Variable Vector Countermeasure Suit (V2Suit) for Space Habitation and Exploration

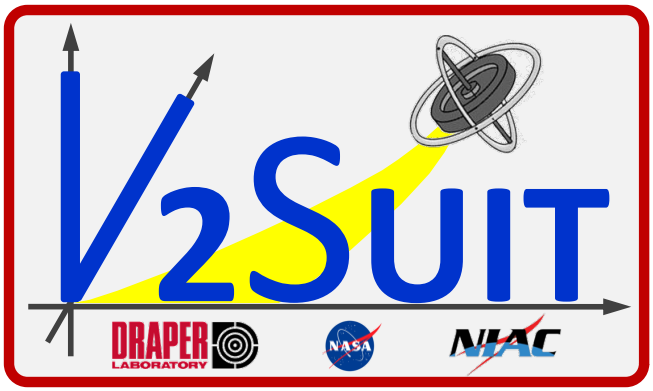

NASA Innovative Advanced Concepts (NIAC)

Phase II Final Report

September 9, 2014

This page intentionally left blank.

Executive Summary

The "Variable Vector Countermeasure Suit (V2Suit) for Space Habitation and Exploration" is a visionary system concept that will revolutionize space missions by providing a platform for integrating sensors and actuators with daily astronaut intravehicular activities to improve human health and performance. The V2Suit uses control moment gyroscopes (CMGs) within a miniaturized module placed on body segments to provide a "viscous resistance" during movements – a countermeasure to the sensorimotor and musculoskeletal adaptation performance decrements that manifest themselves while living and working in microgravity and during gravitational transitions during long-duration spaceflight, including post-flight recovery and rehabilitation. Through an integrated design, system initialization, and control systems approach the V2Suit is capable of generating this "viscous resistance" along an arbitrarily specified direction of "down." When movements are made, for example, parallel to that "down" direction a resistance is applied, and when the movement is perpendicular to that direction no resistance is applied. The V2Suit proposes to be a countermeasure to this spaceflight-related adaptation and de-conditioning and the unique sensorimotor characteristics associated with living and working in 0-G, which are critical for future long-duration space missions.

This NIAC Phase II project leveraged the study results from Phase I and focused on detailing several aspects of the V2Suit concept, including a wearable CMG architecture, control steering laws, human-system integration evaluations, developing a brassboard prototype unit as a proof-of-concept, as well as evaluating the concept in the context of future space exploration missions. A human mission to Mars, such as that outlined in the Mars Design Reference Architecture 5.0, provides a framework for determining the concept of operations and requirements for the V2Suit system. Mars DRA 5.0 includes approximately 180 day 0-G transits to- and from- Mars, as well as a 500 day stay on the surface (~3/8-G) (Figure 3). Accordingly, there are four gravitational transitions associated with this mission: 1-G to 0-G (Earth launch), 0-G to 3/8-G (Mars landing), 3/8-G to 0-G (Mars launch), and 0-G to 1-G (Earth landing). This reference mission provided the basis for developing high-level operational requirements to guide the subsequent study and design of the key V2Suit components.

A detailed simulation architecture was developed to conduct a trade study for inertial measurement unit selection and to demonstrate the performance of the "down" tracking algorithm – a key enabler for the successful implementation of the V2Suit. Throughout the development of the "down" tracking algorithm, two modes of operation were identified – an initialization phase where the direction of "down" is specified by the user, and then stored for the operations phase where the V2Suit system tracks the motion and orientation of each module with respect to that "down" direction. The simulation architecture was also used to conduct a detailed IMU trade study, and CMG trade study with the selected steering laws. Several CMG architectures were evaluate, including scissored pairs, 4- and 5-CMG pyramid configurations,

variable speed CMGs, and reaction wheel assemblies. Key CMG parameters such as flywheel spin rate, gimbal rate, and flywheel inertia were varied within the architecture. A 4-CMG pyramid was selected to generate the required torque – at least 0.1 N-m – in any direction during normal movements.

Initial design of a 4-CMG array was conducted and fabricated using commercial off-the-shelf components, and custom machining when necessary. The goal of this brassboard prototype was to demonstrate the V2Suit concept – closed loop control from "down" tracking to CMG actuation – as well as determine the key engineering and technical challenges required to overcome prior to an operational V2Suit system. It is not the final form factor of the module. Its development identified key challenges and components to further investigate in future systems, including the identification of custom electronics (motors and motor controllers), power consumption and sources, and an initial estimate of human-system integration options. The components were controlled from a desktop computer and powered from a 12 VDC supply. Qualitative and quantitative evaluations of the system demonstrated the ability to initialize and track against a specified direction of "down," command the 4 CMGs independently, and that single module power consumption was approximately 8-10 Watts during operation.

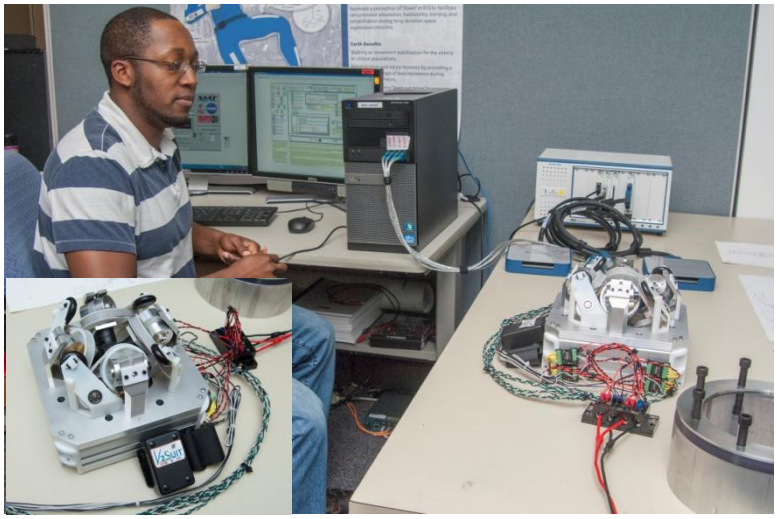

The successful development, integration and operation of the V2Suit will be a be an enabler for space exploration mission technologies, including human health and adaptation countermeasures, autonomous health monitoring, human robotic interfaces, and adaptation and operations during artificial gravity. An integrated and comprehensive countermeasure system has a measurable impact in human performance following a space mission, and mass and volume savings in the spacecraft itself. This type of countermeasure suit also has earth benefits, particularly in gait or movement stabilization for the elderly, or rehabilitating individuals – the gyroscopes could be programmed to provide a kinematic envelope of least resistance during walking. Therefore, providing tactile feedback to the appropriate biomechanical coordination either to assist in gait correction or facilitate recovery following spaceflight.

Table of Contents

The V2Suit Team

CAMBRIDGE, MA

CAMBRIDGE, MA

WORCESTER, MA

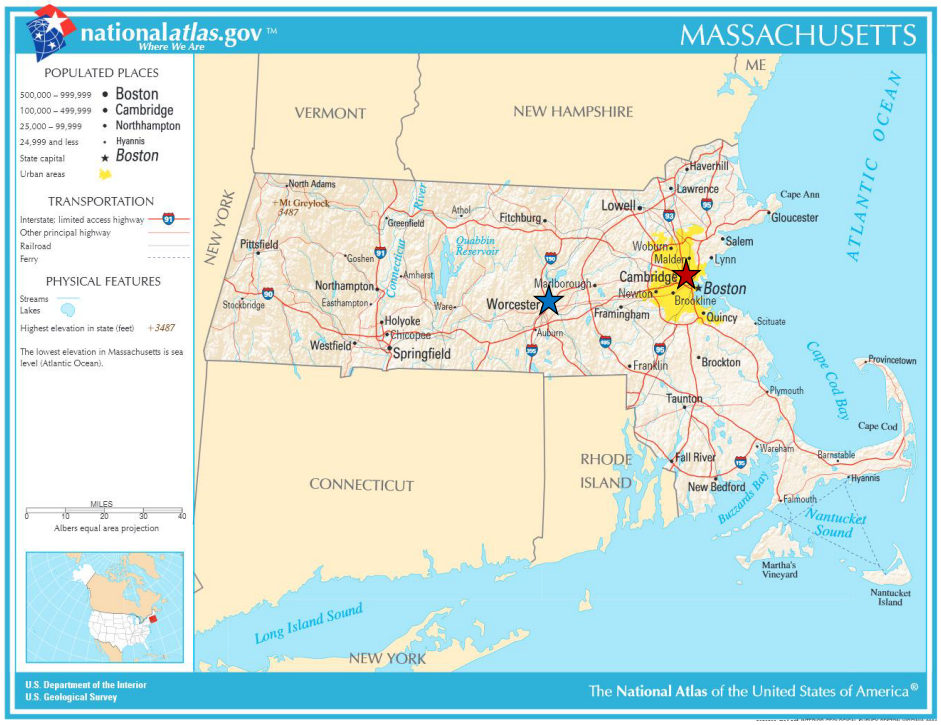

Kevin R. Duda, Ph.D. (Principal Investigator)
The Charles Stark Draper Laboratory, Inc.

Dava J. Newman, Ph.D. (Co-Investigator)
Massachusetts Institute of Technology

Shane E. Jacobs, Ph.D. (Co-Investigator)
David Clark Company, Inc.

John J. West
The Charles Stark Draper Laboratory, Inc.

Akil J. Middleton
The Charles Stark Draper Laboratory, Inc.

Rebecca Vasquez
Massachusetts Institute of Technology

Mitchell Hansberry
The Charles Stark Draper Laboratory, Inc.

Acknowledgements

The V2Suit team would like to thank Mitch Hansberry (Draper Lab) for his contributions to mechanical design and fabrication of the V2Suit module prototype; Mark Boyer, Dan Montes, and Dilip Thekkoodan for their contributions to the human-system interaction evaluations; Ostin Zarse (MIT) for developing the parameterized LabVIEW code for controlling the module prototype; Kevin Hoxie (Draper Lab) for motor wiring and harnessing. We would also like to thank the members of our External Advisory Team for their insightful comments and review of the V2Suit progress through the Phase II study: Jacob J. Bloomberg, Ph.D., Jonathan Clark, M.D., Kent Copeland, William Paloski, Ph.D., Scott Parazynski, Ph.D., Steve Hart, M.D., and Jennifer Rochlis Zumbado, Ph.D. Finally, we would like to thank the NIAC staff for their support and coordination as we were able to study this exciting topic for enabling future human space exploration missions.

1.0 Introduction, Motivation and Objectives

The "Variable Vector Countermeasure Suit (V2Suit) for Space Habitation and Exploration" is a novel concept for integrating spaceflight adaptation countermeasures with daily intravehicular activities, and testing the interactions between countermeasures to assure astronaut health, performance and safe operations (Figure 1-1). The V2Suit integrates control moment gyroscopes (CMGs) within a wearable module on the major segments of the body to provide a "viscous resistance" during movements – a countermeasure to the sensorimotor and musculoskeletal adaptation performance decrements that manifest themselves during gravitational transitions associated with long-duration spaceflight. The V2Suit addresses the "Human Health, Life Support and Habitation Systems" Technology Area (TA06) within NASA's Office of the Chief Technologist Space Technology Roadmaps, specifically the area within "Human Factors and Performance" (6.3.4). The successful development and integration of the V2Suit will be a be an enabler for space exploration mission technologies, including human health and adaptation countermeasures, autonomous health monitoring, human robotic interfaces, and adaptation and operations during artificial gravity. In addition to the measurable impact an integrated and comprehensive countermeasure system has on human performance following a space mission, it also has the potential to enable significant mass and volume savings of required countermeasure equipment within the spacecraft itself.

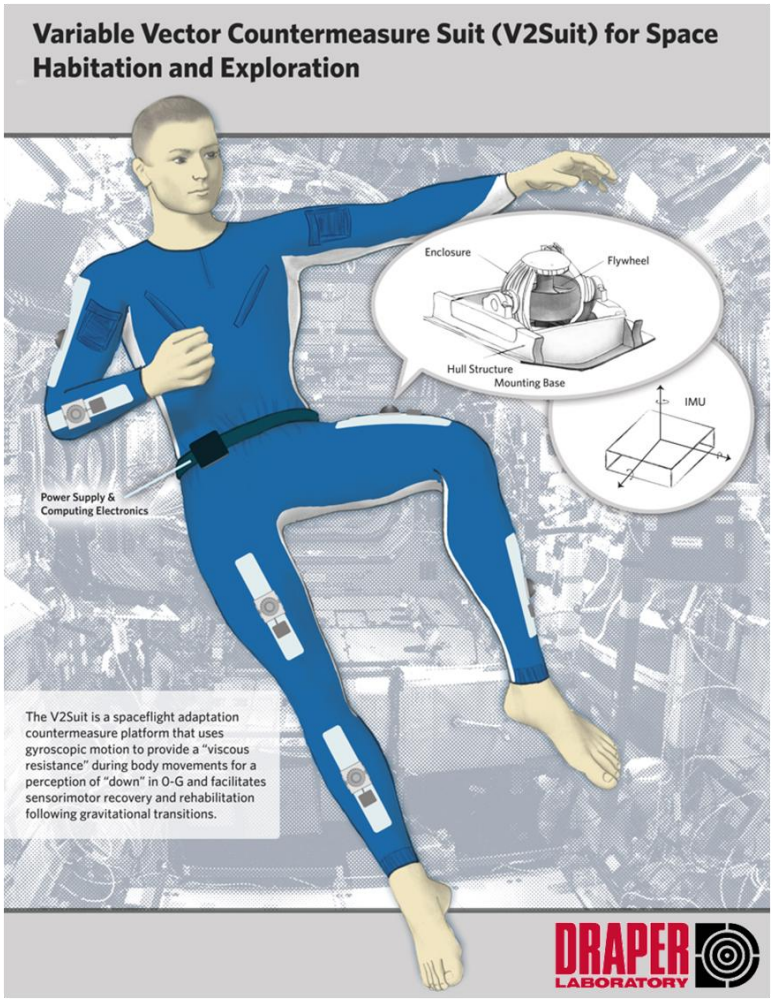

Figure 1-1: Variable Vector Countermeasure Suit (V2Suit)

Exposure to the weightless environment of spaceflight is known to result in sensorimotor adaptation and physiological de-conditioning that includes spatial disorientation, space motion

sickness, reductions in muscle volume, muscle strength, and bone mineral density [3, 4]. Most astronauts report that the effects related to sensorimotor adaptation are the most obvious and prevalent (NSBRI Sensorimotor Research Team Annual Report, 2009). It has been noted that these changes – postural instability, gait ataxia, eye-head-hand control – typically manifest themselves during gravitational transitions and during post-flight activities [5-7]. Gravitational transitions also often coincide with the time critical maneuvering phases of a mission, just when physical and cognitive performance must be high to ensure mission safety and success. Launch, rendezvous and docking with orbiting platforms or bodies, and return to a gravitational environment requires precise, time-critical interactions with complex vehicle systems. In addition, self-orientation perception in 0-G is dynamic since gravitational "down" cues are absent, and visual cues may be ambiguous [1]. Teleoperation and docking tasks are three dimensional and require integration of sensory information from multiple reference frames (NSBRI Sensorimotor Research Team Annual Report, 2009), and performance may be affected due to sensorimotor adaptation.

Anecdotally, one of the ISS Expedition 6 crewmembers was paraphrased following the off-nominal return that they "[C]ompleted about thirty minutes of work in six hours…since there wasn't any real rush" (Soyuz TMA-1 re-entry and descent was a ballistic trajectory landing approximately 300 miles short of the planned area). However, given a long-duration space mission to a solar system destination without ground-based support personnel the outcome of an off-nominal scenario could be significantly different and even jeopardize mission safety.

The NASA Human Research Program has identified a "Risk of Impaired Control of Spacecraft, Associated Systems and Immediate Vehicle Egress Due to Vestibular/Sensorimotor Alterations Associated with Space Flight" which states that, "*Given that there is an alteration in vestibular/sensorimotor function during and immediately following gravitational transitions manifested as changes in eye-head-hand control, postural and/or locomotor ability, gaze function, and perception, there is a possibility that crew will experience impaired control of the spacecraft during landing along with impaired ability to immediately egress following a landing on a planetary surface (Earth or other) after long-duration spaceflight*" [8]. Currently, there are no in-flight countermeasures directly targeting the physiologic changes that affect the sensorimotor system, and the V2Suit system offers a promising solution.

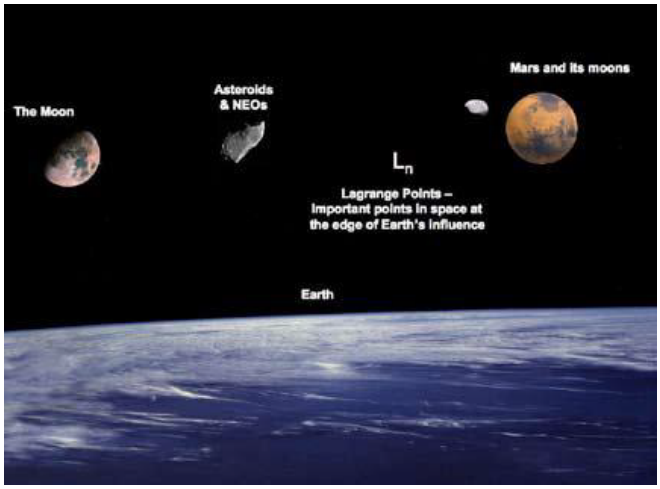

Figure 1-2: Potential destinations for the U.S. human spaceflight program [2]

Missions to future solar system destinations – the moon, asteroids and near earth objects, Lagrange points, and Mars and its moons (Figure 1-2) [2] – will all have varying mission durations, gravitational transitions during entry, descent, and landing or rendezvous maneuvers, and operational requirements upon arrival. These missions will likely include exercise protocols to mitigate the physiologic adaptation and enable operational performance immediately upon arrival. The V2Suit aims to target the sensorimotor system adaptation that results in postural instability, gait ataxia, and eye-head-hand coordination. However, the V2Suit system and wearable sensors are designed to enable the integration of countermeasures against bone and muscle loss, provide radiation protection using novel active and passive materials, and continuously monitor astronaut health and status – all required for deep-space exploration missions. Integrating these countermeasures with daily activities and operations without requiring specialized equipment, may eliminate as much as 2.5 hours per day in allocated exercise time [3, 9] and would significantly reduce the required mass and volume for exercise equipment. Mars missions may utilize artificial gravity via centrifugation, and the V2Suit's sensorimotor adaptation capabilities may be used to counter Coriolis accelerations, and therefore eliminate the need for biomechanical adaptation or compensation within a rotating environment [10].

The V2Suit is an integrated platform for spaceflight-related physiological adaptation and de-conditioning countermeasures and training through the use of wearable control moment gyroscopes to produce a torque that results from the change in direction of the angular momentum vector of the flywheels. This Phase I project investigated the human-system integration challenges of interfacing the wearable modules with human to transmit the gyroscopic torque, as well as developed a system architecture for initializing the modules, tracking their movement, and commanding the flywheels to generate the required gyroscopic torque. The properties of the control moment gyroscopes and module packaging were investigated through modeling and simulation, and the results are documented. Collectively, this analysis has led to the identification of key enabling technologies, the challenges associated with each, and the identification of alternate uses and Earth benefits.

2.0 Mission Definition and Operational Requirements

2.1 Mission Definition – Mars DRA 5.0

It is envisioned that a fully-operational V2Suit will facilitate sensorimotor adaptation in advance of gravitational transitions and potentially counter the musculoskeletal de-conditioning that accompanies long-duration spaceflight. This could include living and working on the International Space Station (ISS), a mission to asteroids or near-earth objects, or a human mission to Mars and/or its moons. A human mission to mars, such as that outlined in the Mars Design Reference Architecture 5.0 [11], provides a framework for determining the concept of

operations and requirements for the V2Suit system. Mars DRA 5.0 includes approximately 180 day 0-G transits to- and from- Mars, as well as a 500 day stay on the surface (~3/8-G) (Figure 2-1). Accordingly, there are four gravitational transitions associated with this mission: 1-G to 0-G (Earth launch), 0-G to 3/8-G (Mars landing), 3/8-G to 0-G (Mars launch), and 0-G to 1-G (Earth landing).

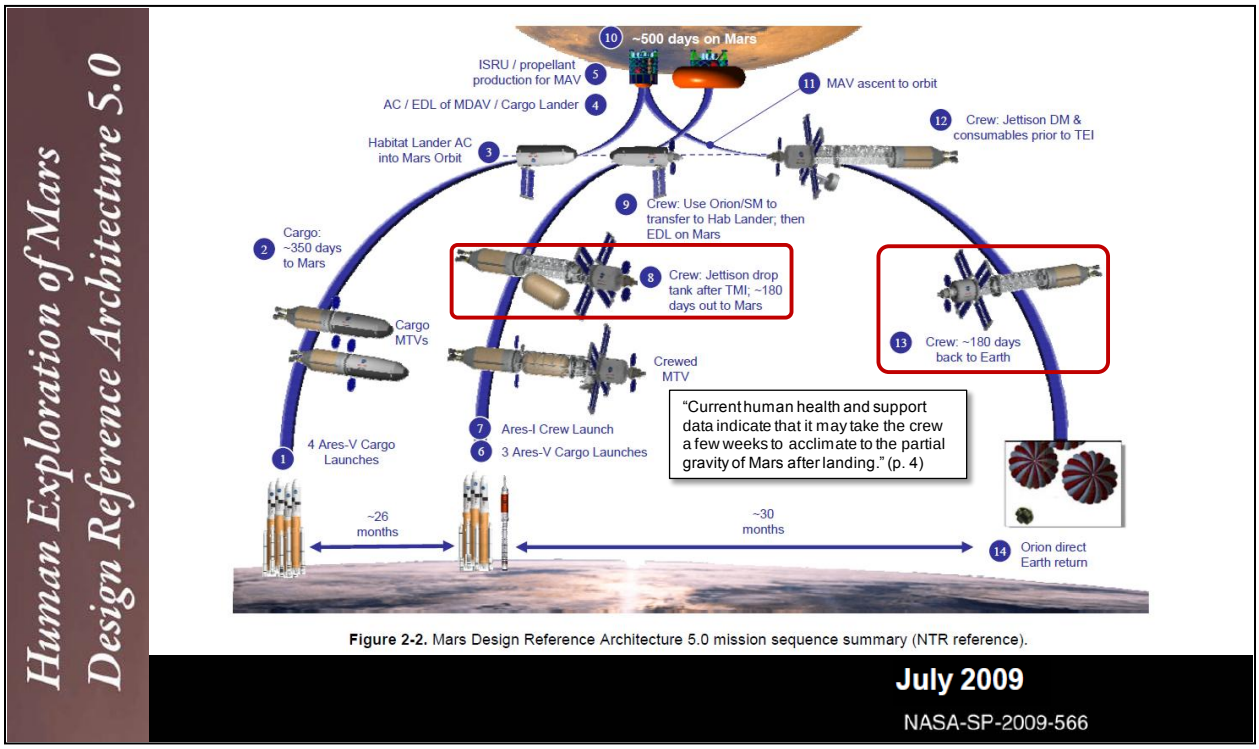

Figure 2-2. Mars Design Reference Architecture 5.0 mission sequence summary (NTR reference).

Figure 2-1: Mars Design Reference Architecture 5.0 (figure modified from [11])

Even though the Mars mission provides the framework for a long-term operational scenario for the V2Suit, many lessons learned and operational experience can be gained from use on the ISS. The Mars DRA 5.0 report states that "The ISS is currently serving as a vital test facility for research that demands long exposures to the reduced-gravity loading conditions in spacecraft and on planetary surfaces. That research will establish the baseline for the 6-month transit from Earth to Mars, and is forming the foundation of the extrapolations and inferences that are necessary for near-term planning for the 18-month Mars surface habitation and the 6-month return transit to Earth." (pp. 64-65) [11]. It was also stated in the report that "Current human health and support data indicate that it may take the crew a few weeks to acclimate to the partial gravity of Mars after landing (p. 4)." This is particularly important given the potential need to support emergency or contingency operations immediately following landing. It has been previously assumed that 50% of the Mars crewmembers will be ambulatory immediately following landing, and in the first 1-3 days activities will be limited to those inside the landing vehicle [12]. Having effective countermeasures to both counter the physiologic adaptation and pre-adapt to the

upcoming gravitational environment onboard a Mars transit vehicle will enable operations in these contingency/emergency situations and facilitate the exiting exploration tasks that await these space explorers safely and quickly following touchdown.

2.2 Key Operational Requirements

The V2Suit, based on the expected torque that can be produced from miniature, wearable CMGs, is aimed at countering the sensorimotor adaptation issues that arise during the gravitational transitions associated with spaceflight. An initial set of operational requirements were specified to capture a high-level list of the required functionality, comfort, and performance parameters for the V2Suit (Table 2-1). These requirements were generated based on a candidate long-duration space mission (e.g., ISS Expedition, human Mars mission), as well as expert input based on operational lessons learned from previous technology developments. This requirements list is mapped against the V2Suit concept of operations to determine the Key Enabling Technologies.

Table 2-1 – V2Suit Operational Requirements

ID	Operational Requirement	Key Enabling Technology
CR-1	The V2Suit shall provide a countermeasure to the sensorimotor adaptation effects that manifest during spaceflight-related gravitational transitions.	• Miniature control moment gyroscopes (CMGs) • CMG steering laws • Motion tracking technology and algorithms
CR-2	The V2Suit system shall be capable of being worn for at least 8 hours (TBR), be comfortable, and be unobtrusive during all nominal activities.	• Miniature CMGs • Human-System Integration
CR-3	The V2Suit shall take less than 5 minutes (TBR) to don/doff in all gravitational (e.g., 0-G, 1-G, 1/6-G) environments.	• Human-System Integration
CR-4	The V2Suit shall have an operational time of at least 1 hour (TBR).	• High-density, miniature batteries • Wireless power

3.0 Background

3.1 Spaceflight-related Physiologic Adaptation and De-conditioning

All future long-duration space missions will result in physiologic adaptation and deconditioning, that include, but are not limited to, bone loss, muscle atrophy, cardiovascular alterations, sensorimotor adaptation [4], and the recent identification of potential changes to the visual system [13]. Each system adapts with a qualitatively different time course. Some have been quantified during space flights up to 6-months in duration, whereas others have no known "0-G Set Point." Each system also recovers to their "1-G Set Point" after returning to Earth at a different pace, ranging from days (sensorimotor) to years (bone). Crewmembers on the International Space Station (ISS) spend approximately 2.5 hours per day exercising in an attempt to prevent this physiological de-conditioning, but have not been completely successful [3, 9].

The muscular system, used for locomotion, postural control, and balance is affected by spaceflight due to the gravitational unloading, the lack of a need for balance, and changes in locomotor strategies in a weightless environment [14]. The major effect of microgravity is muscle atrophy with an accompanying loss of peak force and power [14]. At the whole-muscle level, the maximum power of the lower limbs was reduced to 67% of the preflight levels in astronauts after 31 days in space, and to 45% after 180 days [15]. Head-down bed rest studies, a spaceflight analog, have reported strength losses between 0.4% and 0.6% per day in the arms and lower extremities [16]. Another complication occurs because muscle contractions are also a major source of bone loading. Loss of muscle strength could exacerbate bone loss, so it is necessary to develop countermeasures that address musculoskeletal de-conditioning.

Bone mineral density reductions following spaceflight have been reported as high as 1-2% per month in the lower spine and hip, with smaller losses in the upper body [3, 17, 18]. Studies of Russian Mir cosmonauts found bone losses of up to 1.7% per month in weight bearing areas such as the spine, pelvis, and proximal femur, but no loss in the upper extremities [17]. Similar studies performed on ISS astronauts revealed reductions of 1% per month in the spine, and up to 1.5% a month in the hip. While astronauts lose bone at a rapid rate, they are slow to recover it when they return to earth, and it is unknown whether they ever fully recover. A follow up study on Skylab astronauts showed that not all bone lost during the mission had been recovered even five years after flight [19]. These results are similar to those seen on earth due to immobilization or spinal cord injury [3], which suggests that research into physiological de-conditioning seen in space could have earth benefits.

Changes to the sensorimotor system typically manifest themselves during gravitational transitions and during post-flight activities, which can be observed in terms of postural instability [5] and gait ataxia [6, 7]. The balance system relies on information from the otoliths, semi-circular canals, vision, proprioception, as well as local reflex arcs [20]. Results from spaceflight

suggest that when astronauts enter weightlessness, arm movements are altered and may be inappropriate and inaccurate [21-24] with increased movement variability, reaction time, and duration [25]. Changes in neuromuscular function (e.g., muscle fiber changes, activation potential changes), muscle atrophy, and orthostatic intolerance may also contribute to post-flight posture and stability. The sensorimotor system, however, does recover rapidly. The initial rapid re-adaptation has a time constant on the order of 2.7 hours, whereas the slower, secondary, re-adaptation phase shows a time constant of approximately 100 hours (4 days) [5]. Even though the sensorimotor system appears to re-adapt rather quickly, many critical tasks must occur during the gravitational transition (e.g., piloting tasks) or immediately following it (e.g., landing, vehicle egress).

Vision plays a critical role in maintaining spatial orientation in weightlessness [1]. On Earth we experience no orientation illusions because our sensory systems all agree on the same interpretation of our orientation with respect to the surrounding environment [1]. In space the semi-circular canals and vision continue to provide accurate information, but the otoliths no longer have a tonic input signaling gravity or body tilt, and the feet are rarely in contact with a surface. Cumulatively, this results in a conflict between the senses. During flights, one of the perceptions that can change dramatically is "one's perception of static orientation with respect to the cabin and the environment beyond" (see Figure 3-1) [1], which manifest themselves in the form of 0-G inversion illusions [26, 27] and visual reorientation illusions [26]. There are no countermeasures to these illusions in weightlessness. Providing an external cue to the direction of down may alleviate them, which could have operational benefits for navigation/emergency egress as well as mental rotations and reference frame coordination during teleoperation, docking or berthing operations.

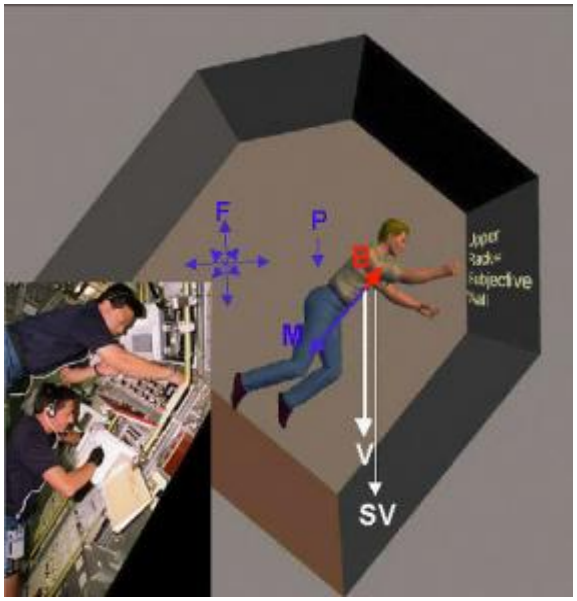

Figure 3-1: A human visual orientation model for working with a canted rack in a spacecraft [1].

3.2 Existing Countermeasures

Sensorimotor— Existing countermeasures for sensorimotor adaptation include pre-flight training procedures which may allow astronauts to more easily adapt their sensorimotor systems to altered vestibular sensory inputs [28-30]. Some of this training includes using virtual reality to expose astronauts to disorientation in order to help the sensorimotor system adapt more quickly to potentially disorienting environments and situations they may encounter [31, 32]. The results

of pre-flight sensorimotor testing as well as ground based virtual reality studies can be used to develop an appropriate training protocol for pre-adaptation to microgravity [33, 34]. It has been shown that previous sensorimotor adaptation facilitates future sensorimotor adaptation; essentially someone's "ability to adapt" can be improved with practice [35].

Musculoskeletal— A variety of countermeasures have been developed to attempt to maintain bone density and muscle strength during space flight. These include exercise, pharmaceutical supplements, a specialized diet, artificial gravity, and countermeasure suits such MIT's Gravity Loading Countermeasure Suit and the Russian Penguin Suit [36, 37]. None of these countermeasures can be shown to be 100% effective at mitigating the effects of microgravity on the musculoskeletal system. Due to differences in individual physiology and an inability to ensure strict compliance to any prescribed countermeasure, it is difficult to evaluate the effectiveness of any given device or practice. Current protocol requires that astronauts spend 2.5 hours per day exercising (with a combination of resistive and cardiovascular equipment) to maintain their fitness while in microgravity, but deconditioning is still an issue [38, 39]. Ground-based studies with simulated microgravity (bed rest) which combine exercise with either centrifuge-induced artificial gravity or lower body negative pressure have been conducted and shown to mitigate deconditioning [40, 41]. Pharmaceutical countermeasures have also been proposed to reduce deconditioning, and the use of bisphosphonates in conjunction with the exercise protocol has been shown to reduce bone loss during spaceflight [42]. Additionally, research has shown that appropriate nutrition (energy intake to maintain body mass and vitamin D) in addition to resistance exercise with the Advanced Resistive Exercise Device (ARED) will help maintain bone mass [43].

The exercise equipment is costly in terms of size and mass (the ARED weighs about 700 lbs.), and the prescribed regime is costly in terms of the large time requirement placed on astronauts [44]. Additionally, use of the current exercise equipment, in particular the ARED, has been hypothesized to lead to other physiological problems such as visual impairment due to intracranial pressure (VIIP syndrome), and there is risk of musculoskeletal injury associated with resistance exercise [45, 46]. Developing additional countermeasures that can be used concurrently with existing countermeasures or other daily activities may enable the crew to spend less time exercising, while also reducing the risk of additional impairment.

3.3 Countermeasure Suits

A number of countermeasures have been developed and used in an attempt to prevent muscle and strength loss during spaceflight. In addition to treadmills, cycle ergometers, and resistive exercise devices, the Russian Cosmonauts have used passive stretch garments (Russian "Penguin Suit") and electrical stimulation. The "Penguin Suit" has "rubber bands woven into the fabric, extending from the shoulders to the waist and from the waist to the lower extremities, to produce

tension on antigravity muscles [16]" (Figure 3-2, Left). More recently, a Gravity Loading Countermeasure Skinsuit (GLCS) was prototyped and evaluated in parabolic flight [36] (Figure 3-2, Right). This type of suit, as well as the "Penguin Suit," is an example platform for integrating with the sensorimotor aspects of the V2Suit. Despite these types of intravehicular suits having been developed, and to a limited extent used operationally, none have proposed to integrate multiple countermeasures (e.g., sensorimotor, bone, muscle, or radiation). These devices also have been completely passive – not containing or requiring any electrically powered components to achieve their intended purpose. The integration and use of intermittent powered components within the V2Suit stands to improve countermeasure systems being developed as well as in-flight training systems for sensorimotor adaptation.

http://www.globaleffects.com/C_pages/Rental/Wardrobe/SpaceSuits/Historical/Russian/Penguin755_hi.jpg

http://www.cnn.com/2010/TECH/innovation/11/05/gravity.space.suit/index.html

Figure 3-2: Left: Russian "Penguin Suit", Right: MIT Gravity Loading Countermeasure Skinsuit

3.4 Wearable Kinematic Measurement Systems

Wearable inertial sensors have previously been used in a variety of kinematic tracking applications. IMUs placed on body segments can measure the angular velocity of the segments, and this data can be integrated to determine the joint angles; IMU drift can be continuously corrected for using inclination estimations from the accelerometers. Inertial sensor network results have been compared to optical tracking systems and found to be accurate with a RMS error of less than 8° [47-49].

There have been a variety of cases of using inertial sensor networks to evaluate athlete performance. Lapinski et al. used 6 DOF IMUs mounted on baseball players' hands and arms to calculate the g-forces at the hand during pitching and batting as well as to estimate bat speed at impact [50]. Brodie et al. used a fusion motion capture system with alpine skiers that combined IMU data with GPS data in order to track both the local orientation and acceleration of the limbs (IMUs) and the global trajectory (GPS) of the athlete [51]. Lai et al. used a network of 4 inertial sensors on the lead arm and trunk of experienced and novice golfers to attempt to find a correlation between swing kinematics and hit accuracy [52].

Inertial sensors have also been used for gait analysis, a concept that has also been extended to navigation. Hung et al. analyzed walking gaits using data from IMUs placed on each shoe combined with a system of a shoe mounted camera and infrared LEDs to measure the attitude between shoes [53]. Li et al. incorporated a similar shoe-mounted IMU system for the Lunar Astronaut Spatial Orientation and Information System (LASOIS), a lunar astronaut navigation system that also incorporated step sensors, suit-mounted cameras, and orbital sensors in order to localize astronauts and analyze their motion on the lunar surface [54]. Space suits in the future will likely include wearable IMUs, cameras, and other sensors and displays to improve astronaut spatial orientation and navigation as well as wearable biological sensors for monitoring astronaut health [55].

Accurately tracking the motion of the V2Suit user is important in determining when and in which direction to apply the resistance. Incorporating the tracking system into the V2Suit using an inertial sensor mechanism similar to those described above would enable the suit to be used anywhere regardless of the existence of external hardware (such as cameras) for motion tracking. The microgravity environment which would be the main use scenario for the V2Suit presents a unique challenge; the gravity vector cannot be used as a reference input to the system as it is in some of the systems described above.

3.5 Control Moment Gyroscopes

Control moment gyroscopes, or CMGs, are momentum actuators that consist of a spinning mass gimbaled about one or more axes. The gimbaling of the mass changes the angular momentum vector of the spinning mass and generates an internal torque. There are a variety of types of CMGs including single gimbal, dual-gimbal, and variable speed CMGs. Traditional single gimbal CMGs have only one gimbal axis and can produce a high output torque vector in a 2-dimensional plane. Dual-gimbal CMGs have two gimbal axes and have a larger momentum envelope but worse power performance than single gimbal CMGs. They also require a more complicated mechanical structure to allow for dual gimbaling. Both single gimbal and dual-gimbal CMGs utilize constant spin rate flywheels. While variable speed CMGs allow for both

gimbaling and changing the flywheel spin rate simultaneously to generate torque, they are power inefficient and generally considered to be of academic interest only. [56]

Arrays of CMGs are controlled with steering laws that command appropriate gimbal rates and/or spin rates (variable speed only) based on the geometric configuration of the CMGs as well as the current gimbal angles in the CMG. Singularities, or orientations in which the CMG array cannot generate torque in a particular direction, may occur and should be taken into account in developing steering laws for the CMG array [56]. There are a variety of steering laws for singularity avoidance and escape being developed, and this is an ongoing area of research as a single steering law is not applicable for every CMG use case [57-59].

Control moment gyroscope arrays are commonly used for spacecraft attitude control. The V2Suit aims to miniaturize a CMG array for use inside modules that have a small enough form factor to be wearable on the individual body segments, and use the gyroscopic torque to affect the wearer's biomechanics. Flanders et al. found that gyroscopic torque can perturb arm motion. The magnitude of the torque required was "about 10% of the maximum joint torque in shoulder elevation and elbow flexion and about 1% of the maximum joint torque in shoulder yaw and humeral rotation" or approximately 0.1 Nm (see Figure 3-3) [60]. This result informed the desired torque output for each V2Suit module.

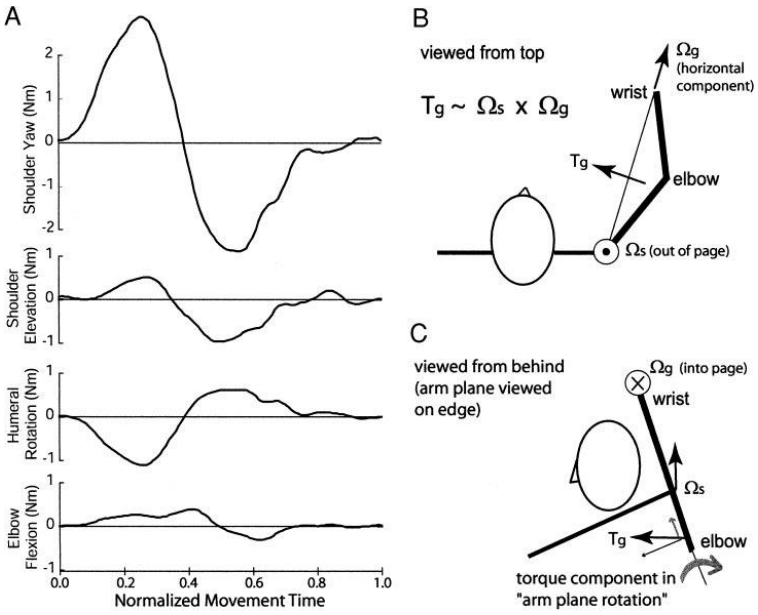

Figure 3-3: Joint torques during reaching motions while holding a spinning flywheel; the gyroscopic torque magnitude was approximately 0.1 Nm [60].

Other considerations when choosing an appropriate array for the V2Suit include the total number of CMGs and actuators for the array, as well as any additional hardware that would be required.

Size is a significant constraint, so minimizing the amount of hardware required inside each module is a key to the success of the design. When considering how to control the CMG array for the V2Suit, significant consideration should be placed on the effect of body motions on the torque output of the system. The movement of the object on which a CMG array is mounted also generates a torque, referred to as a base rate torque [56]. In this case, the CMGs will be mounted on a person's limbs, the motion of which may significantly impact the output torque from the CMG array.

4.0 Key V2Suit Research Areas

Five key V2Suit research areas were investigated as part of the NIAC Phase II Study. These included the development of an integrated simulation architecture; the development of the "down" tracking algorithm for determining the direction to command the CMG torque vector; the design, simulation, and analysis of wearable CMGs; evaluation of human-system integration alternatives; and brassboard prototyping of a unit to demonstrate the V2Suit capabilities. Each of these key research areas will be described in the following sections.

4.1 Integrated Simulation Architecture

An integrated simulation architecture was developed in MATLAB/Simulink for the V2Suit. This integrated architecture enabled several early-stage prototyping efforts as well as a number of trade studies for the CMG architecture and component selections. The architecture, at a high-level, is comprised of two major elements: Central Processing and the V2Suit module (Figure 4-1). Central Processing includes all of the computational elements required for sensing the module state and motion and issuing commands to the CMG for applying a torque in the appropriate direction during movement. In addition, the Central Processing is responsible for system moding and the initialization of parameters. During the initialization phase, maintaining the state record of the local inertial reference frame is the responsibility of Central Processing.

Within each V2Suit module, a model of the onboard IMU is used to determine the module orientation (during the Initialization Mode) and inputs to the "down" tracking algorithm, which is employed during the Operations Mode. Calculation of the "down" vector is accomplished in Central Processing. Commands are received from Central Processing to steer each CMG so that the torque vector is in the appropriate direction with the appropriate magnitude. The CMG controller in each module is responsible for actuating the local hardware. In addition, each V2Suit module model includes a model of the CMG architecture and parameters. Nominally, the simulation flows from the Initialization Mode to Operations Mode.

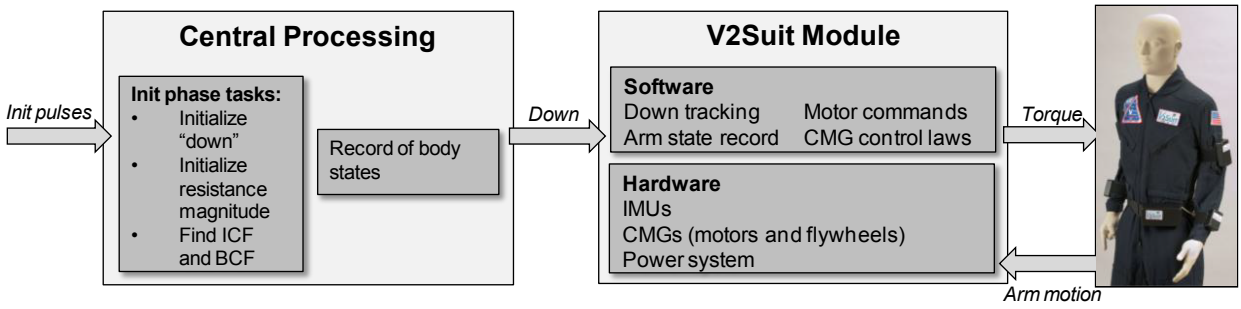

Figure 4-1: High-Level Simulation Architecture

Figure 4-2 provides an overview of the integrated simulation architecture, as implemented in MATLAB/Simulink. Specifically, data files of representative arm motions were created and used to initialize "down" tracking, and then used to track the orientation of the module with respect to that "down" direction during Operations. The CMG model was parameterized for a detailed trade study for wearable architectures.

This integrated simulation architecture proved to be useful in many areas including: validating the "down" tracking algorithm (see Section 4.2), recognizing early potential implementation issues (such as the need for a "down" tracking sampling rate filter), a wearable CMG architecture trade study (see Section 4.3), and selecting an inertial measurement unit (IMU) that would meet the performance requirements of the V2Suit. This final point will be decribed below.

One of the key operational requirements is to operate continuously for at least 1 hour (CR-4, see Table 2-1). Over time, the IMU measurements will drift and result in the algorithm's calculation of 'down' to deviate from its true direction. In order to bound the operational time of the V2Suit before a re-initialization is required, it is necessary to quantify the performance of the IMU inside the V2Suit module to determine how long the system can run before a significant drift from truth is observed.

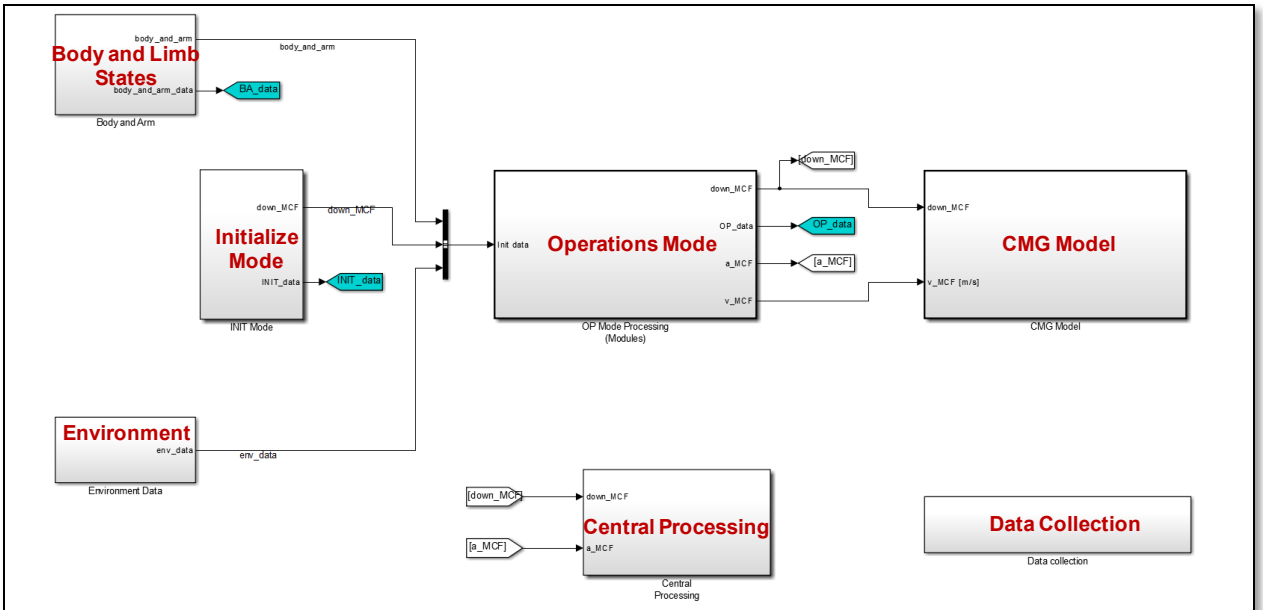

Major Sim Component	Purpose
Body and Limb	States of the limbs and body
Environment Data	Relevant variables from the operational environment
INIT Mode	Logical initialization functions – Initializes down
OP Mode Processing	Logical main operational functions
Central Processing	Remainder of logical CP functions
CMG Model	CMG models and control
Data Collection	Simulation data logger

Figure 4-2: Overview of MATLAB/Simulink Integrated Simulation Architecture

Figure 4-3 shows a potential drift instance. The percent of a calculated 'down' that will align in the direction of true 'down' is the cosine of the angle between the two unit vectors, i.e. it is the projection of the calculated solution onto the vector representing the truth. For example, at a 10-degree offset 98% of the calculated 'down' is the correct direction, at 30 degrees this is reduced to 87%, and at a 41-degree offset it is further reduced to 75%. This percent will end up being the fraction of the generated torque that will be correctly pointed. For this reason, the ideal would be to keep the deviation of 'down' to 10-degrees or less.

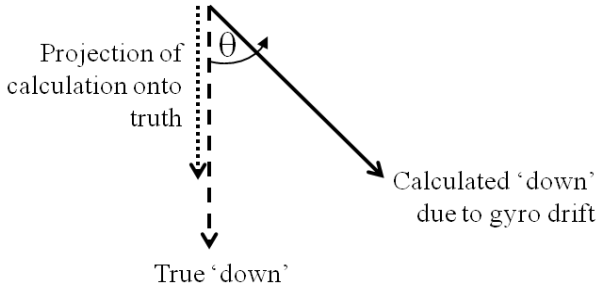

Figure 4-3: An example of drift in the "down" vector. As shown, the calculated 'down' has moved away from the actual 'down' due to gyro imperfections.

The integrated simulation was used to simulate and test three candidate commercial IMUs. The parameters for the simulated IMUs—specifically noise density, bias stability, g-sensitivity, and dynamic range— were obtained from spec sheets or, in the case of IMU #3, from empirically-obtained data. Assumptions made were that a) parameters not listed are set to zero, b) there is a zero gyro bias due to bias removal during initialization, and c) there is a 1 Hz low pass filter at the entrance to down-tracking. For the simulation, the IMUs were set to collect zero-rate data with down in the direction of gravity. The results of the simulation are shown in Figure 4-4.

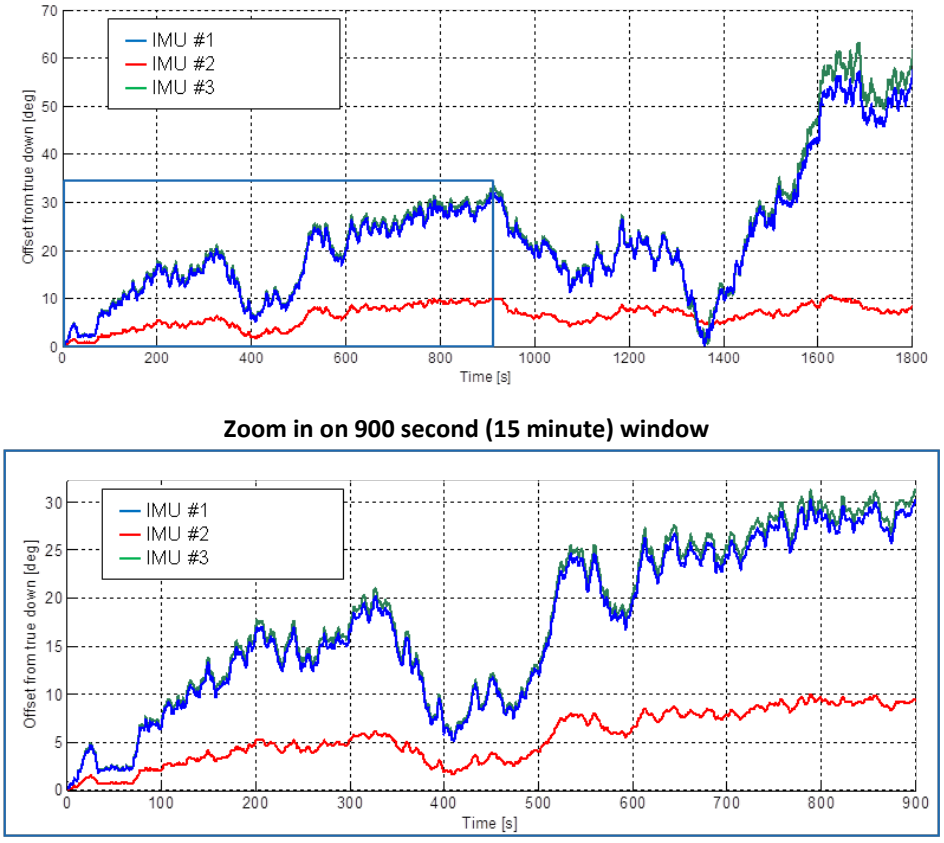

Figure 4-4: IMU performance simulation results. IMU #2 runs for 1 hour with around a 10 degree offset from true down.

Again, the desire was to stay within a 10-degree offset for as long as possible. IMU #2 ran for 1 hour in the simulation and never exceeded a 10 degree offset from true down. Thus it was selected as the desired IMU for the V2Suit module.

The performance of the purchased IMU #2 was subsequently quantified. The IMU was placed in a "rest" position (flat on the table) and the reported 'down' vector was recorded. Then it was secured to a hand for one hour as normal activities were performed. The IMU was returned to the rest position every 10 minutes and the down vector noted. The deviation from the original reported 'down' was calculated at each rest interval (Figure 4-5). It is noted that the offset from the original, true 'down' over the course of an hour does not exceed a degree. Thus, the actual IMU performed better than the simulation predicted and provided confidence in the performance of the IMU to support long-duration operation without requiring re-initialization.

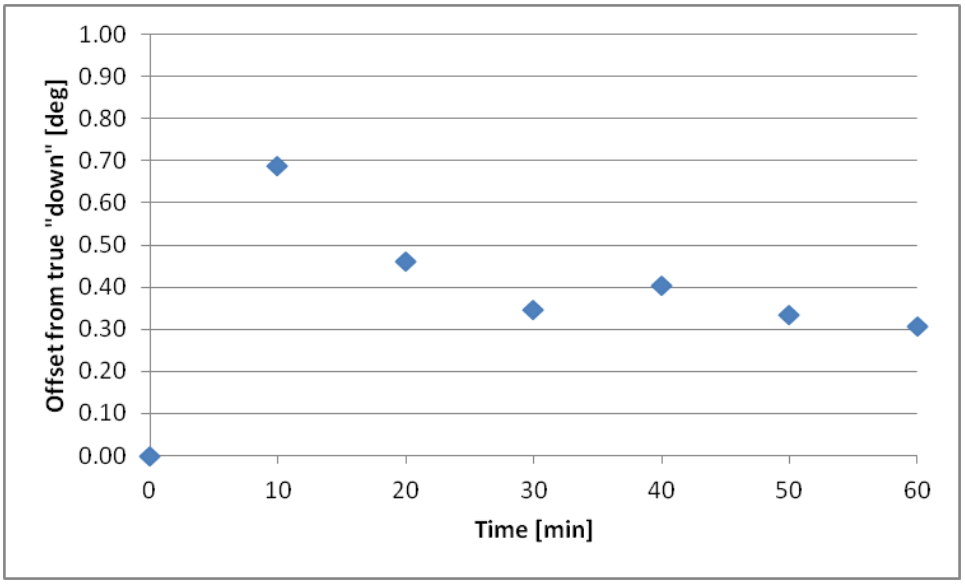

Figure 4-5: Actual IMU performance results. The comparison to true 'down' was taken every 10 minutes.

4.2 "Down" Tracking Algorithm

Two high-level phases of use have been identified for the V2Suit system: the initialization phase and the operations phase (Figure 4-6). The initialization phase is used to set the desired direction of "down" and define the inertial coordinate frame through a specified sequence of motions. Each module's initial orientation can then be determined. During the operations phase the user moves freely and IMUs sense the angular velocity and linear acceleration of each wearable module. This information, along with the orientation information from initialization, is used to track the module position, orientation, and velocity over the course of the motion as well as the direction of inertial "down" in each module's local coordinate frame. This ensures that the resistance that is felt from actuation of the CMGs will be applied in the correct direction.

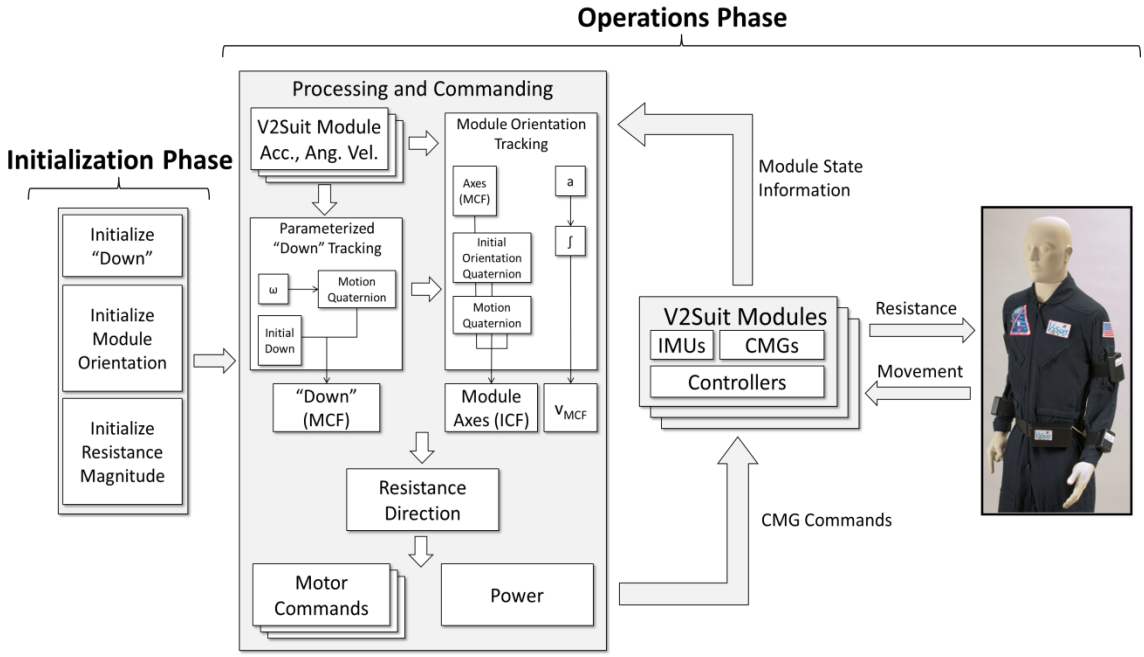

Figure 4-6: V2Suit high level system architecture divided into initialization and operations phases

4.2.1 Coordinate Frames

There are two coordinate frames that are relevant to the V2Suit – the inertial coordinate frame (ICF) and the module coordinate frame (MCF). The ICF is defined by the individual user's "initialization motions" during the initialization phase. It remains fixed in space and does not change until the system is re-initialized. The ICF must be consistent across all V2Suit modules within the same individual to ensure that the direction of the commanded resistance is coordinated across all body segments. Since the ICF is defined in order to specify "down" for the individual user, several users in the same working volume may be tracking against different ICFs. Additionally, the ICF may be specified based on environmental knowledge. For example, the inertial coordinate frame could be specified based on a pre-defined coordinate system associated with a space station module.

The MCF is a local coordinate frame fixed to each of the individual V2Suit modules. It is unique to each module and is non-inertial. The orientation and motion of the MCF is tracked with respect to the ICF (e.g., Figure 4-7) in order to command the CMG actuation to apply the appropriate magnitude and direction of resistance.

As an example, for a module located on the upper arm the MCF is defined as: the module X axis points in the direction of the arm axis, towards the hand. The module Y axis points forward

(right arm) or backward (left arm). The module Z axis points outward from the body to complete the right handed coordinate frame (Figure 4-8).

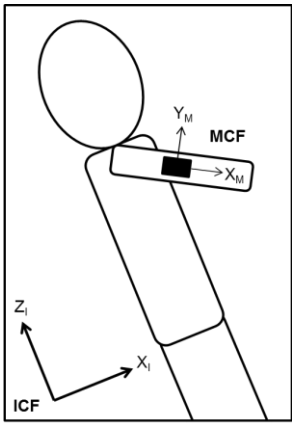

Figure 4-7: Representation of the inertial coordinate frame vs. module coordinate frame

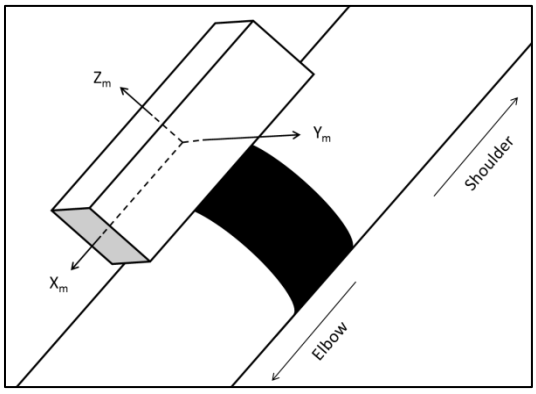

Figure 4-8 – Module coordinate frame convention oriented on an arm.

4.2.2 Algorithm Description

Initialization Phase—The initialization phase defines the direction of inertial "down," determines the initial direction of "down" in module coordinates, and determines the initial orientation of the V2Suit modules with respect to the ICF. In microgravity there is often no obvious up or down direction. Multiple people in the same space may be oriented differently and perceive down differently. The V2Suit user must re-define the inertial coordinate frame each time the system is initialized so that the direction of "down" coincides with the desired direction. Since the initialization process relies on the IMU to determine the module's direction of "down" and the initial orientation, there are required inputs to the system to fully specify these

parameters. These inputs are dependent on the situation or environment in with they are initializing in: in Earth gravity with "down" parallel to gravity, in Earth gravity with "down" in any direction, and in microgravity with "down" in any direction.

The initialization process for the V2Suit requires that the user generate two acceleration pulses in the module that are parallel to two inertial axes – a "Y pulse" and a "Z pulse" (Figure 4-9). One pulse is used to define "down" and the other provides the necessary information to define the orientation of the module with respect to the inertial coordinate frame.

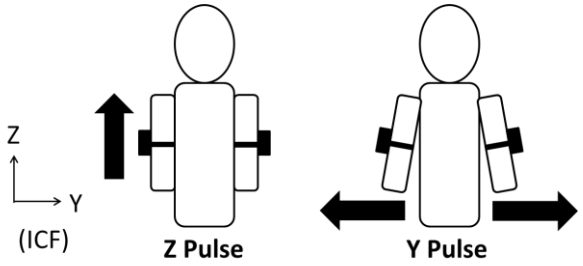

Figure 4-9: The "hop and flap" motion is used to generate two acceleration pulses during initialization to define the direction of inertial down and determine the orientation of the V2Suit module with respect to the ICF.

On Earth, initializing "down" is trivial. "Down" is simply the direction of the IMU acceleration reading due to gravity. Thus, on Earth with "down" aligned to the gravity vector the user must only generate one pulse – the "Y-pulse" or "flap". If the user wishes to initialize "down" on Earth in a direction that is not the same as the direction of gravity, the acceleration reading due to gravity in the IMU must be filtered out so that it does not affect the tracking algorithms and then the initialization process proceeds as it would in microgravity.

In microgravity, the user must provide both the "Y pulse" and "Z pulse" motions. This would be done through a "hop and flap" motion (Figure 4-9). The V2Suit starts in a default initial position of arms by the sides with palms inward. The user then pushes off with his feet. The resulting linear motion is used to define the inertial coordinate frame Z axis. Subsequently, he would move his arms away from his torso to generate a pulse approximately perpendicular to the Z pulse and parallel to the inertial Y axis (see Figure 4-9). (Due to the coordinate convention, the pulse would be in the negative inertial Y direction for the right arm and in the positive inertial Y direction for the left arm.) Inertial down is taken to be the negative inertial Z axis, or the direction opposite of the Z pulse. To find the initial direction of down in the module coordinate frame (MCF) this pulse as detected by the module's IMU is normalized and reversed.

The two "hop and flap" pulses are used to determine the orientation of the module with respect to the ICF [10]. To determine the orientation of the MCF with respect to the ICF, two symbolic

coordinate systems are defined, with $\hat{x}_1, \hat{y}_1$, and $\hat{z}_1$, representing the ICF and $\hat{x}_2, \hat{y}_2$, and $\hat{z}_2$, representing the MCF. The 1-frame is simply the inertial coordinates re-organized for notational purposes (see Equations (4-1) – (4-3)). (Note that calculations shown here are for a module located on the right arm of the user so the Y pulse is in the negative Y inertial direction. The procedure for determining module orientation for the left arm is analogous but $\hat{y}_1$ would be the positive Y inertial axis.)

$$\hat{\boldsymbol{x}}_1 = \boldsymbol{Z}_{Inertial} = [0 \quad 0 \quad 1] \tag{4-1}$$

$$\hat{\boldsymbol{y}}_1 = -\boldsymbol{Y}_{Inertial} = [0 \quad -1 \quad 0] \tag{4-2}$$

$$\hat{\boldsymbol{z}}_1 = \hat{\boldsymbol{x}}_1 \times \hat{\boldsymbol{y}}_1 = [1 \quad 0 \quad 0] \tag{4-3}$$

The 2-frame takes the new $\hat{\boldsymbol{x}}_2$ to be in the direction of the Z-pulse and orthonormalizes the Y pulse to this axis to define the new $\hat{\boldsymbol{y}}_2$(see Equations (4-4) – (4-8)). These $\hat{\boldsymbol{x}}_2$ and $\hat{\boldsymbol{y}}_2$ unit vectors are then used to define $\hat{\boldsymbol{z}}_2$. The orthonormalization process allows for the Y pulse and Z pulse to not be perfectly perpendicular (i.e., the Y pulse need not lie in the inertial XY plane); however the Y pulse must be in the inertial YZ plane to get an accurate orientation.

$$\boldsymbol{x}_2 = \boldsymbol{Z}_{Pulse} \tag{4-4}$$

$$\hat{\boldsymbol{x}}_2 = \frac{\boldsymbol{x}_2}{\|\boldsymbol{x}_2\|} \tag{4-5}$$

$$\boldsymbol{y}_2 = \boldsymbol{Y}_{Pulse} - (\boldsymbol{Y}_{Pulse} \cdot \hat{\boldsymbol{x}}_2)\hat{\boldsymbol{x}}_2 \tag{4-6}$$

$$\hat{\boldsymbol{y}}_2 = \frac{\boldsymbol{y}_2}{\|\boldsymbol{y}_2\|} \tag{4-7}$$

$$\hat{\boldsymbol{z}}_2 = \hat{\boldsymbol{x}}_2 \times \hat{\boldsymbol{y}}_2 \tag{4-8}$$

Once all six unit vectors have been defined, two matrices are formed with the unit vectors as their columns (Equations (4-9) and (4-10)).

$$\boldsymbol{M}_{I(right\ arm)} = \begin{bmatrix} | & | & | \\ \hat{\boldsymbol{x}}_1 & \hat{\boldsymbol{y}}_1 & \hat{\boldsymbol{z}}_1 \\ | & | & | \end{bmatrix} = \begin{bmatrix} 0 & 0 & 1 \\ 0 & -1 & 0 \\ 1 & 0 & 0 \end{bmatrix} \tag{4-9}$$

$$\boldsymbol{M}_M = \begin{bmatrix} | & | & | \\ \hat{\boldsymbol{x}}_2 & \hat{\boldsymbol{y}}_2 & \hat{\boldsymbol{z}}_2 \\ | & | & | \end{bmatrix} \tag{4-10}$$

These matrices are used to find a rotation matrix describing the rotation between the inertial coordinate frame and the module coordinate frame (Equation (4-11)). The rotation matrix can then be converted to a unit quaternion.

$$\boldsymbol{R} = \boldsymbol{M_I M_M}^{\boldsymbol{T}} \qquad (4\text{-}11)$$

The initial orientation quaternion for the module is required to convert between the module coordinate frame (MCF) and the inertial coordinate frame (ICF). To go from the MCF to the ICF, the vector is rotated by the initial orientation quaternion. Conversely, to go from the ICF to the MCF, the vector is rotated by the conjugate of the initial orientation quaternion.

Defining the direction of "down" and finding the orientation of each module with respect to "down" is one aspect of the initialization process. In addition, the initialization phase is used to tare the IMU readings. For this to take place, each V2Suit module would be required to remain stationary while the V2Suit system software tares the IMU acceleration and angular velocity readings to remove any biases in the readings that could affect the stability and long-term "down" tracking performance.

Operations Phase—Once the initialization phase is complete, the system is transitioned to the operations phase. In this phase, the wearer moves freely and the CMG actuation is commanded appropriately. The IMU senses the angular velocity and linear acceleration of each V2Suit module in the MCF and outputs the rotation angles of the IMU relative to its zeroed state. This information is used along with the initial orientation quaternion and the initial direction of down from initialization to keep track of the direction of "down" in the MCF as well as the module's position, orientation, and velocity.

Down Tracking—The CMG-generated torque is perpendicular to the direction of "down" and applied only during movements that are against the direction of "down". Inertial down does not change unless the system is re-initialized, but the direction of "down" in module coordinates changes as the module moves. This direction needs to be tracked to send the appropriate input to the CMG controller. The initial direction of "down" in module coordinates is specified during the initialization phase. During operations phase, rotation angle data (ψ, θ, φ (roll, pitch, yaw)) is converted to a quaternion, q_m, which describes the motion of the module (Equation (4-12)). (The rotation angles may be obtained from the IMU directly if the sensor has that capability or by integrating angular velocity data [11].) The rotation convention used in this algorithm is ZYX. The initial "down" vector is rotated by q_m to give the direction of down in the MCF at each instant throughout the motion (Equation (4-13)).

$$q_m = \begin{bmatrix} \cos\left(\frac{\varphi}{2}\right)\cos\left(\frac{\theta}{2}\right)\cos\left(\frac{\psi}{2}\right) + \sin\left(\frac{\varphi}{2}\right)\sin\left(\frac{\theta}{2}\right)\sin\left(\frac{\psi}{2}\right) \\ \sin\left(\frac{\varphi}{2}\right)\cos\left(\frac{\theta}{2}\right)\cos\left(\frac{\psi}{2}\right) - \cos\left(\frac{\varphi}{2}\right)\sin\left(\frac{\theta}{2}\right)\sin\left(\frac{\psi}{2}\right) \\ \cos\left(\frac{\varphi}{2}\right)\sin\left(\frac{\theta}{2}\right)\cos\left(\frac{\psi}{2}\right) + \sin\left(\frac{\varphi}{2}\right)\cos\left(\frac{\theta}{2}\right)\sin\left(\frac{\psi}{2}\right) \\ \cos\left(\frac{\varphi}{2}\right)\cos\left(\frac{\theta}{2}\right)\sin\left(\frac{\psi}{2}\right) + \sin\left(\frac{\varphi}{2}\right)\sin\left(\frac{\theta}{2}\right)\cos\left(\frac{\psi}{2}\right) \end{bmatrix} \quad (4\text{-}12)$$

$$\vec{d}_{MCF} = q_m \vec{d}_{init} q_m^{-1} \quad (4\text{-}13)$$

4.2.3 Module Orientation and Position Tracking

Tracking each V2Suit module's orientation and position with respect to the ICF are not necessary for sending CMG commands. However, this data is useful for alternate scenarios. For example, a combination of this data with knowledge of elements of the environment could be used to adhere to keep-in or keep-out zones or to track a motion path. Alternately, the IMU-based kinematic measurements could be compared against an optical tracking system to quantify accuracy and drift over time

Tracking each V2Suit module axis orientation during free motion requires that the module axes (in module coordinates) be rotated by the conjugate of the motion quaternion. The resulting vectors represent the module axes in a fixed reference frame aligned with the initial module orientation. To convert from this frame to the inertial coordinate frame, the axes must be rotated again by the initial orientation quaternion which was determined in the initialization phase (Equation (4-14)).

$$X_{MCF}|_{ICF} = q_i(q_m{}^* X_{MCF}(q_m{}^*)^{-1})q_i^{-1} \quad (4\text{-}14)$$

Tracking each module's position requires knowledge about the anthropometry of the user and the placement of the modules on the user's body. The distance from the module center of mass to the joint about which the user's limb rotates (e.g., distance from shoulder to the center of mass of the module on the upper arm) remains fixed under the assumption that the module-body interface does not allow relative motion between the module and the user's body. This distance, multiplied by a unit vector in the direction of the module x axis, gives a position vector from the joint to the module. If additional information about the location of the user with respect to an origin is available through other sensors then this can be combined to determine and track the position and orientation of the module (or some other point of interest) in space (Figure 4-10). Position and orientation tracking may be possible if there were an additional IMU located on the torso to keep track of translation and rotation of the user from a reference starting position.

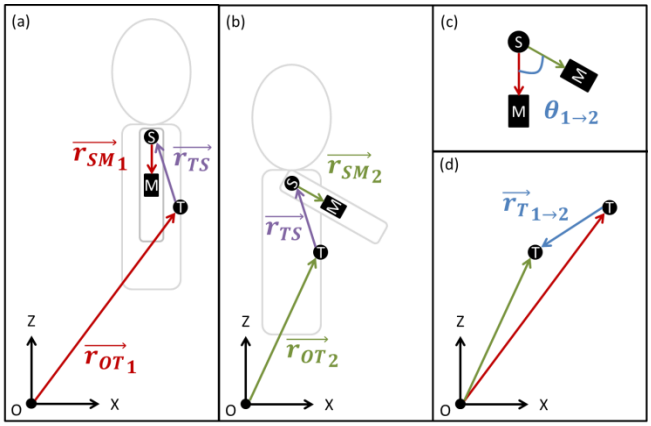

Figure 4-10: The user moves from position (a) to position (b). Figure (c) shows the rotation of the arm from around the shoulder. Figure (d) shows the translational motion of the body. IMU data is used to calculate translation and rotation.

4.2.4 Module Velocity Tracking

The V2Suit system will only command the CMGs to provide a resistance to motions that have a component against "down". The linear velocity of the module is needed to determine the direction of the module's motion. The module IMU measures the linear acceleration over the course of the motion; integrating this gives the linear velocity in module coordinates. If the motion does not have a component in the direction of "down", the dot product of "down" in module coordinates and the linear velocity vector in module coordinates will be equal to zero. If this dot product is non-zero, the CMGs will generate a proportional torque in the direction of "down"; otherwise there will be no torque generated from the V2Suit module.

Direction of Commanded Torque—The CMG generated torque from the V2Suit module should feel like a torque due to gravity. In other words, the direction of this torque should be in the same direction as a gravitational torque would be. The direction of gravitational torque is the cross product of a unit vector starting at the joint and pointing along the body axis and a unit vector in the direction of the force due to gravity. This corresponds in the V2Suit paradigm to the module X axis crossed with the down vector (Equation (4-15)) to specify the direction of the commanded torque in the MCF.

$$\boldsymbol{Torque} = (\mathbf{1} \quad \mathbf{0} \quad \mathbf{0}) \times (\boldsymbol{d_x} \quad \boldsymbol{d_y} \quad \boldsymbol{d_z}) \qquad (4\text{-}15)$$

4.2.5 Algorithm Summary

The "down" tracking algorithm is a critical part of the V2Suit system. It enables the specification of an arbitrary direction of "down" in multiple gravitational environments in order to appropriately command the CMGs to generate a resistance to movements against "down." A

notional sequence of events from the initialization through operations phases is shown in Figure 4-11. It starts with the "hop and flap" motion during Initialization to specify the direction of "down" and orientation of the V2Suit module with respect to that direction. Subsequently, the system transitions to Operations and the user simply lifts their right arm from their side 90-degrees so that it is perpendicular to "down" (note the angular velocity of the module). As a result, the direction of "down" starts off primarily in one of the MCF axes, then is split between two MCF axes, and then returns to being only in one of the MCF axes.

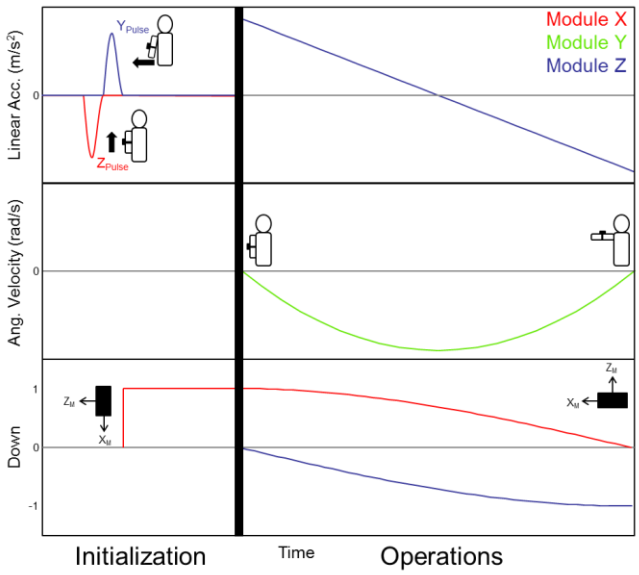

Figure 4-11: Example V2Suit use case. Two acceleration pulses in initialization define down and module orientation, followed by operations with a simple motion and representative notional IMU data. Down tracking is shown in the bottom plot.

4.2.6 Performance Evaluation

Synthetic Data—To test the algorithms two synthetic arm motions were generated in MATLAB. The first motion was an arm lift (1-axis rotation), where the simulated user starts with their arm at their side and lifts it 90 degrees to the side in one second. In this motion there is only rotation about the module Y axis – "Simulated Lift". The second motion also begins with the user's arm at their side, but in this motion the arm is simultaneously raised in the sagittal plane, rotated about its long axis, and rotated in the transverse plane. As a result, the module is rotated around each MCF axis to reach the same final position as the first motion – "Simulated 90-90-90 Rotation". The computer generated IMU data (linear acceleration and angular velocity) from these motions was run through a "down" tracking simulation created in MATLAB/Simulink. Figure 4-12(a) and (b) show the direction of down in the module coordinate frame during the

course of these motions. The illustrations in the boxes depict the module orientation in the inertial frame to give an idea of how the module is moving. The simulated IMU data for the two motions was also run through a module axis tracking simulation. The results of the simulations are shown in Figure 4-13(a) and (b). The figure shows how the module axes move in the inertial coordinate frame over the course of the motion, as well as inertial down for a reference. The trajectory of the module is also indicated.

IMU Data—The same motions were repeated with the selected IMU to capture data from real motions to pass through the algorithm. Unlike the simulated data, these motions were repeated and lasted longer than one second. Due to normal biomechanical movements there is some variability in the start point, trajectory, and module orientation throughout the trajectory. The "down" tracking results from the real arm motions are shown in Figure 4-12(c) and (d). The graphs do not exactly match the simulated data due to differences in the initial starting position and slight differences between the simulated motion and the real motion captured by the IMU. The real IMU data was also passed through the module axes tracking simulation, the results of which are shown in Figure 4-13(c) and (d).

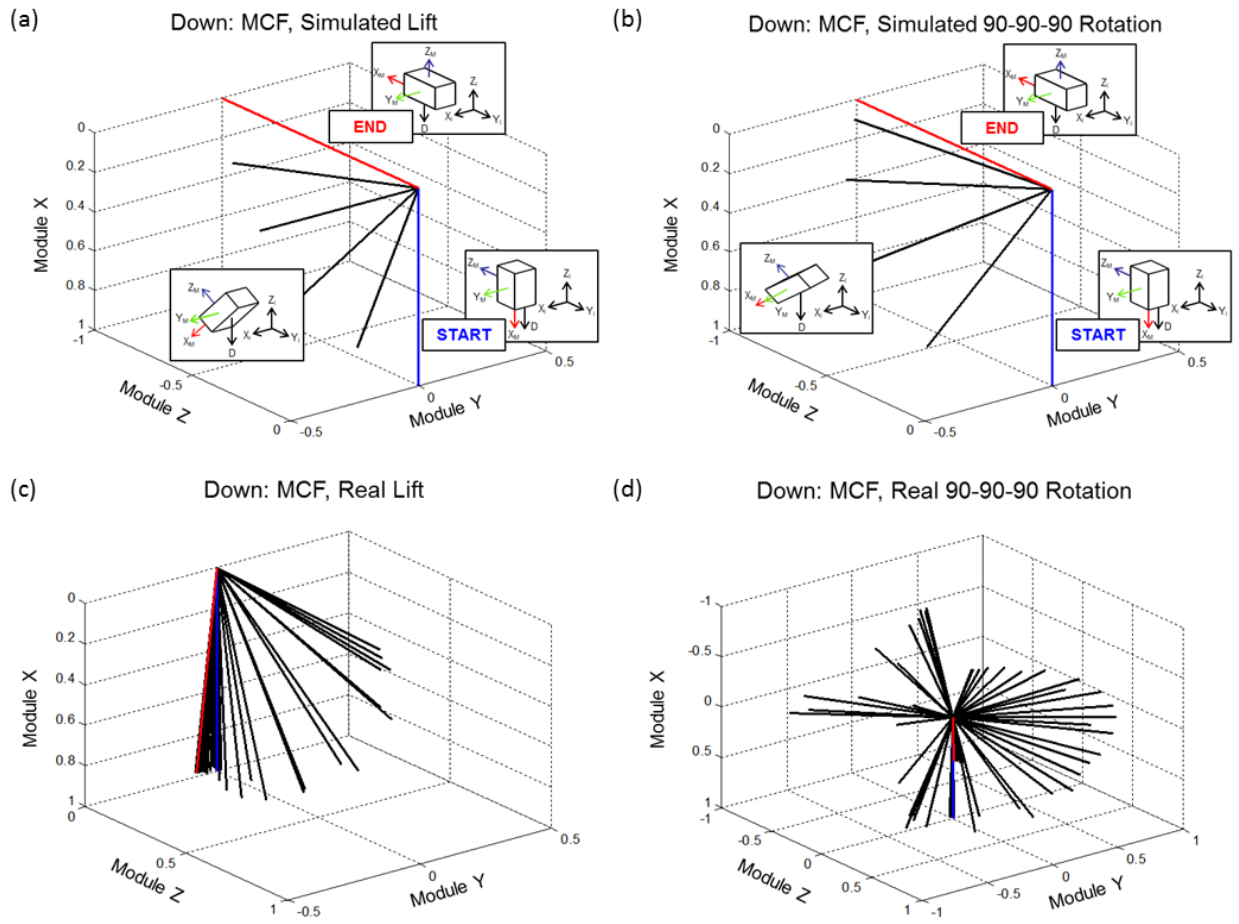

Figure 4-12: Down tracking simulation results: (a) shows the Simulated Lift, (b) shows the Simulated 90-90-90 Rotation, (c) shows the Real Lift, and (d) shows the Real 90-90-90 Rotation. The figures show the direction of "down" in the module coordinate frame over the course of the motion.

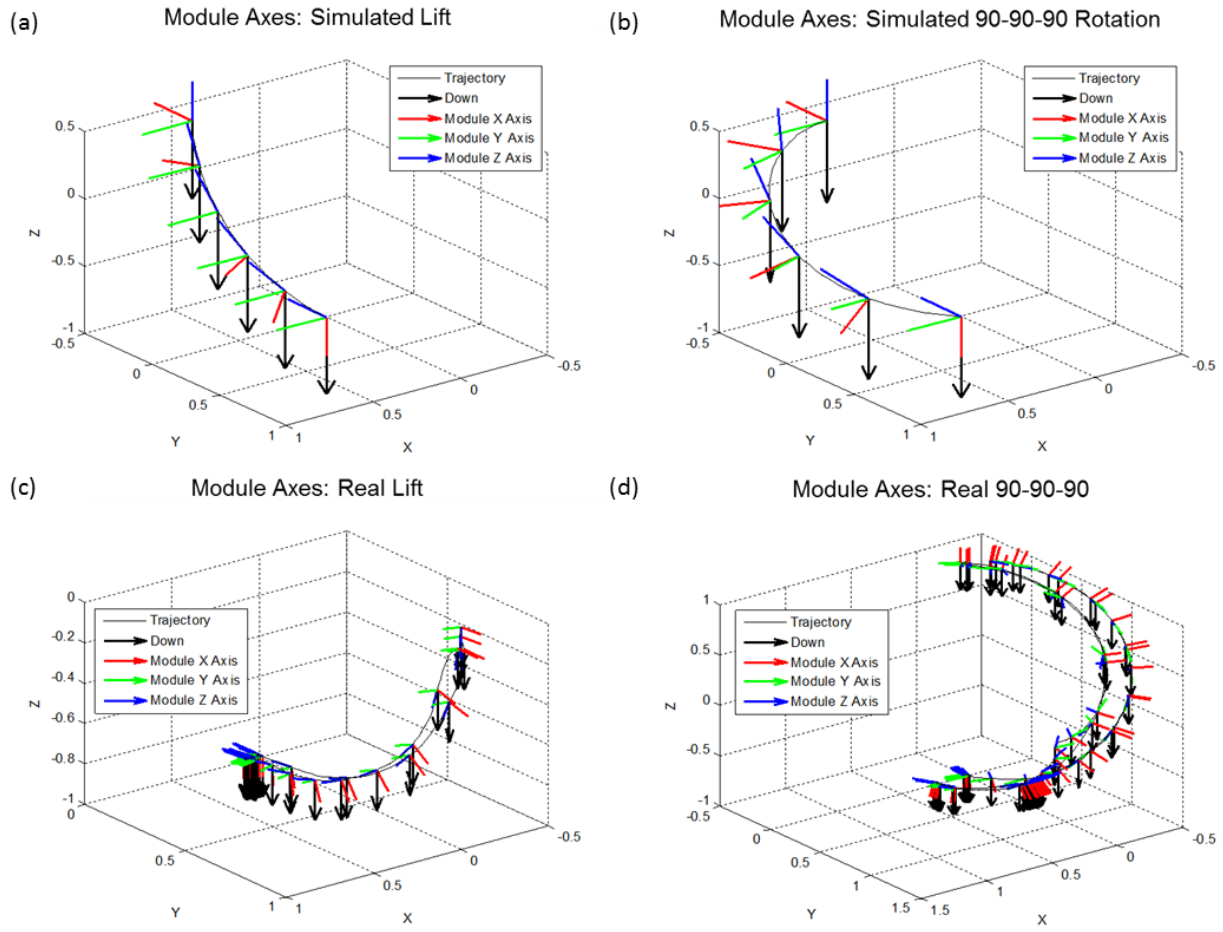

Figure 4-13: Module Axis Tracking simulation results: (a) shows the Simulated Lift, (b) shows the Simulated 90-90-90 Rotation, (c) shows the Real Lift, and (d) shows the Real 90-90-90 Rotation. The figures show the module axes in the inertial coordinate frame over the course of the motion. The trajectory of the module is also shown, and inertial down is given as a reference.

4.3 Wearable CMG Modeling & Simulation

4.3.1 CMG Introduction and Background

Control moment gyroscopes, or CMGs, are momentum actuators that are commonly used on a large scale for spacecraft stabilization and attitude control. CMGs consist of a spinning mass gimbaled about one or more axes to change the direction of the angular momentum vector and thereby generate an internal torque on the system (Figure 4-14). In the majority of CMG designs, the magnitude of the angular momentum vector is constant. However, variable speed CMGs may also be considered for some applications, but they introduce system complexities and inefficiencies. In this thesis, any CMG referred to as a single gimbal CMG (SGCMG) – meaning

that it gimbals only about one axis — has a constant spin rate (constant angular momentum magnitude).

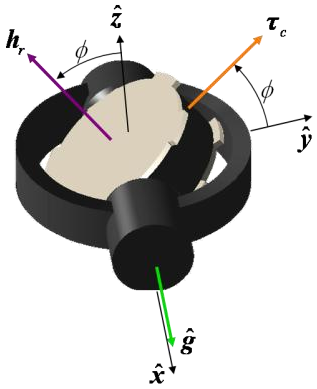

Figure 4-14: Control moment gyroscope diagram [56].

Gimbaling the spinning mass changes the direction of its angular momentum vector, which generates an internal torque on the system. The magnitude of the torque from a SGCMG is dependent on the angular momentum of the spinning mass as well as the gimbal rate. The direction of the torque vector for a SGCMG is dependent on the gimbal angle and is always perpendicular to the gimbal axis. The torque from a SGCMG can be approximated as shown in Equation (4-16) where $\vec{\omega}_g$ is the gimbal rate vector and $\vec{h}_r$ is the angular momentum vector of the spinning mass.

$$\tau = -\vec{\omega}_g \times \vec{h}_r \tag{4-16}$$

This is simplified from taking the time derivative of the SGCMG angular momentum vector and is valid under the assumption that the angular velocity of the body on which the CMG is mounted (typically a spacecraft) is small in comparison to the gimbal rate of the CMG. This is referred to as the base rate. In the case of the V2Suit CMG, the base rate is the angular velocity of the body segment on which the module is located. The effect of the base rate, given in Equation (4-17), might become significant in this case.

$$\tau_B = -\vec{\omega}_B \times \vec{h}_r \tag{4-17}$$

Therefore, the total torque generated by a CMG is $\tau + \tau_B$. In order for the V2Suit to generate the desired torque in the appropriate direction, the base rate effects caused by the motion of the wearer's limbs must be accounted for. In the ideal scenario, the base rate torque is in the desired direction for the specified resistance torque, but this is rarely the case. The base rate torque must be nulled through active gimbaling to prevent undesired perceptions.

A single SGCMG is capable of generating a torque vector that may lie anywhere on a 2 dimensional surface at a given instant. This is one input to an attitude control system- in general, rigid bodies (e.g., spacecraft) have 3 degrees of freedom in attitude. While one CMG may occasionally be able to generate the desired torque for an attitude control system, 3 CMGs are generally necessary and the torque is from a combination of the CMGs. Groups of CMGs controlled together to generate torque are referred to as arrays. Including a 4th CMG in an array allows for redundancy in case of failure and also facilitates singularity avoidance. A singularity is a configuration in which a CMG array cannot generate torque in one or more directions. A CMG array may encounter two types of singularities: external (momentum saturation) and internal (geometric). Figure 4-15 shows a representation of the different types of singularities for an array of 4 planar CMGs. Saturation singularities cannot be avoided without the loss of the effective torque command. Some internal singularities can be avoided by constraining the gimbal motion of the CMGs to prevent them from reaching a singular configuration, but again not without a performance penalty.

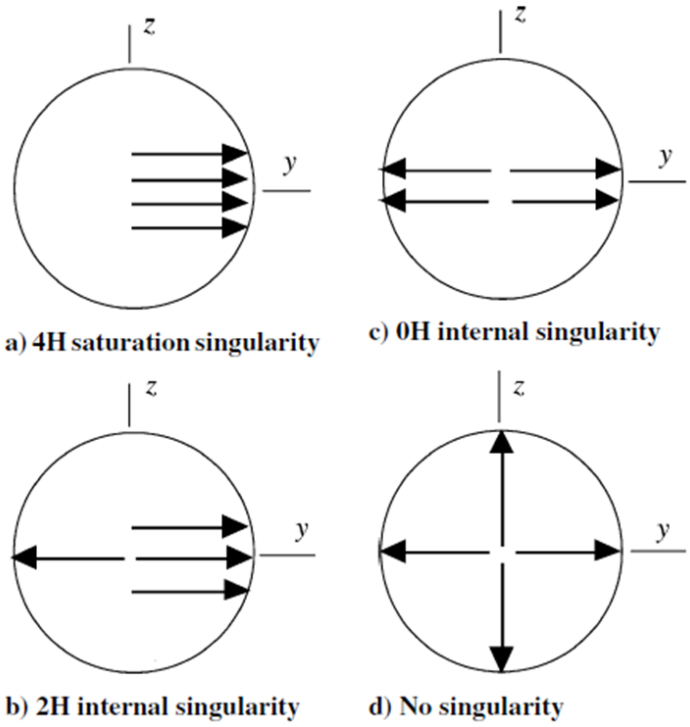

Figure 4-15: Visual explanation of singularities for an array of 4 planar CMGs— (a) shows an external saturation singularity, (b) and (c) show internal singularities, and (d) shows no singularity [58].

The gimbal angles of the CMG are controlled using steering laws that are based on the Jacobian of the array [61]. The Jacobian of a SGCMG array is a matrix of partial derivatives of the angular momentum vector of the array with respect to its gimbal angles. In matrix form, the torque output from a SGCMG is given by Equation (4-18) where *J*, the Jacobian of the array, is a

function of the gimbal angles of the array and ω_g is a vector of the gimbal rates for each CMG in the array.

$$\tau = J\omega_g \tag{4-18}$$

If the desired torque vector is known, it is possible to calculate the required gimbal rates for the CMG array to generate the desired torque. In order to calculate do so, the inverse of the Jacobian must be multiplied by the torque vector (Equation (4-19)).

$$\omega_g = J^{-1}\tau \tag{4-19}$$

The Jacobian for a given array may not be square, so the steering laws often use a pseudoinverse to calculate the gimbal angles as shown in Equation (4-20) which uses the Moore-Penrose pseudoinverse.

$$\omega_g = J^T[J\,J^T]^{-1}\tau \tag{4-20}$$

Other steering laws require adding constraint equations to the Jacobian to make it invertible. This will necessarily limit the motion of the CMG array. If the Jacobian for an array is not invertible at a given operating condition, there is a singularity at that condition. Similarly, if $\det(J\,J^T) = 0$ the pseudoinverse cannot be calculated and there is a singularity. If the Jacobian can be made to be full rank (and therefore invertible) at all times, the array will be singularity free [61, 62].

The V2Suit aims to miniaturize a CMG array for use in a body-worn system to apply torque to the wearer's musculoskeletal joints. The smallest existing CMGs on the market are intended for use on small satellites and are too large for the purposes of the V2Suit. Miniaturizing a CMG array while still generating a large enough gyroscopic torque for suitable resistance is a main challenge in the design of the V2Suit system. Additional challenges include developing steering laws that allow for singularity avoidance and methods of desaturating the CMGs.

4.3.2 Steering Laws

The goal of a steering law for a CMG array is to calculate the gimbal rates that will generate the commanded torque vector taking into account hardware constraints such as gimbal limits and avoiding singularities [62]. For the V2Suit array, there has been a limit imposed on the range of motion for the gimbal of 2 revolutions in either direction. The limit on the gimbal rate for the array is a function of the selected gimbal motor, which has a maximum output speed of 24 RPM. The acceleration capability of the gimbal motor also limits how quickly the array can respond to changes in gimbal rate. Accounting for these factors in the steering logic, as well as incorporating a method of resetting the gimbal angles once the limits have been reached, is important for successful torque generation.

Though the pseudoinverse steering law used in the initial simulations was insufficient in terms of its ability handle singularities, most CMG steering laws use some variation of the pseudoinverse steering logic [62]. There are two types (external and internal) singularities. In an external, or saturation, singularity the total angular momentum of the CMG array has reached the total momentum capability of the array. In other words, all of the angular momentum vectors from the various CMGs in the array point in the same direction. Spacecraft attitude control systems that utilize CMGs must incorporate a method of desaturation for the CMG array to handle external singularities [56, 62].

In an internal singularity, the total angular momentum of the array is within the limit of the momentum capability, but a singularity still exists. There are two types of internal singularities: hyperbolic and elliptic. There is a numerical method for distinguishing between the two types, but generally they differ because hyperbolic singularities can be avoided by incorporating null motion into the steering logic and elliptic singularities cannot [63].

4.3.3 Singularity Avoidance using Null Motion

Null motion is defined as motion of the gimbals that does not produce any net torque. The pseudoinverse steering logic does not naturally incorporate null motion into the gimbal rate commands, and as a result it tends to steer the gimbal angles towards singular states [62]. There are a variety of ways to incorporate null motion into the steering logic for an array, one of which will be discussed here. Bedrossian et al. presented a non-directional method of adding null motion to the pseudoinverse steering logic that adds significant null motion to the array even when it is not near a singularity. Equation (4-17) can be considered to be a particular solution to Equation (4-18); the homogeneous solution is obtained by Equation (4-21) below where n is a vector that spans the null space of the Jacobian [62].

$$Jn = 0 \tag{4-21}$$

The particular solution to Equation (4-21) is then

$$\omega_g = J^T[\,J\,J^T]^{-1}\tau \;+\; \gamma n \tag{4-22}$$

where γ specifies the amount of null motion to be added. The method for calculating n and γ is presented below in Equations (4-23) – (4-27):

$$\gamma = \begin{cases} m^6 & for\ m \geq 1 \\ m^{-6} & for\ m < 1 \end{cases} \tag{4-23}$$

$$m = \sqrt{det\,(JJ^T)} \tag{4-24}$$

$$n = \begin{bmatrix} C_1 \\ C_2 \\ C_3 \\ C_4 \end{bmatrix} \tag{4-25}$$

$$C_i = (-1)^{i+1} M_i \tag{4-26}$$

$$M_i = det(J_i) \tag{4-27}$$

In the above equations, m is a so-called singularity measure for the array. The C_i are the order 3 Jacobian cofactors, and the M_i are the order 3 Jacobian minors for the array. J_i is the Jacobian of the array with the ith column removed. This method of applying null motion does not guarantee singularity avoidance; indeed since it is non-directional the null motion may actually end up steering the array towards a singularity in some instances [64]. While this may help singularity avoidance for the V2Suit system, it may not be the ideal choice of steering logic in this instance.

4.3.4 Singularity Robust Inverse

The reason singularities occur is that the steering logic is attempting to solve Equation (4-18) exactly which is not always possible; allowing for some deviation from the desired torque and using a singularity robust inverse steering logic is a way to get around this [64]. A variety of singularity robust inverses have been developed, one of which, given in Equation (4-28) and referred to as a generalized singularity robust inverse, is capable of passing through and escaping from any internal singularity.

$$J^{\#} = J^T [JJ^T + \lambda E]^{-1} \tag{4-28}$$

In Equation (4-28), $J^{\#}$ is the singularity robust inverse of the Jacobian. The matrix E is given by Equation (4-29).

$$E = \begin{bmatrix} 1 & \varepsilon_1 & \varepsilon_2 \\ \varepsilon_3 & 1 & \varepsilon_1 \\ \varepsilon_2 & \varepsilon_3 & 1 \end{bmatrix} > 0 \tag{4-29}$$

In the above equations, λ and ε_i should be selected so that $J^{\#}u \neq 0$ for any non-zero constant u. If this can be accomplished the array will never encounter a singularity [59].

Using this method for singularity avoidance for the V2Suit could be problematic as high accuracy in torque generation is desirable. However, further study into how much deviation from the desired torque direction and magnitude is acceptable before the countermeasure loses efficacy may make this a possibility moving forward.

4.3.5 Generalized Inverse Steering Law

Asghar et al. presented an exact steering law based on the generalized-inverse for a 4CMG pyramid array. The steering law will restrict the gimbal motion to a hyper-surface that will not encounter any internal elliptic singularities. The steering law is defined in Equations (4-20) and (4-30) below.

$$\omega_g = A^T(JA^T)^{-1}\tau \tag{4-30}$$

$$A = J + J_0 \tag{4-31}$$

In Equation (4-31), J_0 is a 3x4 matrix of column vectors chosen to be perpendicular to the column vectors in the Jacobian, J. For the V2Suit array, a possible choice for the matrix J_0 is given in Equation (4-32).

$$J = h\begin{bmatrix} (sin\,\varphi_1 - cos\,\alpha\,cos\,\varphi_1) & (-sin\,\varphi_2 - cos\,\alpha\,cos\,\varphi_2) & \dots \\ (-sin\,\varphi_1 - cos\,\alpha\,cos\,\varphi_1) & (-sin\,\varphi_2 + cos\,\alpha\,cos\,\varphi_2) & \dots \\ 0 & 0 & \dots \\ \dots & (-sin\,\varphi_3 + cos\,\alpha\,cos\,\varphi_3) & (sin\,\varphi_4 + cos\,\alpha\,cos\,\varphi_4) \\ \dots & (sin\,\varphi_3 + cos\,\alpha\,cos\,\varphi_3) & (sin\,\varphi_4 - cos\,\alpha\,cos\,\varphi_4) \\ \dots & 0 & 0 \end{bmatrix} \tag{4-32}$$

The generalized inverse steering law was tested in simulation and found to give exact torque control while avoiding internal singularities [65]. This makes it a good candidate for use as a potential steering law for the V2Suit.

4.3.6 V2Suit CMG Trade Study

In order to select an appropriate CMG array and design parameters for use in the V2Suit a detailed trade study was conducted including a variety of simulated CMG arrays. Simulations of each of the candidate arrays were created in MATLAB and Simulink. The simulations included scissored pairs SGCMG arrays, pyramid SGCMG arrays, and variable speed CMG arrays. For comparison, a reaction wheel array was also included. The goal of the trade study was to narrow down the candidate arrays so that a more detailed parameterized simulation study could be conducted to determine the appropriate CMG array architecture and specifications for use in the V2Suit. The performance of the arrays in terms of generating the desired torque to apply resistance to movements parallel to "down" was quantified. The purpose of the first round of simulations was to determine whether the arrays could generate the desired torque based on the simple steering laws without exceeding reasonable gimbal and spin limits. Additional criteria used to down-select the array candidates included considerations of the overall size of the array, keeping in mind the system requirement for a wearable array form factor.

Simulation Design

The basic simulation architecture for the SGCMGs is shown in the diagram in Figure 4-16. The simulation is for a single CMG array mounted on the V2Suit user's arm. In the figure, the boxes outlined in red represent aspects of the simulation that are unique to each individual CMG array.

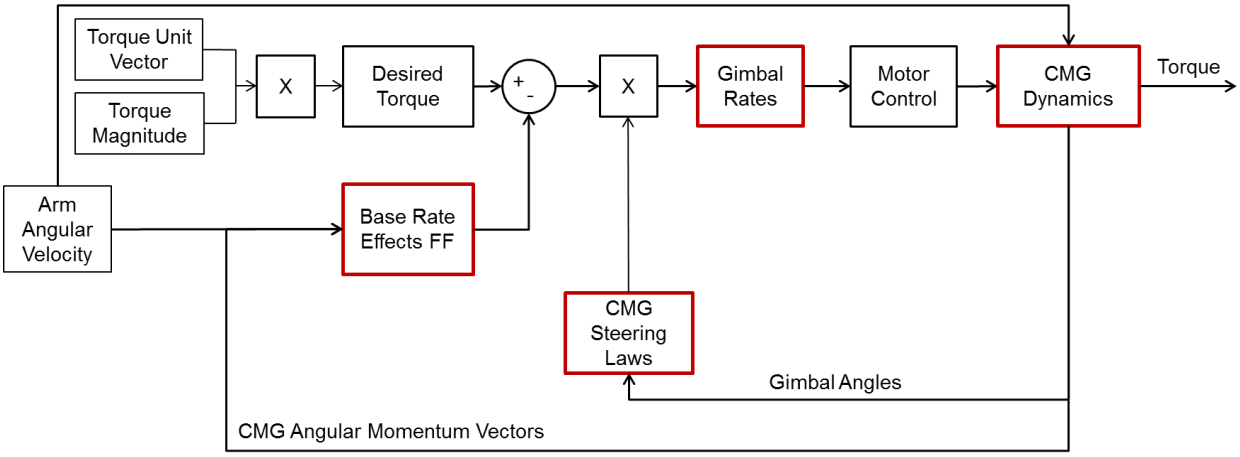

Figure 4-16: SGCMG simulation architecture to select an array for the V2Suit. The CMG simulation begins at the end of the initialization phase. The inputs to the simulation are the direction of the torque vector in the module coordinate frame (determined by "down" tracking), the desired torque magnitude, and the angular velocity of the arm. The red boxes indicate aspects of the simulation that are unique to each array.

The CMG simulation begins at the end of the initialization phase. The inputs to the simulation are the direction of the torque vector in the MCF (determined by "down" tracking), the desired torque magnitude, and the angular velocity of the arm from simulated IMU data. The desired torque magnitude is multiplied by the direction of the torque vector to get the desired perceptible torque for the V2Suit module. This is the magnitude and direction of the torque that the user will feel while wearing the V2Suit. The desired perceptible torque from the V2Suit module is different from the command torque sent to the CMG controller. The command torque will be generated only by the gimbaling of the CMGs in the array and is based on the gimbal rate commands sent to the CMG controller. This torque may differ from the desired perceptible torque due to the need to account for the motion of the module.

Unless the module is stationary, there is a base rate effect torque due to the angular velocity of the arm that must be fed forward into the torque command sent to the CMG controller. In the simulation, computer generated IMU data representing an arm motion is provided to calculate the base rate torque (Equation (4-17)). This torque is subtracted from the desired perceptible torque to determine the command torque to send to the CMG steering laws (Equation (4-33)).

$$\tau_{CMD} = \tau_{perceptible} - \tau_B \tag{4-33}$$

For the SGCMGs the simulation uses very basic steering laws to determine the appropriate gimbal. The Jacobian of the array is calculated at each time step in the simulation using the gimbal angles as inputs. The pseudoinverse of the Jacobian is taken and then multiplied by the command torque vector to generate the gimbal rate commands. These commands are sent to the simulated CMG dynamics, as well as the arm motion to generate the base rate torque. The final output of the simulation is the torque generated by the array based on the gimbal rate commands combined with the base rate torque to give the perceptible torque. The steering laws to command the spin rates for the variable speed arrays and the reaction wheel array are different and will be discussed in more detail in the following sections. The overall architecture of the simulation remains the same, but instead of gimbal rate commands the CMG controller is being sent spin rate commands.

The simulations were initiated using MATLAB scripts that allow for parameterization so that changes in flywheel size and material (flywheels were cylindrical), spin rate (for the constant spin rate CMG's), gimbal rate (for the variable spin rate CMG's), can be incorporated easily at the start of each simulation. These scripts run a one-second long arm motion simulation with the given array parameters and output the perceptible torque and the gimbal rates and gimbal angles at each time step in the simulation. In addition to changing the array parameters, the simulation also allowed for a variety of arm motion conditions to be tested. The motions implemented included a test case where there was no motion (i.e., the module was stationary) and the two simple motions (lift arm and 90-90-90) used previously in the formulation of the down tracking algorithm.

As previously stated, the purpose of the initial simulation was to determine whether it is possible to generate the desired torque magnitude using each CMG array and a very basic steering law. A simulation with a stationary module was conducted, as well as simulations with two simple arm motions. The desired torque magnitude was set to 0.1 Nm (see Section 3.5) [60]. The plots of the commanded torque vector for each motion are shown in Figure 4-17. For a successful simulation, the output torque from the simulated CMG array should closely match this command torque for each motion. Additionally, the gimbal/spin rates that were required to generate the torque were examined to determine whether they exceeded feasible limits.

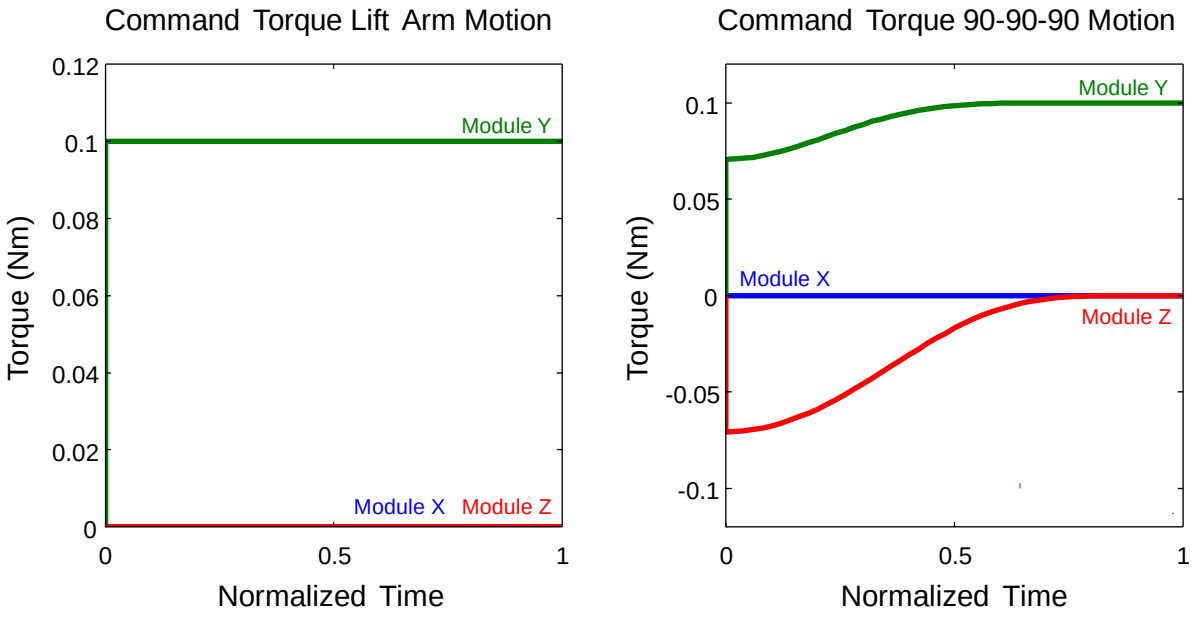

Figure 4-17: Command Torque for the lift arm motion (left) and the 90-90-90 motion (right). For the simple lift arm motion, the desired torque vector always points in the module Y direction. The 90-90-90 motion is more complicated due to the extra rotation that occurs during the motion.

Candidate Arrays and Simulation Results

Scissored Pairs Array— A scissored pair is a grouping of two SGCMGs that act together to generate torque in one direction. They are gimbaled at equal and opposite rates which results in a net torque vector from the pair in a constant direction. Figure 4-18 shows an array of 3 scissored pairs and the directions in which they generate torque. The CMGs in this array are aligned so that each pair generates torque along one of the module's principal axes. Variations of this array could include multiple CMG pairs pointing along the same axis, or a pair oriented in a different direction that might be useful.

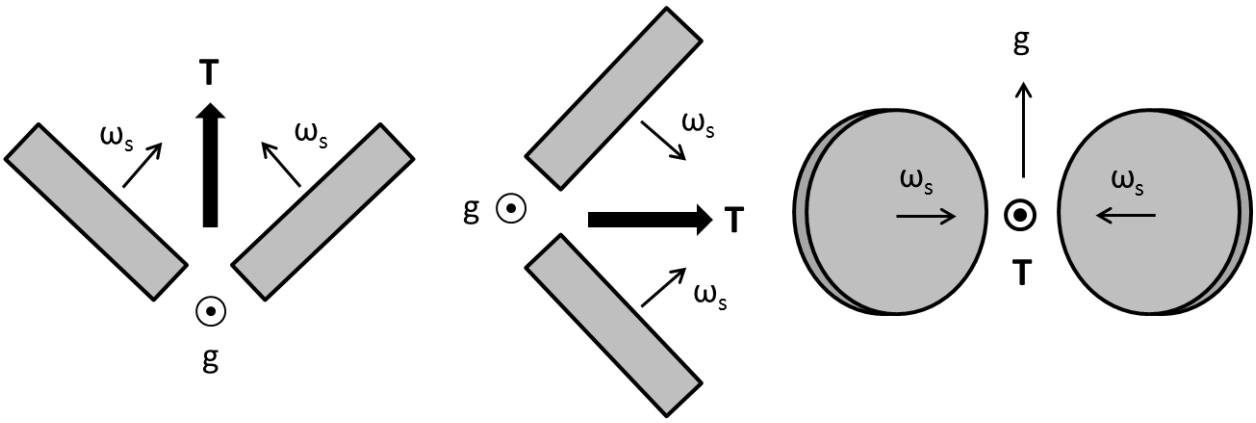

Figure 4-18: 3-Scissored pairs array. Each pair controls torque along one module axis.

The Jacobian for the scissored pair array can be seen in Equation (4-34) where h is the magnitude of the angular momentum of a single CMG spin mass, and φ_i are the gimbal angles of each CMG. The bottom three rows of the Jacobian result from constraint equations imposed on the scissored pairs array (Equations (4-35) through (4-37)). These equations state that within a scissored pair the gimbal rates must be equal and opposite. In the physical system this would be taken care of by a gear mechanism linking the two CMGs of a pair together to the same gimbal motor.

$$J_{3SP} = \begin{bmatrix} h\cos\varphi_1 & h\cos\varphi_2 & h\sin\varphi_3 & h\sin\varphi_4 & 0 & 0 \\ h\sin\varphi_1 & h\sin\varphi_2 & h\cos\varphi_3 & h\cos\varphi_4 & h\sin\varphi_5 & h\sin\varphi_6 \\ 0 & 0 & 0 & 0 & h\cos\varphi_5 & h\cos\varphi_6 \\ 1 & -1 & 0 & 0 & 0 & 0 \\ 0 & 0 & 1 & -1 & 0 & 0 \\ 0 & 0 & 0 & 0 & 1 & -1 \end{bmatrix} \tag{4-34}$$

$$\dot{\omega}_{g1} + \dot{\omega}_{g2} = 0 \tag{4-35}$$

$$\dot{\omega}_{g3} + \dot{\omega}_{g4} = 0 \tag{4-36}$$

$$\dot{\omega}_{g5} + \dot{\omega}_{g6} = 0 \tag{4-37}$$

One main benefit of the scissored pair array is that it is commonly used. It is also singularity robust within its operating capabilities. This means that as long as the gimbal angle does not exceed ± π/2 radians (90-degrees) for any given scissored pair, there will be no internal singularities and the array will be able to generate torque in all 3 principal module axes. Gimbal limits can be imposed on the scissored pairs array can be limited to prevent the gimbal angle from exceeding ± π/2 radians, which would mean array also has the advantage of not requiring slip rings. This would help to keep the overall size of the array at a minimum. However, this also limits the amount of time that torque can be generated in a given direction. If a pair reaches the gimbal angle limit then it must be re-set so that it can resume generating torque again; this means there would be periods of time where torque could not be generated along a certain direction. The process of resetting the gimbal angle for the scissored pair could potentially generate torque in the opposite direction of the desired torque. A spacecraft would need to use fuel and an alternate attitude control mechanism to account for this. In a system like the V2Suit where there is no alternate mechanism for torque generation, there will be a period of time where the torque vector is incorrectly directed as the gimbal angles are re-set. As previously stated, there is potential to include additional scissored pairs in the array. Multiple pairs along the same axis may be coordinated to enable one pair to take over from another when it reaches its gimbal angle limit and needs to be re-set to reduce or eliminate any incorrect torques.

Pyramid Arrays— Pyramid arrays consist of a group of SGCMGs arranged so that their gimbal axes are perpendicular to the faces of a pyramid with a skew angle of α. Two pyramid arrays were examined for potential use in the V2Suit: a 4-CMG pyramid and a 5-CMG pyramid (Figure 4-19). The skew angle was set to 54.73 degrees, which creates a nearly spherical momentum envelope for the 4 CMG pyramid array [57]. The momentum envelope of an array is the surface that defines the maximum angular momentum of the array in any direction in 3-space and determines in which directions torque can be generated by the array [66].

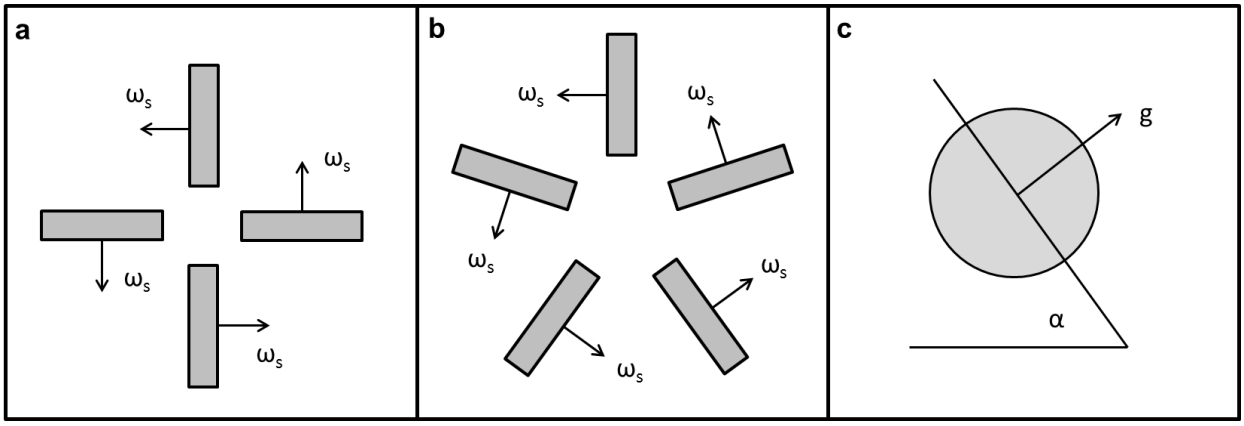

Figure 4-19: 4-CMG Pyramid (a) and 5-CMG Pyramid (b) arrays. The gimbal axes of the CMGs are perpendicular to a pyramid with a skew angle of α=54.73 degrees.

Pyramid arrays are also commonly used. Unlike the scissored pairs array, there is no need to impose gimbal limits on the pyramid array in terms of singularity robustness. A pyramid array would require a slip ring or another mechanism to allow for continuous rotation of each of the CMGs. The Jacobian for the 4 CMG pyramid array is given by Equation (4-38). Again h is the magnitude of the angular momentum of a single CMG spin mass, φ_i are the gimbal angles and α is the skew angle of 54.73 degrees. The array assumes that the base of the pyramid defining the array is a square with edges aligned with the module axes. The Jacobian for the 5 CMG pyramid is given by Equation (4-39), where θ is equal to $^{2\pi}/_{5}$ which defines the base of the pyramid as a regular pentagon. Neither pyramid Jacobian is a square matrix, meaning the arrays will most likely encounter singularities and eventually require either constraint equations added to the Jacobians or more complicated steering laws than those given by Equations (4-19) and (4-20).

$$J_{Pyr4} = \begin{bmatrix} -h\cos\alpha\cos\varphi_1 & h\sin\varphi_2 & h\cos\alpha\cos\varphi_3 & -h\sin\varphi_4 \\ -h\sin\varphi_1 & -h\cos\alpha\cos\varphi_2 & h\sin\varphi_3 & h\cos\alpha\cos\varphi_4 \\ h\sin\alpha\cos\varphi_1 & h\sin\alpha\cos\varphi_2 & h\sin\alpha\cos\varphi_3 & h\sin\alpha\cos\varphi_4 \end{bmatrix} \quad (4\text{-}38)$$

$$J_{Pyr5} = \begin{bmatrix} -h\cos\alpha\cos\varphi_1 & -h\sin\theta\sin\varphi_2 - h\cos\theta\cos\alpha\cos\varphi_2 & -h\sin 2\theta\sin\varphi_3 - h\cos 2\theta\cos\alpha\cos\varphi_3 & \dots \\ -h\sin\varphi_1 & -h\cos\theta\sin\varphi_2 + h\sin\theta\cos\alpha\cos\varphi_2 & -h\cos 2\theta\sin\varphi_3 + h\sin 2\theta\cos\alpha\cos\varphi_3 & \dots \\ h\sin\alpha\cos\varphi_1 & h\sin\alpha\cos\varphi_2 & h\sin\alpha\cos\varphi_3 & \dots \\ \dots & h\sin 2\theta\sin\varphi_4 - h\cos 2\theta\cos\alpha\cos\varphi_4 & h\sin\theta\sin\varphi_5 - h\cos\theta\cos\alpha\cos\varphi_5 & \\ \dots & -h\cos 2\theta\sin\varphi_4 - h\sin 2\theta\cos\alpha\cos\varphi_4 & -h\cos\theta\sin\varphi_5 - h\sin\theta\cos\alpha\cos\varphi_5 & \\ \dots & h\sin\alpha\cos\varphi_4 & h\sin\alpha\cos\varphi_5 & \end{bmatrix} \quad (4\text{-}39)$$

SGCMG Results and Discussion— Sample results from the simulations are shown in Figure 4-20 and Figure 4-21. The results are for simulations with 4CMG pyramid array that has a steel flywheel of radius 2 cm and height 1 cm. Figure 4-20 is the simulation with the lift arm motion and Figure 4-21 is the simulation with the 90-90-90 motion. At a high level, the results show that the 4 CMG pyramid array is successful in generating the desired torque vector in the appropriate direction for the two simulated arm motions. For the lift arm motion, the average deviations of the torque in magnitude and direction were $1.0\text{x}10^{-17}$ Nm and 0 degrees. For the 90-90-90 motion, the average deviations were $2.3\text{x}10^{-17}$ Nm and $3.4\text{x}10^{-7}$ degrees. These deviations are likely to increase when motor dynamics are added to the simulation. Both the 3 scissored pairs array and the 5 CMG pyramid array were also capable of generating the desired torque vector in the appropriate direction (data not shown). For the lift arm motion, the average deviations of the torque in magnitude and direction were $3.1\text{x}10^{-17}$ Nm and 0 degrees for the 3 scissored pairs array and $7.6\text{x}10^{-16}$ Nm and 0 degrees for the 5 CMG pyramid array. For the 90-90-90 motion, the average deviations were $4.1\text{x}10^{-17}$ Nm and $3.9\text{x}10^{-7}$ degrees for the 3 scissored pairs array and $1.3\text{x}10^{-17}$ Nm and $3.4\text{x}10^{-7}$ degrees for the 5 CMG pyramid array.

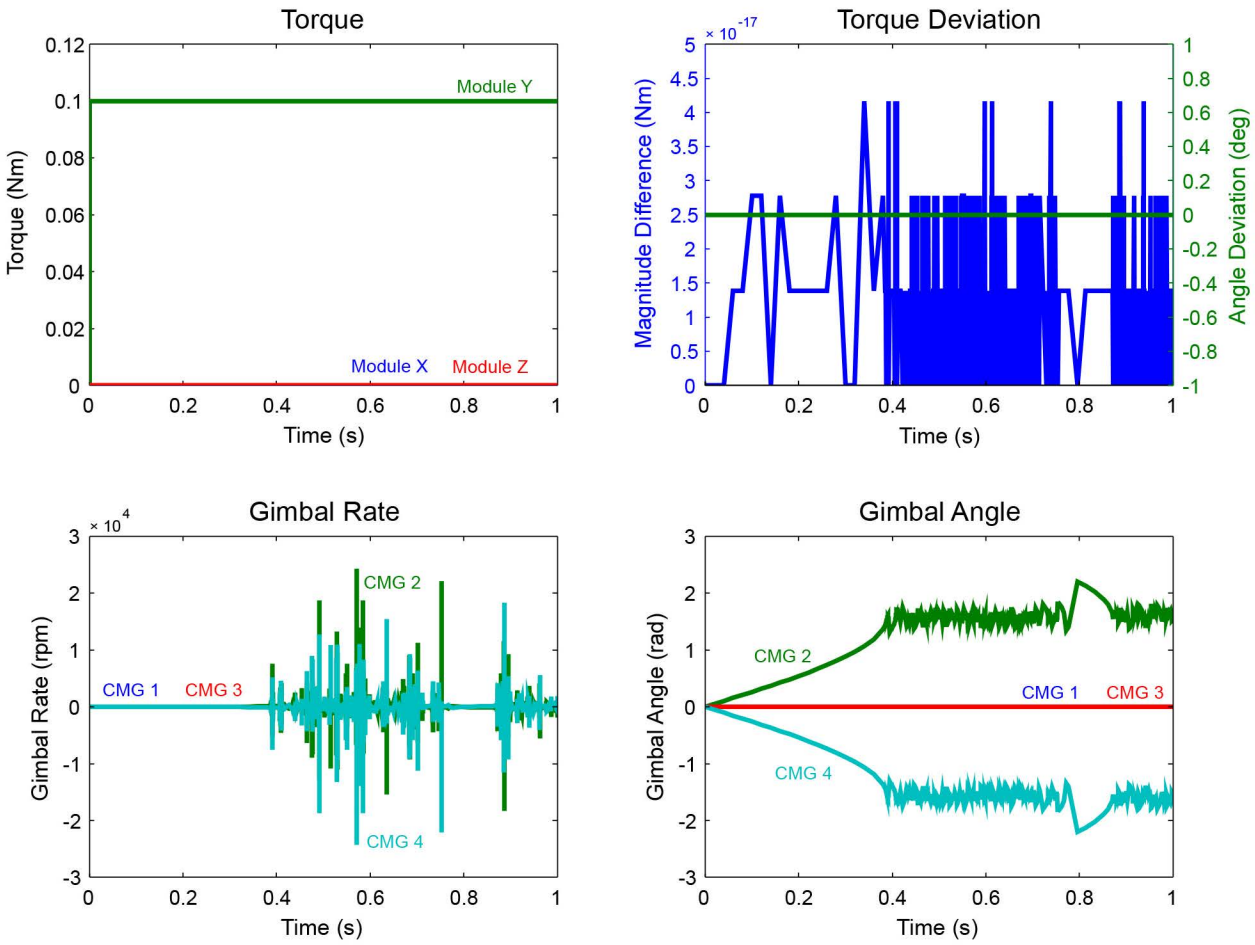

Figure 4-20: Results from the initial 4 CMG pyramid simulation with the lift arm motion for an array with steel flywheels of radius 2 cm and height 1 cm. The torque output (upper left) does not deviate significantly from the command torque, as seen in the figure in the upper right corner (mean deviations of 1.0×10^{-17} Nm and 0 degrees). The gimbal rate (lower left) and gimbal angles (lower right) are also given.

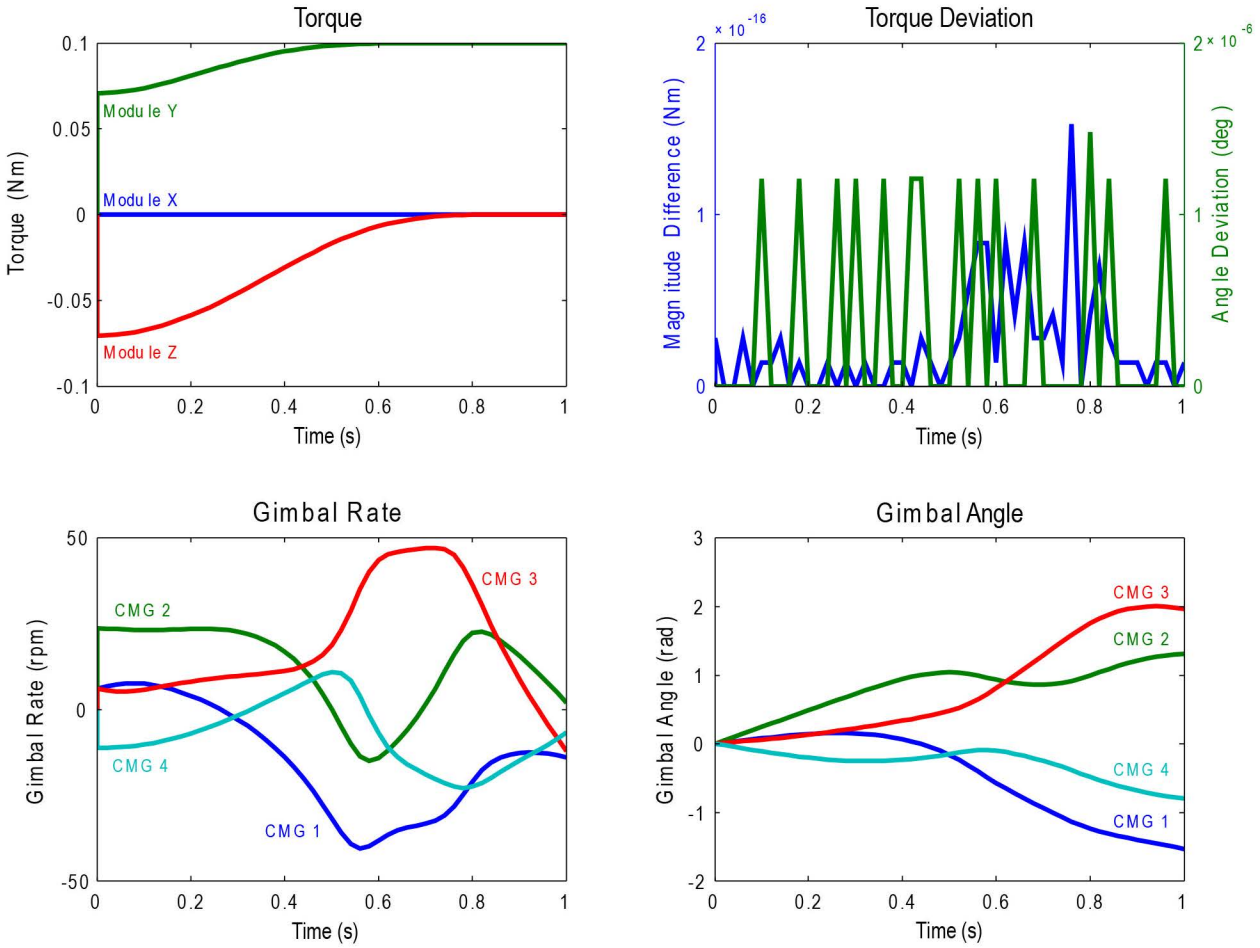

Figure 4-21: Results from the initial 4 CMG pyramid simulation with the 90-90-90 motion for an array with steel flywheels of radius 2 cm and height 1 cm. The torque output (upper left) does not deviate significantly from the command torque, as seen in the figure in the upper right corner (mean deviations of 2.3×10^{-17} Nm and 3.4×10^{-7} degrees). The gimbal rate (lower left) and gimbal angles (lower right) are also given.

The results for the SGCMG array simulations show that, without considering the physical limitations of motors or gimbal restrictions on the arrays, it is possible to command almost exactly the desired torque over the course of the two simple arm motions with these three arrays. However, the results do not indicate complete success. There were various cases in which the commanded gimbal rate (not limited in the simulation) far exceeded a reasonable value in order to generate the desired torque. For example, in the 4 CMG pyramid array results in Figure 4-20 the gimbal rate command quickly reaches a value of roughly $2x10^4$ RPM, orders of magnitude larger than would be reasonable to expect from the gimbal motor. Ideally the gimbal rate command would be a smooth curve over the course of the motion without exceeding roughly 60 RPM (as seen in Figure 4-21). The spikes seen in the commanded gimbal rates in Figure 4-20 exist because the arrays are approaching singular states, and in order to generate torque near a singularity the gimbal rate must be large. The gimbal angle plot in this figure shows a case where the array oscillated around the singularity. The gimbal rate command never allowed the array's gimbal angles to get far enough from the singularity to not be affected by it, and so the array could not escape from the singularity. More complex steering laws will be required moving forward for singularity avoidance and escape. These results show that there may be situations where the V2Suit system is unable to provide the exact desired torque based on limitations in gimbal motor speed acceleration. It is worth noting that the simulations with the better results (those that did not exceed reasonable gimbal rate commands) were those where the 90-90-90 motion was being tested. Intuitively, since the lift arm motion only requires a commanded torque in the Y direction, it puts a great strain on the CMGs responsible for controlling torque in that direction, and so they are more likely to quickly approach a singular state. It is unlikely that a real arm motion would exclusively require torque generation along one axis for an extended period of time, which is promising with respect to the potential for improvement in performance with real arm motions.

Variable Speed CMGs— The initial concept for the V2Suit CMG array was a variable speed array consisting of 16 total small CMGs arranged into groups of 4 (Figure 4-22). Each grouping of 4 is arranged around a central gimbal axis and canted at an angle α. The CMGs are gimbaled at a constant rate around the central axis, and the speed of each flywheel is varied. The combination of gimballing and speed control is what generates the output torque from the variable speed CMG array.

A second variable speed array was proposed, with only minor changes from the first array (Figure 4-23). Again the array consists of 16 total small CMGs arranged into groups of 4. Within the groups of 4, the CMGs are gimbaled about a central axis and the individual spin rates of the flywheels are controlled as before. However, in this case rather than canting each group of 4, each individual CMG has an elevation angle of α.

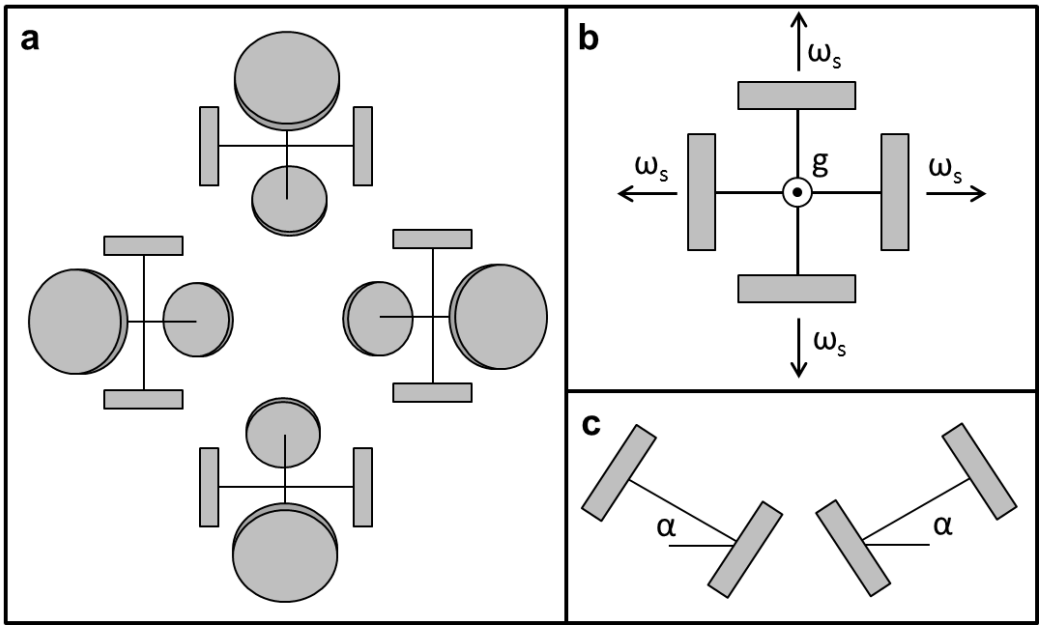

Figure 4-22: Variable speed CMG array 1 with 16 CMGs arranged into groups of 4 (a). Within each group of 4, the CMGs are gimbaled at a constant rate around the central axis (b). Each grouping is canted at an angle α (c).

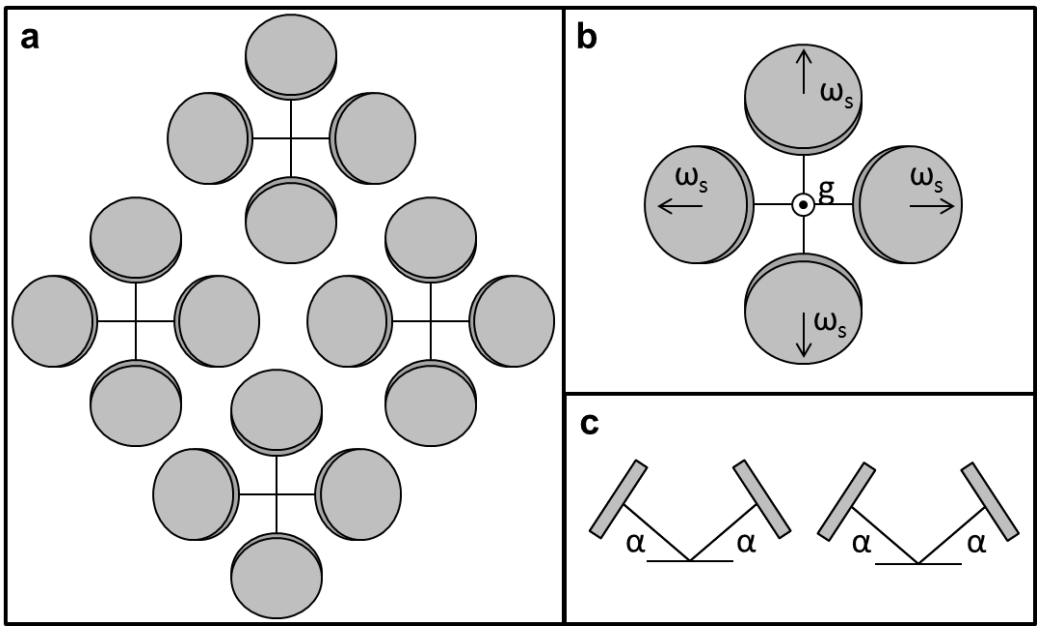

Figure 4-23: Variable speed CMG array 2 with 16 CMGs arranged into groups of 4 (a). Within each group of 4, the CMGs are gimbaled at a constant rate around the central axis (b). Each CMG has an elevation angle of α (c).

The dynamics of variable speed CMGs differs from those of constant speed CMGs because both the changing of both the gimbal angle and the spin rate of the CMG contribute to torque generation. Equation (4-18) above does not apply to the torque output from variable speed CMGs because it does not take into account the changing spin rate. For a variable speed array the torque is given by Equation (4-40) which was derived from the fact that torque is equal to the time derivative of the angular momentum of a system. In Equation (4-40), J_{ω_g} is the gimbal Jacobian, J_{ω_s} is the spin Jacobian, and $\dot{\omega}_s$ is a matrix containing spin acceleration values for each CMG in the array.

$$\tau = J_{\omega_g}\omega_g + J_{\omega_s}\dot{\omega}_s \tag{4-40}$$

The spin Jacobian is a matrix of partial derivatives of the angular momentum vector of the array with respect to the spin vector, and the gimbal Jacobian is a matrix of partial derivatives of the angular momentum vector of the array with respect to the gimbal angles. The Jacobians for the first variable speed array considered in this trade study are given in Equations (4-41) and (4-42). The matrices shown below are 3x16 — in actuality they are 11x16. The bottom 8 rows of the gimbal Jacobian are all zeroes, but the bottom 8 rows of the spin Jacobian are filled by constraint equations given in Equations (4-43) and (4-44).

$$J_{\omega_g} = I\begin{bmatrix} -\omega_{s11}\cos\alpha\sin\varphi_1 & -\omega_{s12}\cos\alpha\cos\varphi_1 & \omega_{s13}\cos\alpha\sin\varphi_1 & \omega_{s14}\cos\alpha\cos\varphi_1 & -\omega_{s21}\cos\varphi_2 & \dots \\ \omega_{s11}\cos\varphi_1 & -\omega_{s12}\sin\varphi_1 & -\omega_{s13}\cos\varphi_1 & \omega_{s14}\sin\varphi_1 & -\omega_{s21}\cos\alpha\sin\varphi_2 & \dots \\ -\omega_{s11}\sin\alpha\sin\varphi_1 & -\omega_{s12}\sin\alpha\cos\varphi_1 & \omega_{s13}\sin\alpha\sin\varphi_1 & \omega_{s14}\sin\alpha\cos\varphi_1 & -\omega_{s21}\sin\alpha\sin\varphi_2 & \dots \end{bmatrix}$$

$$\begin{matrix} \dots & \omega_{s22}sin\varphi_2 & \omega_{s23}cos\varphi_2 & -\omega_{s24}sin\varphi_2 & \omega_{s31}cos\alpha\,sin\varphi_3 & \omega_{s32}cos\alpha\,cos\varphi_3 & -\omega_{s33}cos\alpha\,sin\varphi_3 & \dots \\ \dots & -\omega_{s22}cos\alpha\,cos\varphi_2 & \omega_{s23}cos\alpha\,sin\varphi_2 & \omega_{s24}cos\alpha\,cos\varphi_2 & -\omega_{s31}cos\varphi_3 & \omega_{s32}sin\varphi_3 & \omega_{s33}cos\varphi_3 & \dots \\ \dots & -\omega_{s22}sin\alpha\,cos\varphi_2 & \omega_{s23}sin\alpha\,sin\varphi_2 & \omega_{s24}sin\alpha\,cos\varphi_2 & -\omega_{s31}sin\alpha\,sin\varphi_3 & -\omega_{s32}sin\alpha\,cos\varphi_3 & \omega_{s33}sin\alpha\,sin\varphi_3 & \dots \end{matrix}$$

$$\begin{bmatrix} \dots & -\omega_{s34}cos\alpha\,cos\varphi_3 & \omega_{s41}cos\varphi_4 & -\omega_{s42}sin\varphi_4 & -\omega_{s43}cos\varphi_4 & \omega_{s44}sin\varphi_4 \\ \dots & -\omega_{s34}sin\varphi_3 & \omega_{s41}cos\alpha\,sin\varphi_4 & \omega_{s42}cos\alpha\,cos\varphi_4 & -\omega_{s43}cos\alpha\,sin\varphi_4 & -\omega_{s44}cos\alpha\,cos\varphi_4 \\ \dots & \omega_{s34}sin\alpha\,cos\varphi_3 & -\omega_{s41}sin\alpha\,sin\varphi_4 & -\omega_{s42}sin\alpha\,cos\varphi_4 & \omega_{s43}sin\alpha\,sin\varphi_4 & \omega_{s44}sin\alpha\,cos\varphi_4 \end{bmatrix} \tag{4-41}$$

$$J_{\omega_s} = I\begin{bmatrix} cos\alpha\,cos\varphi_1 & -cos\alpha\,sin\varphi_1 & -cos\alpha\,cos\varphi_1 & cos\alpha\,sin\varphi_1 & -sin\varphi_2 & \dots \\ sin\varphi_1 & cos\varphi_1 & -sin\varphi_1 & -cos\varphi_1 & cos\alpha\,cos\varphi_2 & \dots \\ sin\alpha\,cos\varphi_1 & -sin\alpha\,sin\varphi_1 & -sin\alpha\,cos\varphi_1 & sin\alpha\,sin\varphi_1 & sin\alpha\,cos\varphi_2 & \dots \end{bmatrix}$$

$$\begin{matrix} \dots & -cos\varphi_2 & sin\varphi_2 & cos\varphi_2 & -cos\alpha\,cos\varphi_3 & cos\alpha\,sin\varphi_3 & cos\alpha\,cos\varphi_3 & \dots \\ \dots & -cos\alpha\,sin\varphi_2 & -cos\alpha\,cos\varphi_2 & cos\alpha\,sin\varphi_2 & -sin\varphi_3 & -cos\varphi_3 & sin\varphi_3 & \dots \\ \dots & -sin\alpha\,sin\varphi_2 & -sin\alpha\,cos\varphi_2 & sin\alpha\,sin\varphi_2 & sin\alpha\,cos\varphi_3 & -sin\alpha\,sin\varphi_3 & -sin\alpha\,cos\varphi_3 & \dots \end{matrix}$$

$$\begin{bmatrix} \dots & -cos\alpha\,sin\varphi_3 & sin\varphi_4 & cos\varphi_4 & -sin\varphi_4 & -cos\varphi_4 \\ \dots & cos\varphi_3 & -cos\alpha\,cos\varphi_4 & cos\alpha\,sin\varphi_4 & cos\alpha\,cos\varphi_4 & -cos\alpha\,sin\varphi_4 \\ \dots & sin\alpha\,sin\varphi_3 & sin\alpha\,cos\varphi_4 & -sin\alpha\,sin\varphi_4 & -sin\alpha\,cos\varphi_4 & sin\alpha\,sin\varphi_4 \end{bmatrix} \tag{4-42}$$

$$\omega_{si1} + \omega_{si3} = 0 \tag{4-43}$$

$$\omega_{si2} + \omega_{si4} = 0 \tag{4-44}$$

To generate the desired torque with a given gimbal rate for a variable speed CMG array, Equation (4-45) is used to determine the appropriate spin acceleration commands to send to the array controller. To reiterate, the gimbal rate in these variable speed arrays is constant.

$$\dot{\omega}_s = (J_{\omega_s})^{-1}[\tau - J_{\omega_g}\omega_g] \tag{4-45}$$

A down side to variable speed CMGs is that they are not commonly used. They are less efficient in terms of power than constant speed CMGs and changing the momentum of the flywheel causes different types of singularities [56]. However, some research suggests that the ability to change the speed of a CMG might be beneficial for avoiding traditional CMG singularities [67].

The variable speed arrays were found to be unsuccessful with the basic steering law presented in Equation (4-45). The goal of that steering law was to command spin accelerations that would generate the desired torque as each group of 4 VSCMGs was gimbaled around the group's central axis (ref. Figure 4-22, Figure 4-23). Rather, it appeared that gimballing the groups of 4 interfered with the torque output and the variable speed arrays were being controlled as reaction wheels. In other words, when the gimbal rate was set to 0 RPM the array could generate the desired torque, but when the gimbal rate was increased the torque output deviated from the command (Figure 4-24).

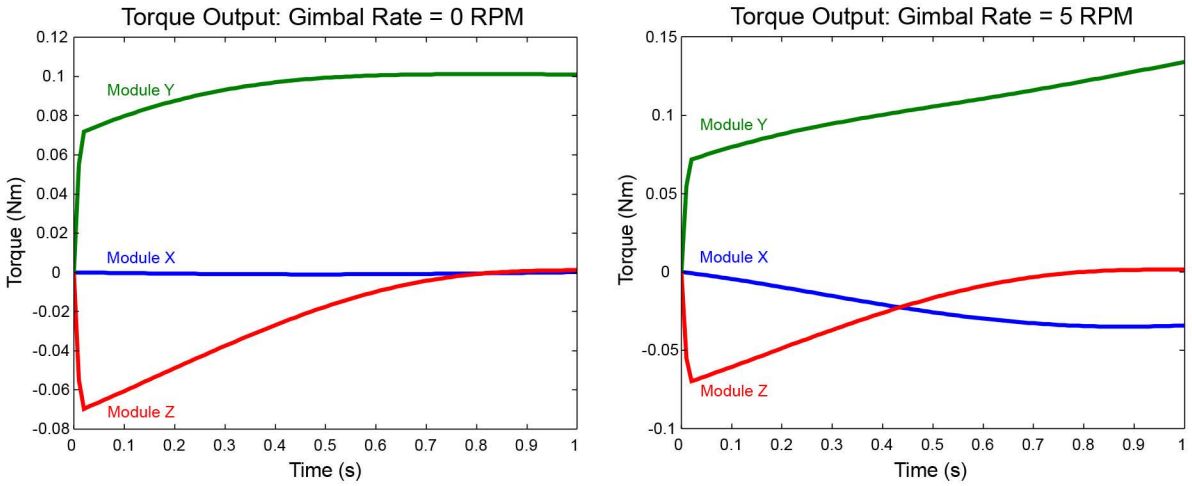

Figure 4-24: Results from a variable speed simulation with the 90-90-90 motion. The left graph shows the torque output of the array with a gimbal rate of 0 RPM. The right graph shows the torque output of the array with a gimbal rate of 5 RPM. This result deviates from the commanded torque.

Reaction Wheel Array— In order to compare the performance of reaction wheels against a CMG array, an array of three reaction wheels was included in the trade study. The array is shown in Figure 4-25. The array consists of three flywheels with their spin axes aligned along one of the principle module axes. Changing the spin rate of the flywheel generates a torque aligned with the spin vector (there is no gimballing of the spin mass). This means that each reaction wheel controls the torque along one axis. The reaction wheel array will need to account for base rate effects in the same manner as the CMG arrays.

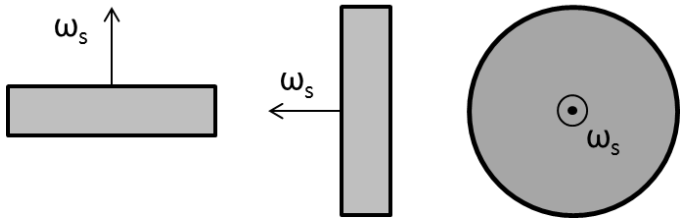

Figure 4-25: Reaction wheel array. Each wheel controls torque along one module axis.

The Jacobian for the reaction wheel array is given in Equation (4-46) and is simply a diagonal matrix with entries equivalent to the moments of inertia of the flywheels about their spin axes.

$$J_{RW} = \begin{bmatrix} I_{x,s} & 0 & 0 \\ 0 & I_{y,s} & 0 \\ 0 & 0 & I_{z,s} \end{bmatrix} \tag{4-46}$$

The simulated reaction wheel array was tested with the same 90-90-90 motion seen above to determine its feasibility. This array used cylindrical flywheels with radius 1.25 cm and height 1 cm. The torque output results are shown in Figure 4-26, which indicates a successful simulation as the output torque from the array matches the commanded torque.

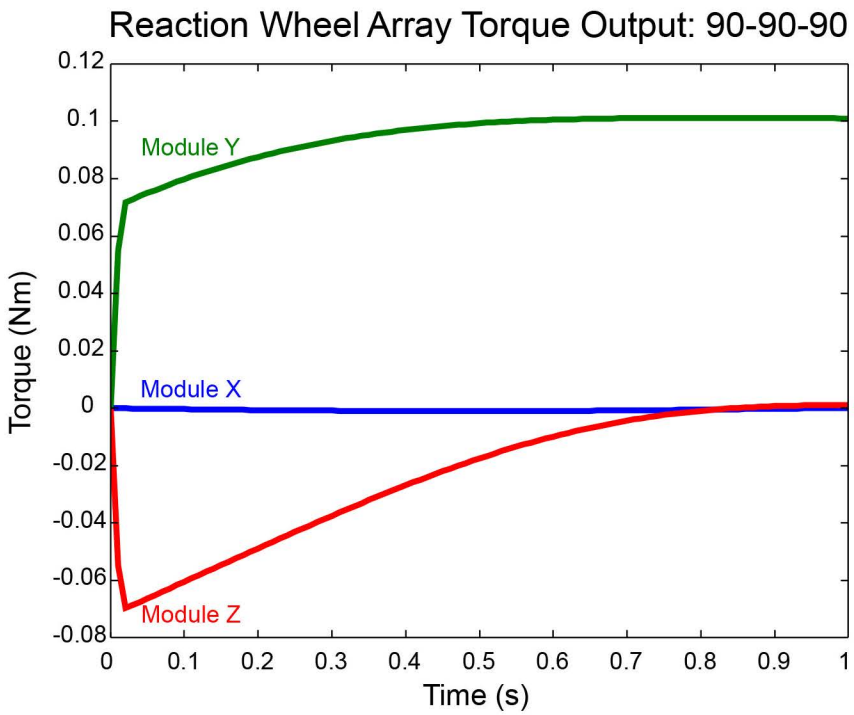

Figure 4-26: Torque output from a simulated reaction wheel array with 3 flywheels of radius 1.25 cm and height 1 cm tested with the 90-90-90 motion.

However, further examination of the simulation results were less promising in terms of the feasibility of a reaction wheel array. The spin rates required by the flywheels in this array over the course of the motion to generate the desired torque are plotted in Figure 4-27. The spin rate very quickly exceeds a reasonable value meaning the reaction wheels would be rapidly maxed out in terms of their torque generating ability.

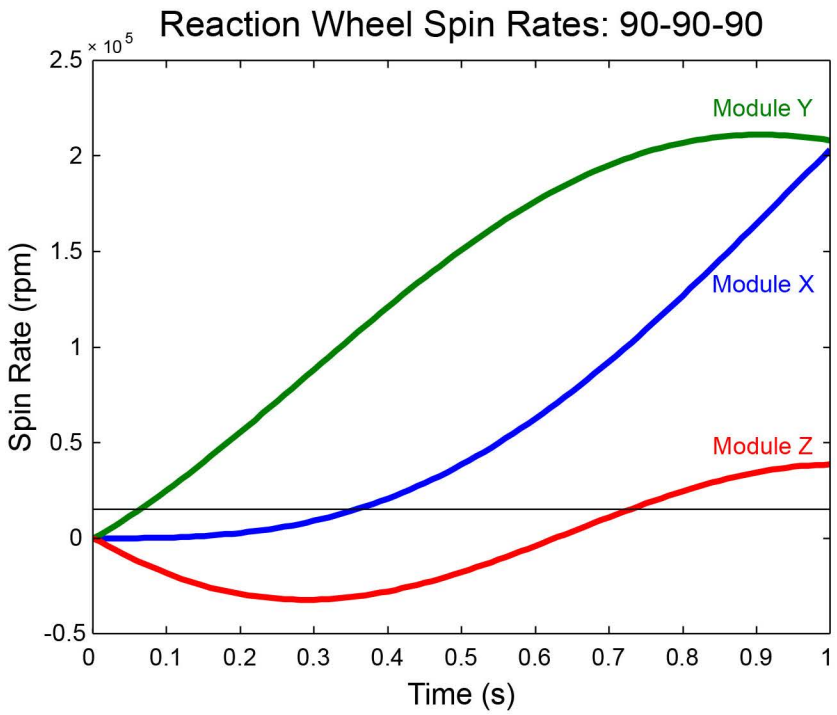

Figure 4-27: Commanded spin rates to generate the desired torque from the reaction wheel array in the 90-90-90 simulation.

Discussion

All of the arrays considered in the trade study have benefits and drawbacks, some of which were mentioned above. The most important consideration in the selection of a CMG array for use in the V2Suit is whether or not the array can generate the desired magnitude of torque in the desired direction over the course of motions. While this criterion is heavily dependent on the mechanical array design, it also depends on the steering laws used to control the CMG array that will need to be developed in detail once an array has been chosen. Another main concern for the design of a CMG array for the V2Suit is minimizing the overall size of each wearable module. The number of flywheels and actuators has a large impact on the final module size, and the number and size of the flywheels limits the potential torque output from the array. A larger number of smaller CMGs may be a better solution than a smaller number of larger CMGs (or vice versa) if one allows for enough torque generation and has a smaller form factor than the other. A comparison of the CMG arrays, the hardware that they require, and the high level simulation results is summarized in Table 4-1.

Table 4-1: Comparison of candidate V2Suit CMG Arrays

Array	Number of Spin Masses	Number of Spin Motors	Number of Gimbal Motors	Generates Desired Torque?	Notes
3 Scissored Pairs	6	6	3	Y	Gearing to connect pairs
4 CMG Pyramid	4	4	4	Y	Slip ring or cable management
5 CMG Pyramid	5	5	5	Y	Slip ring or cable management
Variable Speed 1	16	16	4	N	Slip ring(s)
Variable Speed 2	16	16	4	N	Slip ring(s)
Reaction Wheels	3	3	0	Y	Unreasonable spin rates required

The results of the initial round of simulations allowed the candidate arrays to be narrowed down to the scissored pairs array and the two pyramid arrays. Following the down-selection of the initial array candidates, a more detailed simulation needs to be created in order to determine the specific parameters for the V2Suit array. Aside from the actual array architecture, the inertial properties of the flywheel need to be selected, as well as the operating spin rate for the array, to generate the desired torque magnitude within reasonable gimbal limits.

4.3.7 Parameterized CMG Simulation

The results of the initial round of simulations allowed the candidate arrays to be narrowed down to the scissored pairs array and the two pyramid arrays. Following the down-selection of the initial array candidates, a more detailed simulation needs to be created in order to determine the specific parameters for the V2Suit array. Aside from the actual array architecture, the inertial properties of the flywheel need to be selected, as well as the operating spin rate for the array, to generate the desired torque magnitude within reasonable gimbal limits.

Simulation Design

In the second round of simulation some changes were made to all of the remaining arrays, including adding the dynamics from candidate spin and gimbal motors to the Simulink model for each array. This was done to give a better idea of how quickly the array will be able to respond to the commanded gimbal rates and how much the output torque will deviate from the command as a result of this delay. Additionally, the simulations were changed to vary flywheel inertia rather than varying height, radius, and material as this would allow for various flywheel shapes to be tested. A script was written to determine the other parameters (radius, height, inertia tensor, etc.) for a variety of possible spin mass shapes based on a given inertia and material.

The pyramid array models were not changed in any other way during this round of simulation. However, the scissored pairs array was altered to add an additional pair in each of the module Y and Z directions. This resulted in an array with 5 scissored pairs total, one in the module X direction and 2 in the module Y and Z directions. This decision stems from the fact that there will never be a commanded perceptible torque in the module X direction. The direction of the V2Suit torque was defined to be the direction given by the cross product of the arm axis (module X axis in this case) and the direction of "down" in the MCF, meaning that the torque vector always lies in a plane perpendicular to the module X axis. The scissored pair that controls torque in the module X direction will only ever be activated to balance out base rate effect torques and there would likely be less need for a large amount of torque to be produced in that direction. The Y and Z directions, in comparison, would be responsible for generating the desired perceptible torque as well as accounting for base rate effects, so the extra pair would be more useful here.

In summation, the second round of simulations included 3 candidate arrays: a 5 scissored pairs array, a 4 CMG pyramid array, and a 5 CMG pyramid array. New Matlab scripts were written to allow for the simulations to be run multiple times at once with all possible combinations of the two important parameters: spin rate from 1000 to 15000 RPM, spin mass inertia from 10^{-8} to 10^{-4} kgm^2. The goal of these simulations was to determine the best combination of these parameters for each candidate CMG array to generate the desired amount of torque (0.1 Nm) in the appropriate direction without exceeding a gimbal rate of 60 RPM over the course of the arm motion. The results of the simulation informed the selection of the CMG array architecture for the V2Suit module, as well as the required momentum properties for the CMG flywheel.

Simulation Results

The simulations were run with the lift arm motion so the commanded perceptible torque is the same as shown in Figure 4-17. The output of the simulation was a 3 dimensional bar chart like that seen in Figure 4-28 below, which is for the 4CMG pyramid array simulation. Each bar represents a different set of parameters for the simulation, identified by the spin rates and flywheel inertias on the two lower axes. The vertical axis is the maximum gimbal rate reached by the motor during the course of the simulated arm motion. If the gimbal rate exceeded 60 RPM, the bar was cut off at 60 RPM. The best combination of parameters in this case has been defined by the smallest flywheel inertia possible spinning at the slowest rate possible such that the gimbal rate does not exceed 60 RPM during the motion. These simulations were run with a command torque magnitude of 0.1 Nm and assumed cylindrical tungsten flywheels with density 18269 kg/m^3.

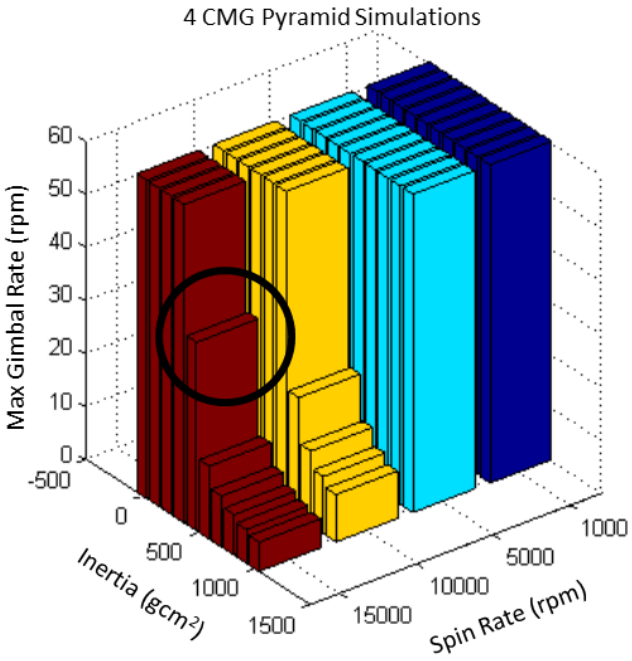

Figure 4-28: Results from the 4 CMG pyramid simulations with motor dynamics. The best set of parameters is a spin rate of 15,000 RPM and flywheel inertia of roughly 450 gcm^2. This is the smallest flywheel possible spinning at the slowest rate possible to generate 0.1 Nm of torque without exceeding a gimbal rate of 60 RPM.

In the bar chart, the circled bar represents the ideal set of parameters for the array. For the 4 CMG Pyramid array the ideal configuration was a flywheel of inertia roughly 450 gcm^2 spinning at 15,000 RPM. For the 5 scissored pairs array the ideal configuration was a flywheel of inertia roughly 200 gcm^2 spinning at 10,000 RPM. Finally for the 5 CMG pyramid the ideal configuration was a flywheel of inertia 300 gcm^2 spinning at 15,000 RPM. While this is a useful starting point for further testing, there is no indication in this data of the performance of the simulated array in terms of accuracy of torque generation. Each simulation was run again with its ideal set of parameters for both the lift arm and 90-90-90 motions. The plots in Figure 4-29 show the results of each of the 4 CMG pyramid array simulation for the lift arm motion including the perceptible torque from the array, the deviation from the commanded torque, and gimbal rates, and the gimbal angles for each CMG in the array.

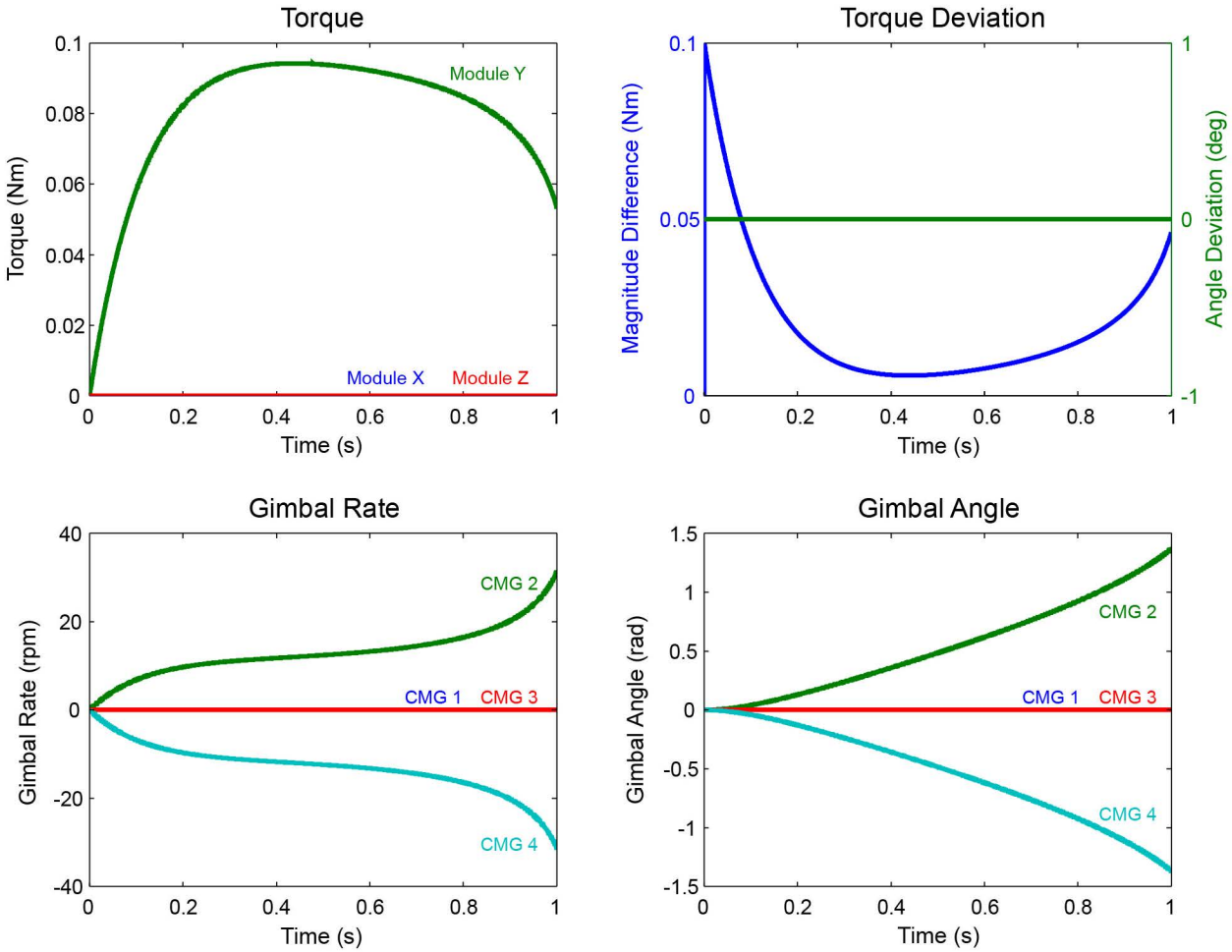

Figure 4-29: Results from the parameterized 4 CMG Pyramid simulation with the lift arm motion for an array with flywheels of inertia of 450 gcm^2 spinning at 15,000 RPM. The torque output (upper left) does not deviate significantly from the command torque, as seen in the figure in the upper right corner (mean deviations of 0.0201 Nm and 0 degrees). The gimbal rate (lower left) and gimbal angles (lower right) are also given.

These plots show that the simulated 4 CMG pyramid array with the motor dynamics added in is still essentially capable of generating torque in the correct direction. This holds true for the other two arrays as well. However, the amount of error between the commanded torque vector and the perceptible torque output from the array has increased from the initial simulations. The average deviations of the torque in magnitude and direction were 0.0201 Nm and 0 degrees for the 4 CMG pyramid array, 0.0190 Nm and 0 degrees for the 5 scissored pairs array, and 0.0123 Nm and 0 degrees for the 5 CMG pyramid array. The increase in deviation is due to the fact that the gimbal rates are no longer reached instantaneously after they are commanded; this is limited by the dynamics of the gimbal motor. These simulations still used the basic pseudoinverse steering law to control the CMGs. There is potential to account for the delay caused by the motor acceleration in a more complex steering law.

4.3.8 Array Selection and Discussion

In general, the simulations of the CMG arrays confirm that it is more likely that a larger flywheel spinning faster would generate the 0.1 Nm of torque without exceeding the 60 RPM gimbal limit than a smaller flywheel spinning slower. Exactly how small a mass and how slow it can spin before reasonable gimbal limits are exceeded is the question to answer. Each array had a different set of ideal parameters. The results of the simulation are summarized for convenience in Table 4-2.

Table 4-2: Final CMG simulation results summary

	Motion	Flywheel Inertia (gcm^2)	Flywheel Spin Rate (RPM)	Torque Deviation (Nm—deg)	# of Flywheels	# of Actuators	Notes
5 Scissored Pairs	Lift Arm	200	10,000	0.0190—0	10	15	Gearing Mechanism required
	90-90-90	200	10,000	0.0238—19			
4 CMG Pyramid	Lift Arm	450	15,000	0.0201—0	4	8	Slip ring/cable management required
	90-90-90	225	15,000	0.0193—7			
5 CMG Pyramid	Lift Arm	300	15,000	0.0123—0	5	10	Slip ring/cable management required
	90-90-90	125	15,000	0.0127—5			

Selecting an appropriate array requires comparing how close the output torque from each array was to the command torque, as well as taking into account other design considerations that will influence size such as the total number of actuators in each array. The 5 scissored pairs array allowed for the smallest flywheel inertia and the slowest spin rate. However, the mean angle deviation in the 90-90-90 simulation for the scissored pairs array was significantly larger than the angle deviation for the other arrays. It is possible that this could be minimized with appropriate steering laws, but there are other disadvantages to the scissored pairs array such as the fact that it requires many more actuators and double the number of flywheels than the other two arrays. As such, this array was not chosen.

There was no significant improvement in torque generation between the 4 CMG pyramid and the 5 CMG pyramid. Although the 5 CMG pyramid allows for a smaller flywheel than the 4 CMG pyramid, it also requires an additional flywheel and two additional actuators. The 5 CMG pyramid was eliminated from consideration as a possible array. The 4 CMG pyramid required the largest flywheel and the fastest spin rate of the 3 candidate arrays, but also the fewest number of flywheels and actuators. It also generated the desired torque without any concerning deviations in magnitude and angle; the existing deviation will likely be reduced with the choice of appropriate steering laws for the array. When all of these factors are taken into account, the 4 CMG pyramid array becomes the best candidate for the V2Suit array due to the importance of minimizing the module size.

4.4 Integrated V2Suit Module Design

The major design goal for the V2suit module is to minimize the overall size of the module so that the form factor will be wearable and unobtrusive. The main challenge is packaging the CMG array and associated electronics, cables, and assembly hardware into a functional and minimally sized module. A module size requirement was not imposed; rather the research associated with the design will be used to specify a size requirement. Additional design considerations for the module include safety and comfort for the wearer. Ultimately there will need to be considerations for how to power the module, likely from a separate power and processing module worn on the user's belt; in this iteration of the design the assumption is that the V2Suit will be operated tethered to a wall outlet. Based on these design considerations, a final V2Suit module design was formulated to create a brassboard prototype module. The module was built using a combination of off the shelf and custom machined components. It will be used to test the basic control and steering laws for the CMG array as well as measure the torque output from the CMG array.

4.4.1 CMG Array Mechanical Design

The selection of the 4 CMG pyramid array structure is a key factor that will determine the overall design of the V2Suit module. Again, the main consideration in the module design is

minimizing the size while maintaining the functional CMG array inside. The 4 CMG pyramid array utilizes the fewest number of CMGs of any of the candidate arrays, which is beneficial from a size minimization standpoint. The module needs to contain 4 CMG assemblies and the associated circuitry and electronics to control them as well as the IMU. One final major component of the design is the management of the wiring and cables inside the module. The module design is broken down into a few sub-assemblies and categories: the spin assembly, the gimbal assembly, cable management, and the overall module assembly.

Motor Selection

The selected CMG array requires a total of 8 motors: 4 spin motors and 4 gimbal motors. Both categories of motor have their own specific set of requirements, though size is an important consideration in each case. The smallest motor possible for each is desirable. The spin motor must spin the flywheel via direct drive at a constant rate of up to 15,000 RPM. The amount of time it takes for the motor to spin up from rest to the desired spin rate is not critical. However, maintaining the specified spin rate during operations is necessary. The motor chosen for use as the spin motor is the Micromo 1226M012B brushless DC servo motor. This motor is capable of spinning the required mass at the desired velocity and is of minimal size. On the end of the drive shaft there is a pinion that will be utilized in the coupling between the motor and the spin mass. The motor has rate feedback so the actual angular velocity of the spin mass (assuming no failure in the coupling mechanism) can be estimated.

The gimbal motor must actively change the direction of the angular momentum of the spin mass to generate the desired torque. A gear motor is preferable for this purpose due to their high-torque capabilities. Additionally the direction of rotation for the gimbal motor must be reversible. The motor chosen for use as the gimbal motor is the Micromo 2619S012SR 207:1 IE2-16. This motor has a gear ratio of 207:1 and can output 180 mNm of torque which is enough to gimbal the spin assembly. The direction of drive for this motor is reversible. The maximum output speed for this motor is 24 RPM. The gimbal motor has a built in encoder that allows for position and rate feedback. Position feedback is critical because the gimbal angles are required for the CMG steering laws.

4.4.2 Spin Assembly Design

The V2Suit CMG spin assembly consists of the spinning mass, the spin motor, an enclosure to surround the spinning mass, and other associated bearings and assembly hardware. An exploded view of the spin assembly can be seen in Figure 4-30 showing the spin enclosure (part 1), the spin bearing holder assembly (part 2), and the spin motor mount assembly (part 3).

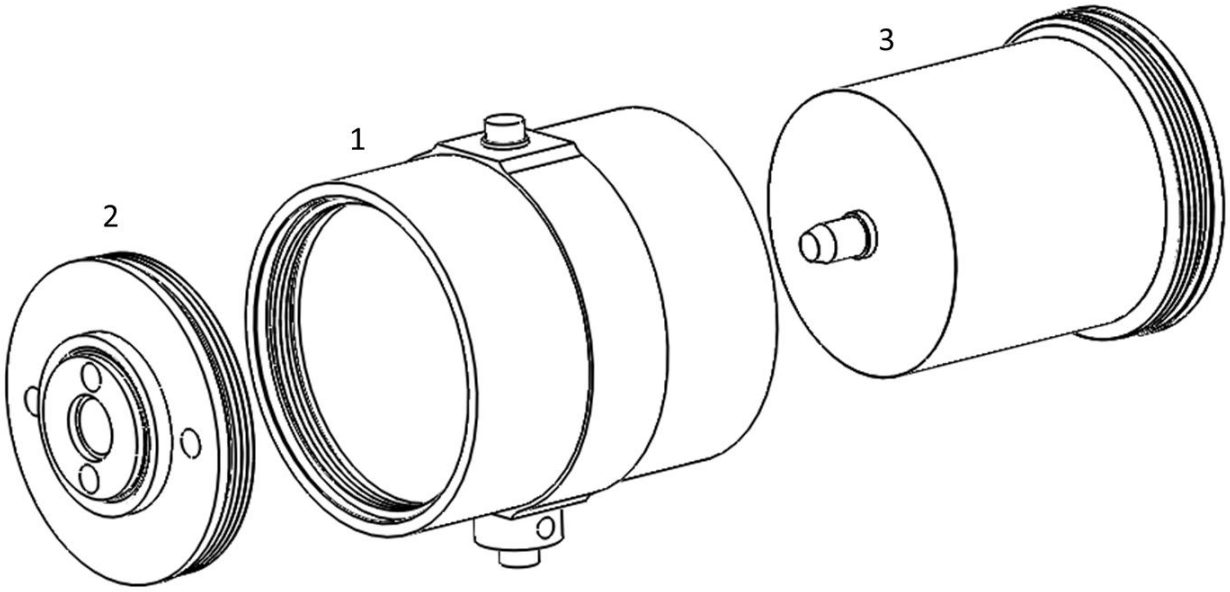

Figure 4-30: Exploded view of the V2Suit CMG spin assembly showing (1) the spin enclosure, (2) the spin bearing holder assembly, and (3) the spin motor mount assembly.

Spin Mass Design— The inertia of each spinning mass for the CMG within the 4 CMG pyramid array was specified at 450 gcm^2 The design for the spin mass must achieve an inertia as close to this as possible in order to generate the desired torque. For perspective, a stainless steel cylindrical flywheel would need to be 2 cm in radius and 2 cm in height to have this inertia. There are tradeoffs to consider when selecting a shape and material for the spinning mass. Using a more dense material such as tungsten (or a tungsten alloy) will enable the use of a smaller flywheel, but it might be more costly or more difficult to machine than a less dense material such as steel. An alternative shape for the mass (instead of a cylinder) might also be beneficial in terms of adding inertia without increasing size significantly, but the machining will be more complex. Ultimately for the V2Suit spin mass a cup shape (shown in Figure 4-31) was chosen. The hollow part of the spin mass fits around the spin motor, which is attached in the middle of the mass. The motor coupling will be discussed in more detail, as well as the bearings that will support the spin mass at either end.

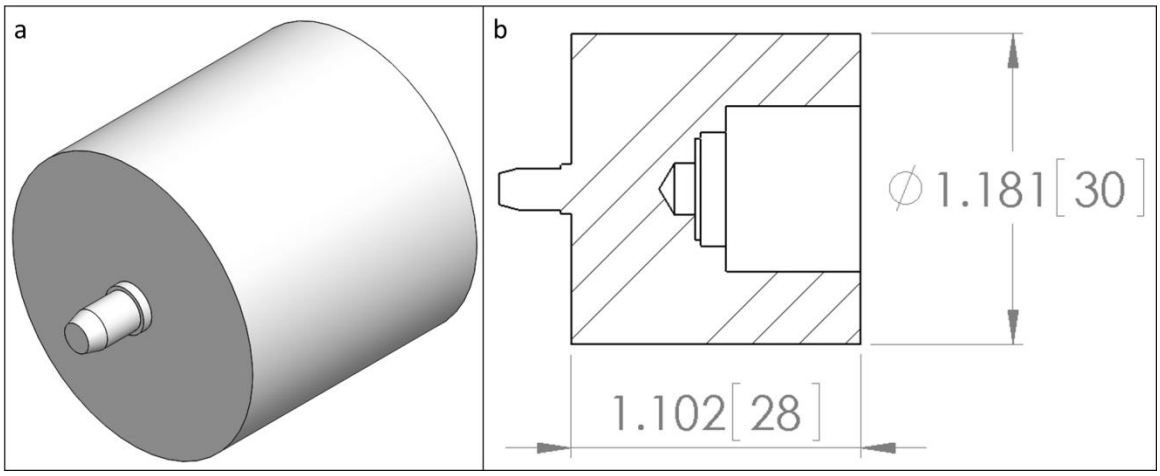

Figure 4-31: V2Suit spin mass. Figure (a) shows an isometric view of the spin mass and (b) shows a cross section view. The mass is cup-shaped to fit around the spin motor. Dimensions are in inches [millimeters].

The spin mass was machined out of ASTM B777 tungsten alloy which has a density of 17 g/cm^3 The alloy was chosen as it retains a high density and is more easily machinable than pure tungsten. Based on the design of the spin mass, its mass is approximately 288 g and the inertia around the spin axis is approximately 364 gcm^2. (Note that this is less than the desired inertia previously stated as 450 gcm^2.) However, there are other spinning components (e.g., bearings, the rotor inertia) that will contribute some to the total inertia that is being spun. Additionally, this inertia is more than capable of generating the desired 0.1 Nm of torque in any direction (as shown by the possible torque output of the array with a flywheel of this size in Figure 4-32). The responsibility for maximizing the torque generation from the array lies in the selection of appropriate steering laws. Indeed in the future it may be possible to reduce the size of the spin mass and thereby reduce the overall size of the array, assuming a sufficiently effective steering law can be developed.

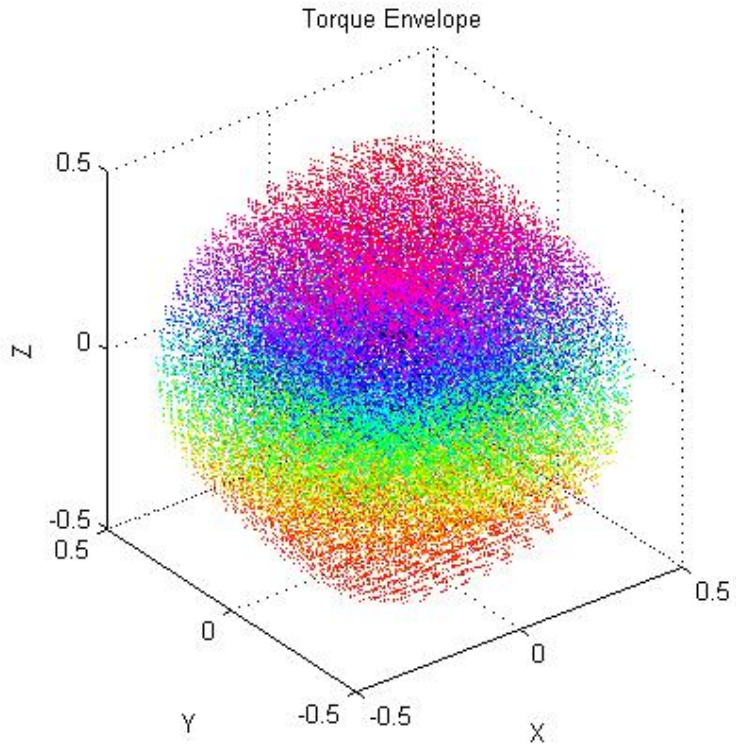

Figure 4-32: Possible Torque output of a 4 CMG pyramid array with a flywheel inertia of 363 gcm^2 assuming a maximum gimbal rate of 30 RPM.

Spin Gear Insert— The spin mass is coupled to the spin motor via a small insert bonded into the inside of the spin mass. The insert is cylindrical with a shape cut out of the center that mates to the pinion attached to the rotor of the spin motor. When the motor spins the gear will engage with the insert and turn the spin mass. The insert can be seen in Figure 4-33. The gear profile was created using wire electrical discharge machining with 7075 aluminum. This method for attaching the motor was chosen to eliminate the necessity of threading a hole through the tungsten spin mass for a set screw. Additionally the motor rotor is only 1 mm in diameter, so using a set screw is undesirable. The insert also prevents the spin motor from being axially loaded by the spin mass and reduces the stress on the spin motor bearings.

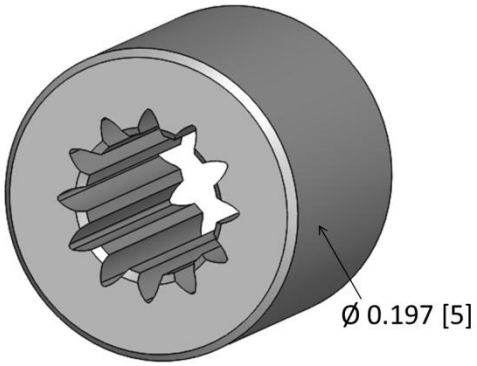

Figure 4-33: The spin gear insert will be bonded into the interior of the spin mass using epoxy and will serve as the coupling between the spin motor and the spin mass. The gear profile has been designed to match the pinion on the end of the spin motor. Dimensions are in inches [millimeters].

Spin Enclosure Design— The spin mass is encased inside a spin enclosure, both as a safety precaution and as a way to prevent anything inside the module from coming into contact with the spinning mass. The enclosure also provides a way to support the spin mass and spin motor, as well as the interface between the spin assembly and the gimbal structure. The spin enclosure can be seen in Figure 4-34.

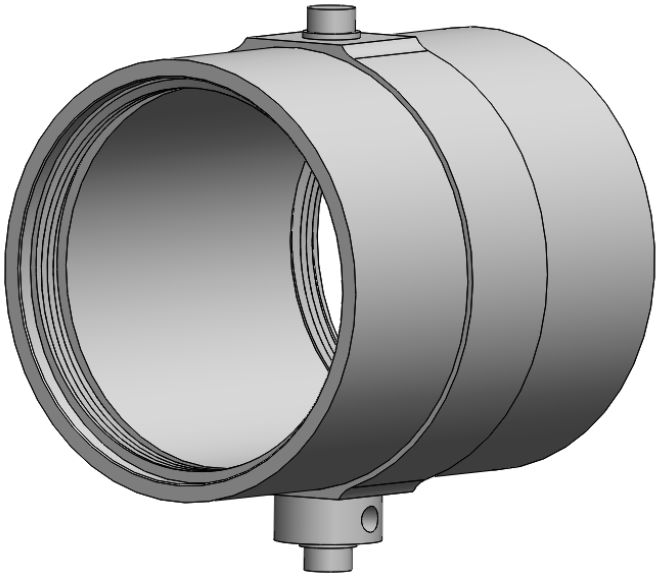

Figure 4-34: The spin mass enclosure encases the spin mass for safety and provides a way to support the spin mass and mount the spin motor. The enclosure is attached to the gimbal motor.

A cross section view of the enclosure can be seen in Figure 4-35. This part has a cylindrical interior that surrounds the spin mass. The ends of the internal cylinder are threaded with 32 pitch threads to enable the two end caps to screw onto the enclosure; the end caps provide

means of supporting the spin motor and the spin mass. The cylindrical bosses protruding from the exterior surface of the enclosure are aligned with the gimbal axis and serve as the interface with the gimbal motor and bearings in the gimbal structure. The gimbal motor shaft fits into a hole in the lower boss and there is a tapped hole to allow for a set screw to secure the gimbal motor to the spin assembly. The general cylindrical shape for the exterior minimizes the size of this part, the largest in the spin assembly. The raised ring and flat surfaces present on the exterior surface are features that were included to simplify the machining process. Allowing this raised ring enabled the two ends of the part to be machined on a lathe, while leaving a larger ring that was then removed to create the cylindrical bosses. The enclosure was machined out of 7075 aluminum stock.

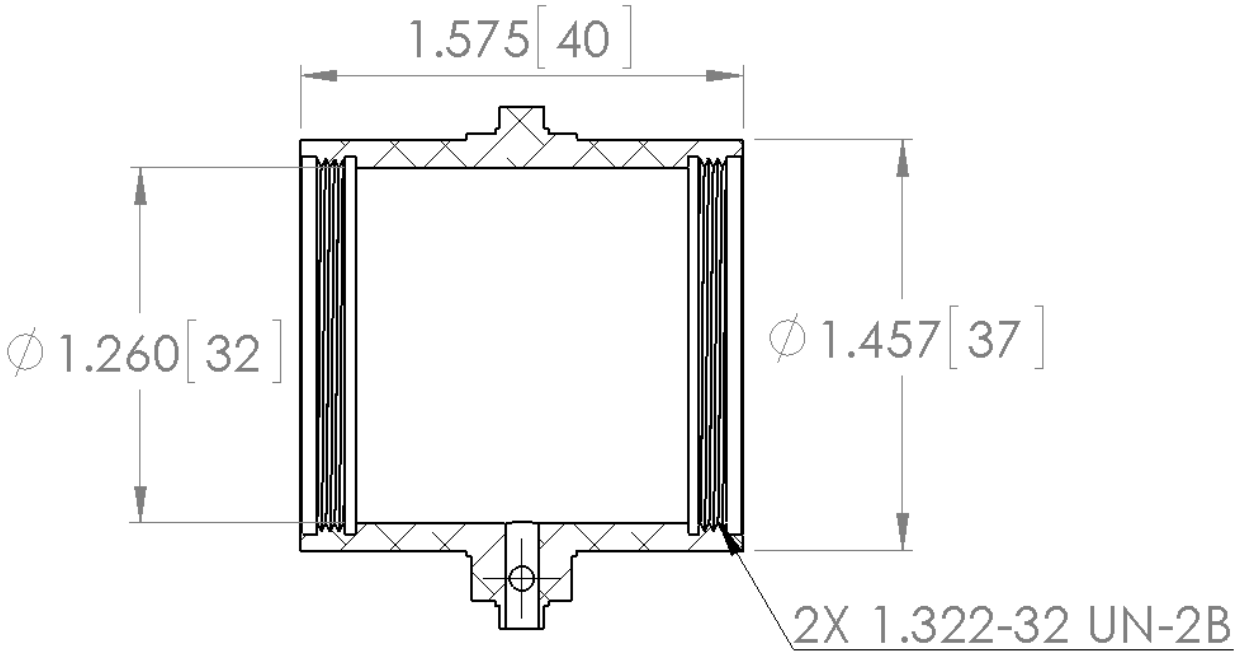

Figure 4-35: Cross section view of the enclosure. The two end caps screw into the threaded regions at either end. The bosses on the top and bottom of the enclosure interface with the gimbal motor and bearings. Dimensions are in inches [millimeters].

Spin Bearing Holder Assembly Design— One end of the spin mass (seen as the left side of the mass in Figure 4-31 (b)) has a small cylindrical feature to interface with a bearing (referred to here as the spin bearing). The spin bearing holder assembly (see Figure 4-36) was designed as a way to support this end of the spin mass with a pre-loaded radial bearing. This assembly is one of the two end caps mentioned previously that will fit into one end of the spin enclosure.

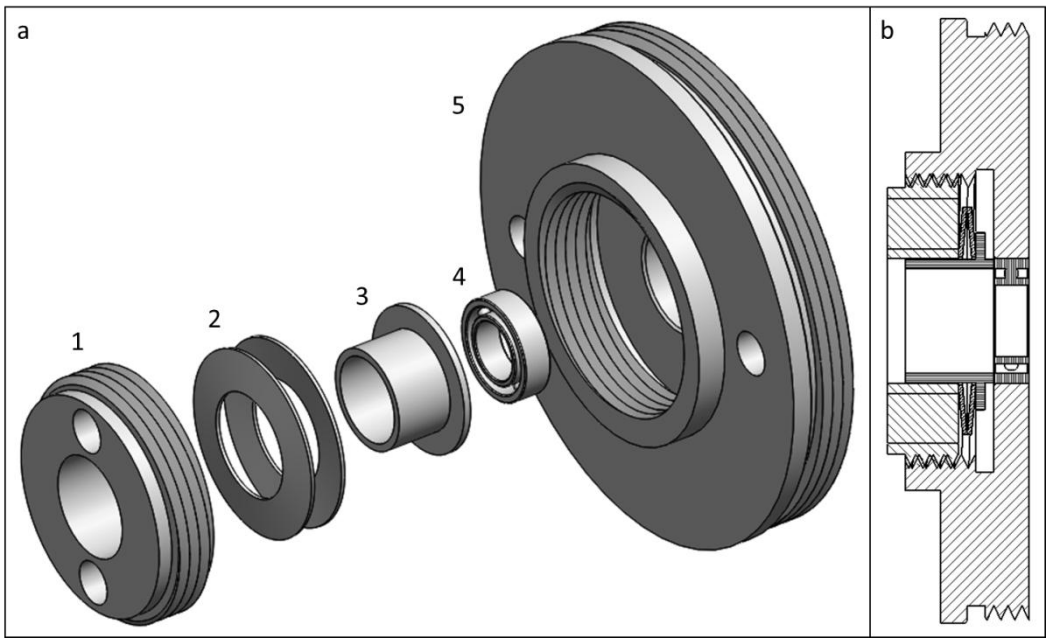

Figure 4-36: (a) Exploded view of the spin bearing assembly with parts: 1. Spin bearing cap, 2. Disc springs, 3. Pre-load sleeve, 4. Spin bearing, 5. Spin bearing holder. (b) Cross section view of assembly showing the pre-load on the outer race of the spin bearing.

The bearing fits into the center of the spin bearing holder (part 5 in Figure 4-36, also see Figure 4-37) which has external 32 pitch threads to allow it to be screwed into one end of the enclosure. When fully attached, the exterior surface of the spin bearing holder is flush with the side of the spin enclosure which minimizes the size of the assembled enclosure. In order to facilitate assembly, two holes have been included on this surface to enable the use of a spanner wrench to screw the parts together. The largest cylindrical exterior surface shown in Figure 4-37 is a precision diameter used to align the spin bearing holder and the enclosure more accurately than the threads would allow for. The spin bearing holder was machined out of stainless steel rather than aluminum to prevent any potential assembly issues stemming from having two aluminum parts repeatedly screwed together.

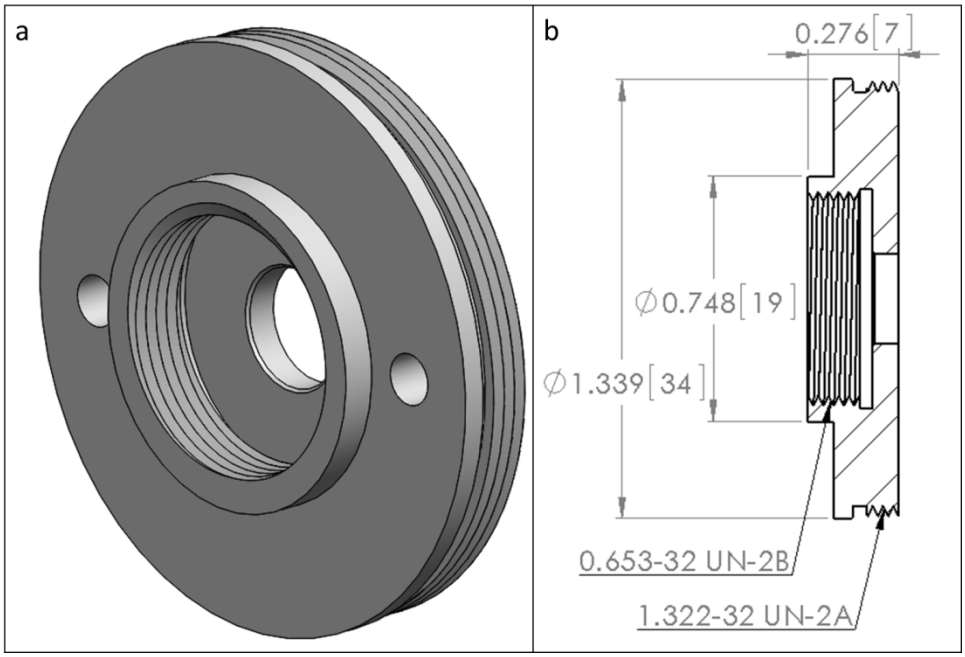

Figure 4-37: Spin bearing holder (a) and cross section (b). The spin bearing holder screws into one side of the spin enclosure. It supports the spin mass on one side with a pre-loaded radial ball bearing.

The spin bearing holder also allows for a way to pre-load the spin bearing. The bearing is pre-loaded using disc springs in series. The pre-load mechanism is housed inside the smaller cylindrical boss protruding from the face of the spin bearing holder. The disc springs interact with the bearing through the pre-load sleeve (part 3 in Figure 4-36 (a)), a simple part designed to center the springs inside the housing and direct the spring force onto the outer race of the bearing. The interior surface of the housing is threaded with 32 pitch threads, and the spin bearing cap (part 1 in Figure 4-36 (a)) is threaded to fit into it. This allows the spin bearing cap to be tightened down onto the disc springs using the same spanner wrench used to attach the spin bearing holder to the spin enclosure. This allows for control over the level of pre-load on the bearing. A cross section of the complete assembly is shown in Figure 4-36 (b).

Spin Motor Mount Assembly Design— The second end cap for the spin enclosure is the spin motor mount assembly. The purpose of this assembly is to complete the spin enclosure as well as support the motor and the other end of the spin mass. The entire spin motor assembly can be seen in Figure 4-38. It consists of the spin mass and the spin gear insert (part 1 in Figure 4-38 (a)), the spin motor bearing (part 2), the spin motor mount (part 3) and the Micromo 1226M012B spin motor (part 4). A cross section view showing how this assembly goes together is shown in Figure 4-38 (b).

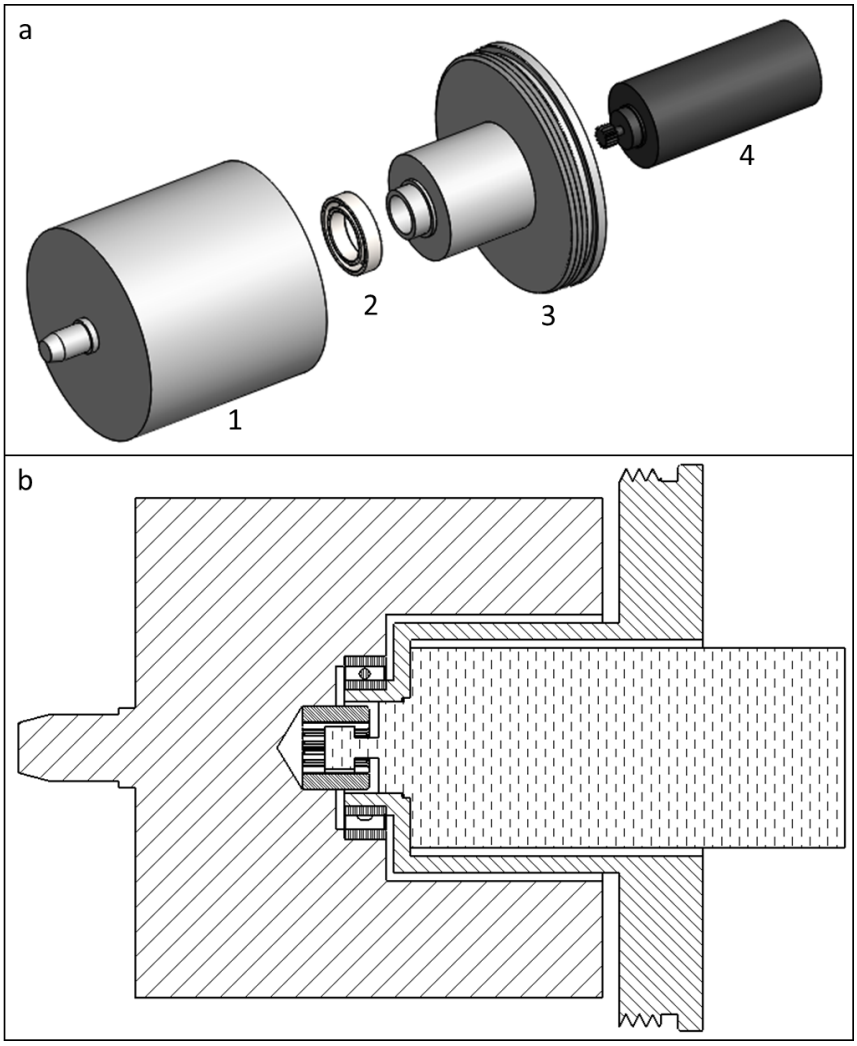

Figure 4-38: (a) Exploded view of the spin motor assembly with parts: 1. Spin mass assembly, 2. Spin motor bearing, 3. Spin motor mount, 4. Spin motor. (b) Cross section view of the spin motor assembly.

As with the other end cap, the motor mount (shown in Figure 4-39) is flush with the spin enclosure when assembled, and there are holes on the exterior face for a spanner wrench to be used in assembly. The spin motor mount was designed to interface with the Micromo 1226M012B spin motor, which has a threaded boss on its front surface. The mount has an interior threaded surface that allows the motor to be screwed into place. There is also a small precise cylindrical feature on the end of the spin motor to allow for more precise positioning of the rotor, and there is a corresponding feature on the interior face of the spin motor mount. This precision diameter feature ensures that the spin axis is centered in the spin enclosure. The spin motor mount fits inside the spin mass with clearance all around so the mass spins around it. There is a radial bearing to support the spin mass on the spin motor side (part 2 in Figure 4-38 (a)). The bearing fits around the end of the spin motor mount and the small boss on the exterior surface of the mount interfaces with the inner race of the bearing; the outer race of the bearing interfaces with a surface in the interior of the spin mass (see Figure 4-38 (b)). The spin motor mount

was machined out of brass. Brass was chosen instead of stainless steel (used for the bearing holder) due to its higher heat conductance in the hopes that this will help with heat transfer from the spin motor.

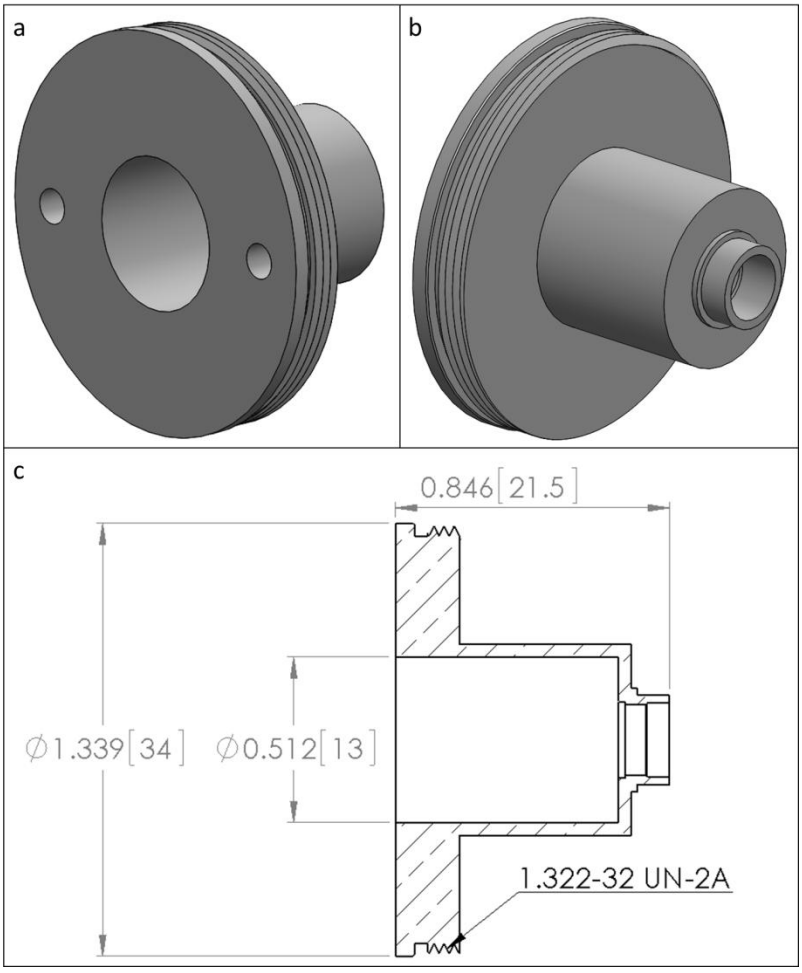

Figure 4-39: Two views of the sin motor mount (a, b). The spin motor bearing fits onto the small cylindrical surface shown in (a) and the motor is housed inside the larger cylindrical opening shown in (b). The spin motor mount screws into one end of the spin enclosure. Figure (c) shows a cross section view of the motor mount. Dimensions are in inches [millimeters].

Spin Assembly— A cross section view and an isometric view of the completed spin assembly are shown in Figure 4-40. The spin assembly is supported by the gimbal assembly and interfaces with the cable management system which will be discussed in the following section.

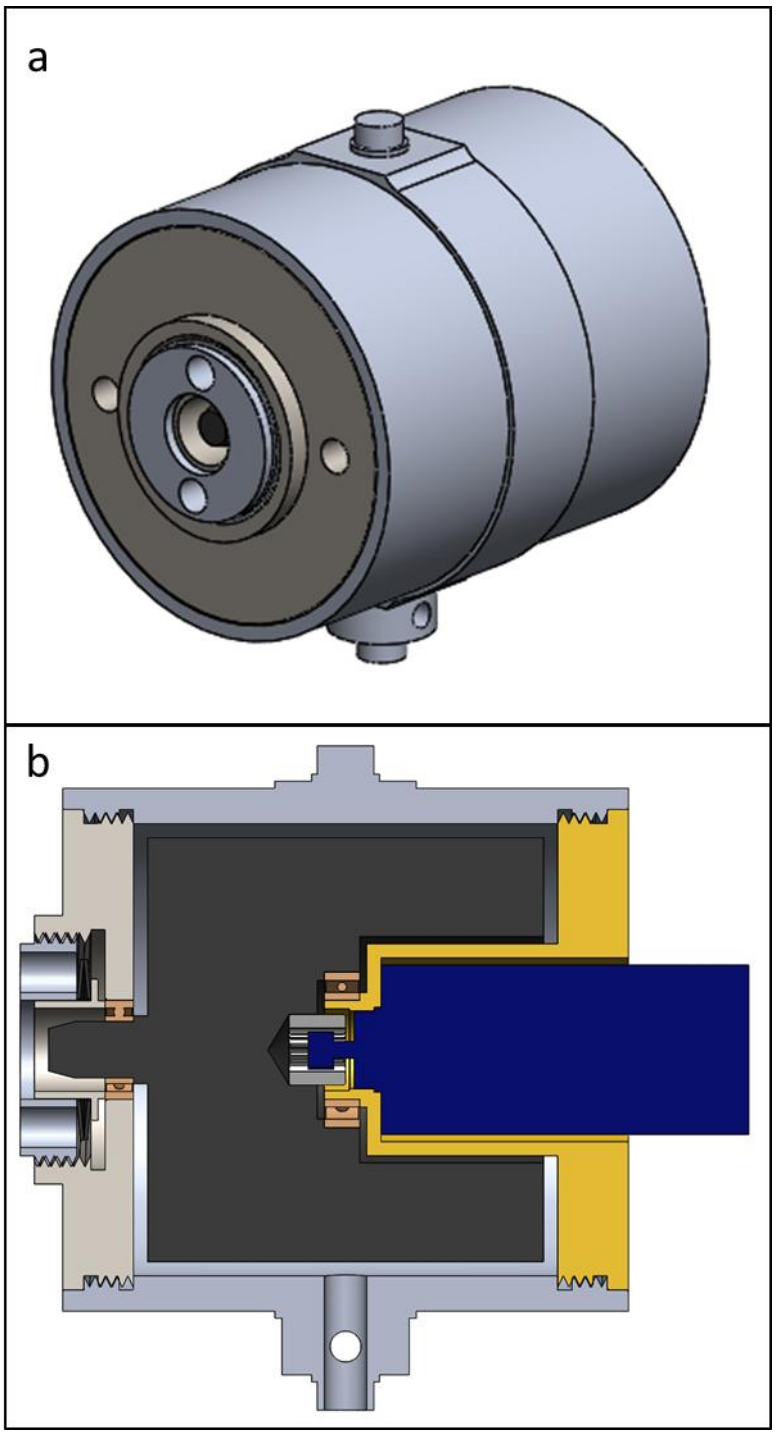

Figure 4-40: Completed V2Suit spin assembly isometric (a) and cross section (b) views.

4.4.3 Cable Management

As mentioned previously, there are not any limits imposed on the gimballing of the CMGs in the pyramid array. Allowing continuous gimballing would require incorporating slip rings into the design, which would increase the overall size significantly. To avoid this, a limit of ± 2

revolutions was put on the gimbal angle for each CMG, meaning there needs to be enough cable available running to the spin motor to account for this range and a means of managing the cable as the CMG gimbals. The idea behind the design of the cable management system is to have two spools for the cable to wrap around.

One spool (called the gimbal spool) is attached to and surrounds the spin assembly (see Figure 4-41). The cable running from the motor fits into a slot in the spool. At a gimbal angle of 0 there is no cable wrapped around this spool. As the CMG gimbals in either direction, the cable winds around the gimbal spool. For the brassboard CMG array the gimbal spools will be 3D printed. The spool is attached to the spin enclosure with a small screw.

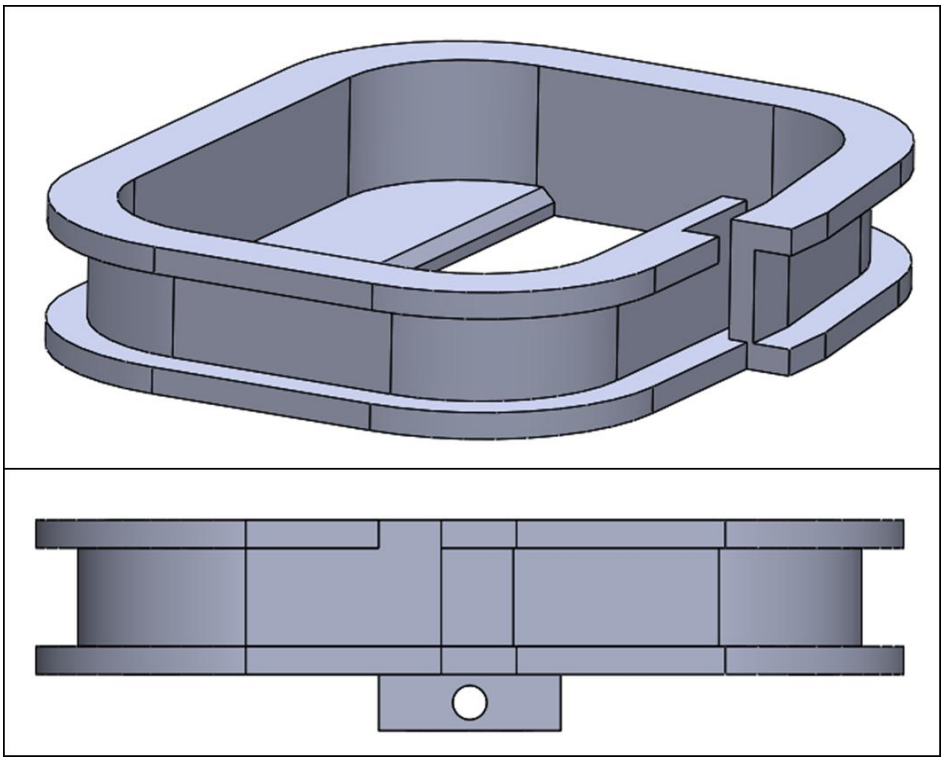

Figure 4-41: The gimbal spool fits around the spin assembly and is attached by a small screw at the base. The cable wraps around the gimbal spool as the CMG gimbals.

The second spool (called the spring-loaded spool) for each CMG is located inside the module adjacent to the CMG. At a gimbal angle of 0 deg all of the extra cable is wound around this spool. As the CMG gimbals in one direction, the spring-loaded spool is unwound and the cable winds around the gimbal spool. When the CMG is gimbaled the other direction, the cable is unwound from the gimbal spool. A constant force spring attached to the spring-loaded spool then causes the free cable to be re-wound around this spool. It is important that the spring is strong enough to wind up the loose cable but not too strong so as to interfere with the action of the gimbal motor. The assembly for the spring-loaded spool can be seen in Figure 4-42.

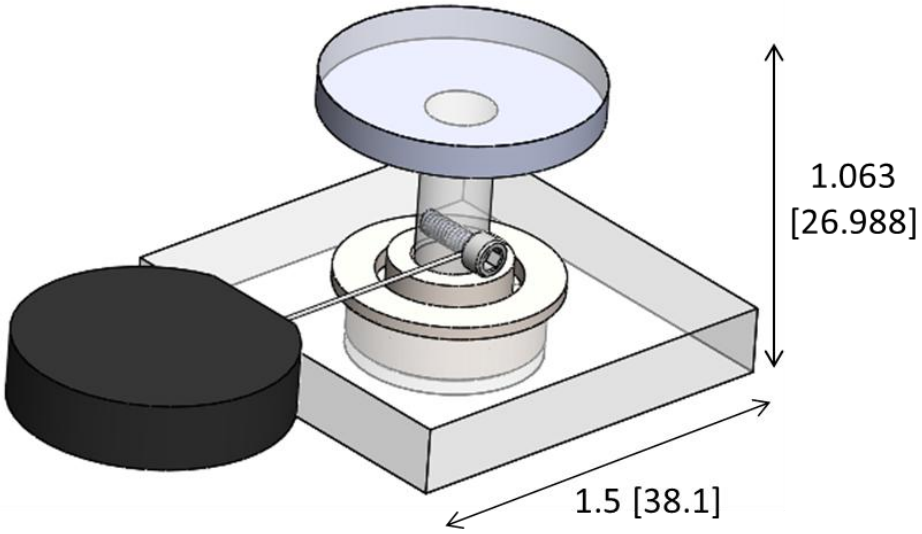

Figure 4-42: The spring-loaded spool holds the excess cable when it is not wrapped around the gimbal spool. There is a constant force spring attached to this spool so that when there is loose cable it will be re-wound automatically. Dimensions in inches [millimeters].

4.4.4 Gimbal Assembly

The spin assembly is canted so that the gimbal axis is at an angle of 35.27 degrees relative to the base of the module. This makes it perpendicular to the face of an imaginary pyramid with an elevation angle of 54.73 degrees, as specified previously [57]. The gimbal assembly consists of two main parts that will serve to support the gimbal motor, the spin assembly, and two gimbal bearings. The entire assembly can be seen in Figure 4-43.

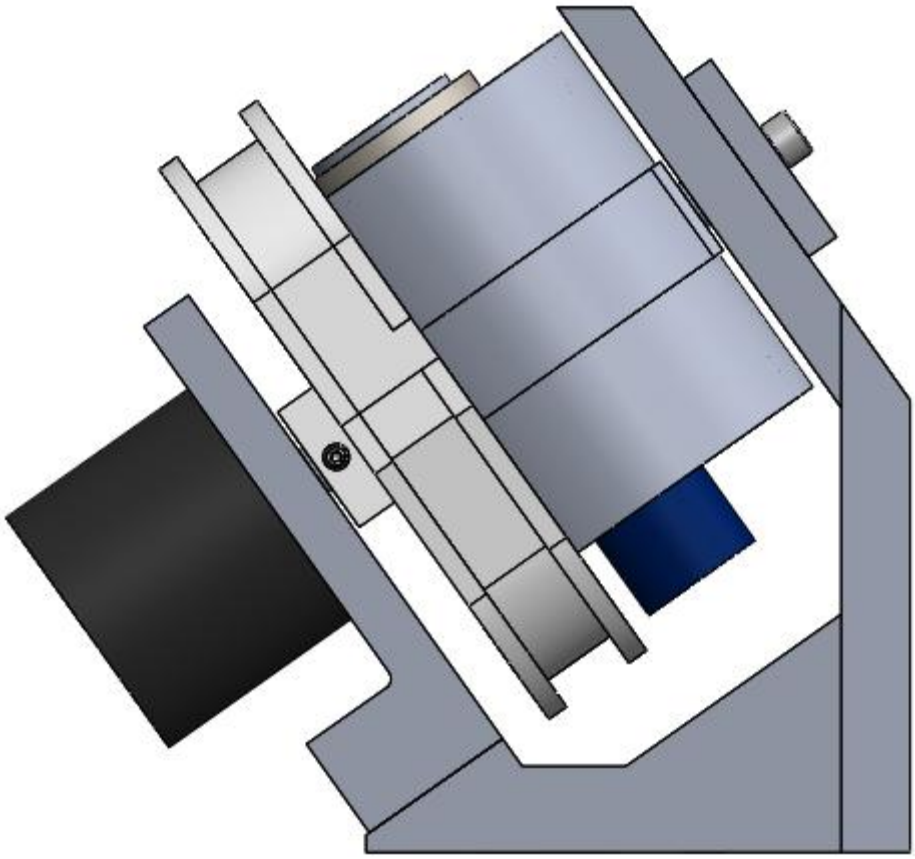

Figure 4-43: The gimbal assembly for a single CMG consists of the gimbal motor, the gimbal support structure, the gimbal spool, and the spin assembly.

The two parts of the gimbal support structure can be seen in more detail in Figure 4-44. They were designed keeping in mind the complete gimbal sweep of the spin assembly. The gimbal motor mount (Figure 4-44 a) was designed to attach to the gimbal motor and hold one of the two gimbal bearings. This part is attached to the gimbal support (Figure 4-44 b) on a surface that is at an angle of 35.27 degrees relative to the flat base of the part. The top portion of the gimbal support holds the second gimbal bearing and allows for the bearing to be pre-loaded using disc springs and another pre-load sleeve like the one from the spin assembly.

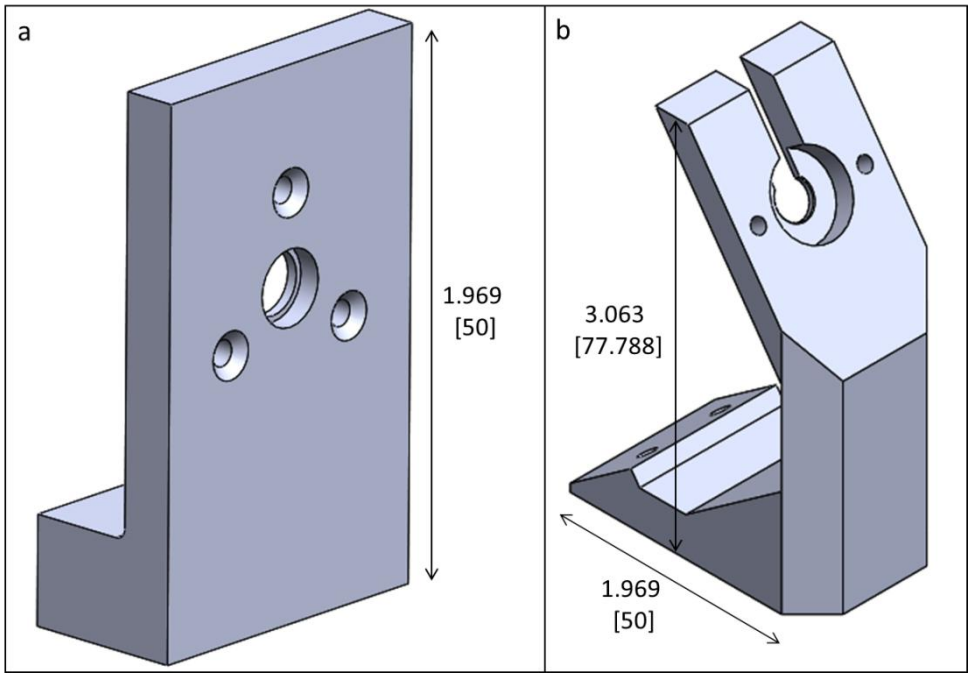

Figure 4-44: The gimbal support structure is made up of the gimbal motor mount (a) and the gimbal support (b). Dimensions in inches [millimeters].

An exploded view of the gimbal assembly is shown in Figure 4-45 below. For assembly, the gimbal motor (part 1) must first be attached to the motor support (part 2). The gimbal bearing (part 3) is then placed into its position in the motor support, and the spin assembly (part 4) is placed on the motor shaft and inserted into the bearing. The spin assembly is attached to the motor shaft using a small set screw. This assembly is then attached to the gimbal support (part 9). The top of the spin assembly slides through the slot in the top of the gimbal support and the gimbal motor mount is screwed in from the base of the gimbal support. Finally the other gimbal bearing (part 5) is placed around the top of the spin assembly and pre-loaded appropriately.

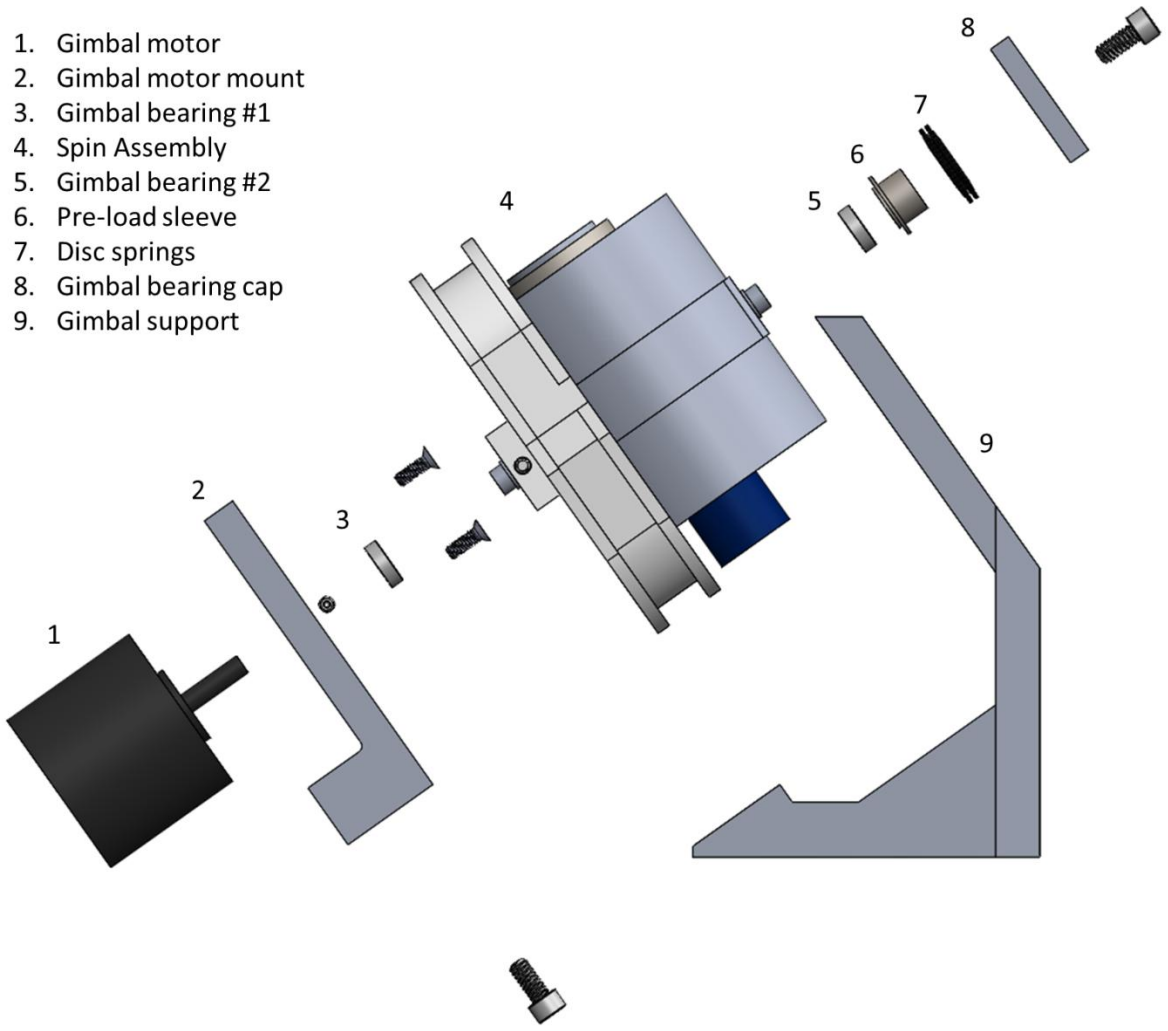

Figure 4-45: The exploded view of the gimbal assembly shows how it goes together. The gimbal motor is attached to the motor mount and then to the spin assembly with a bearing. The motor mount is attached to the gimbal support and then the second bearing is put in place and pre-loaded.

4.4.5 Complete Module Design

The V2Suit module will need to contain the 4 CMGs in the array as well as the cable management spools for each CMG. Additionally the module will ultimately contain an IMU and assorted electronics for controlling the CMG motors. For the brassboard unit, the motor electronics will be located elsewhere. A basic layout for the V2Suit module can be seen in Figure 4-46. The module has a 6 in. square footprint and is 3.5 in. tall.

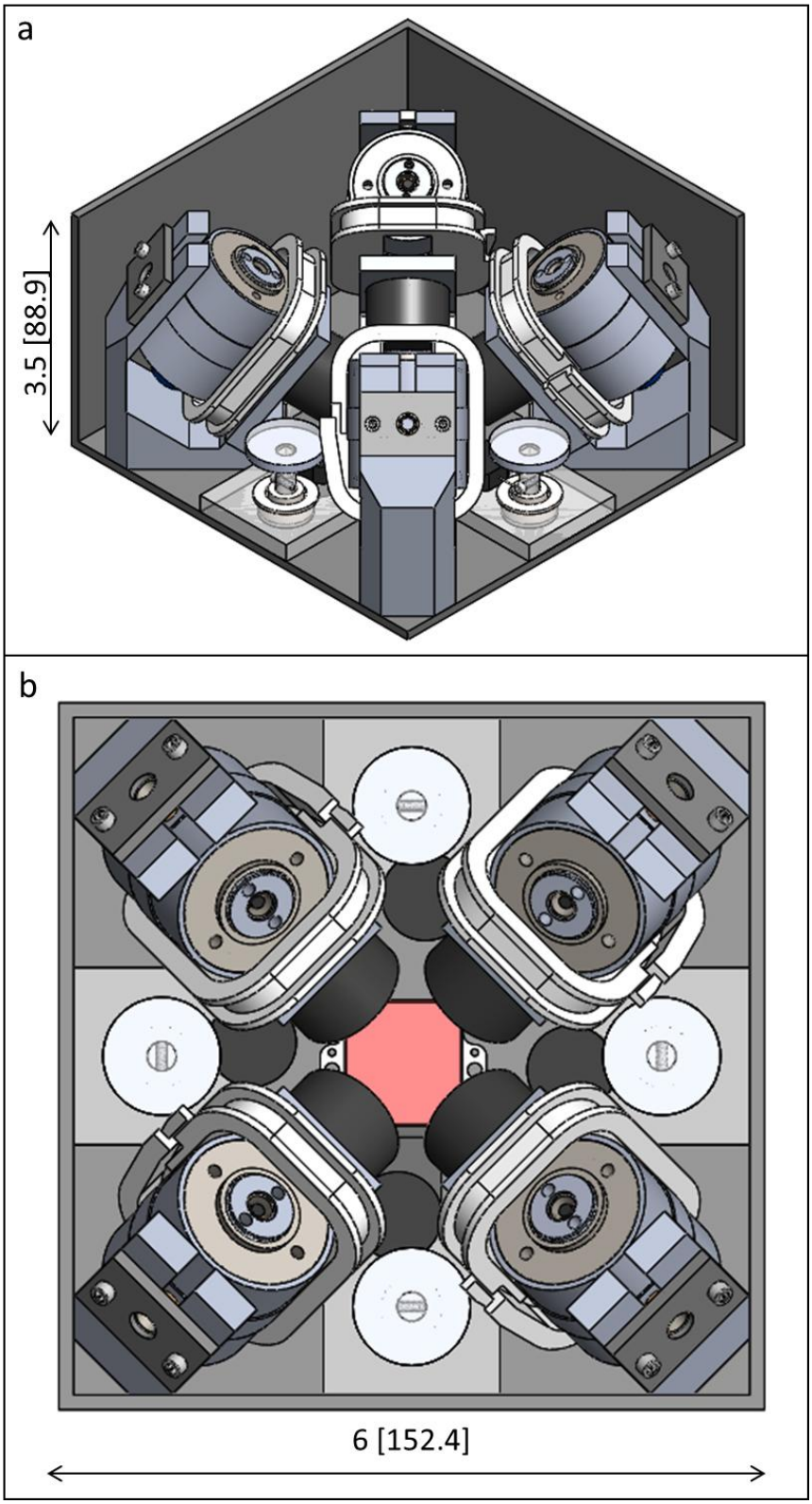

Figure 4-46: Each CMG fits into the corner of a 6”x6”x3.5” module. This leaves enough room for the gimbal sweep and the cable management system. The IMU fits in the center of the module. Electronics for motor control will likely be placed along the side walls of the module. Dimensions in inches [millimeters].

In Figure 4-46 (b) the IMU can be seen in the center of the module. It is possible that in future iterations the motor electronics would be located along the walls of the module or on a raised platform in the center of the module above the IMU. The spools for cable management for each CMG can be seen in the space adjacent to the CMGs.

Orienting the CMGs into the module's corners rather than having them aligned with the module axes allows the overall size of the module to be smaller. The new orientation of the 4 CMGs with respect to the module coordinate frame changes the Jacobian of the array from the one given by Equation (4-38). The Jacobian of the V2Suit 4 CMG pyramid array is given by Equation (4-47).

$$J = h\begin{bmatrix} \frac{\sqrt{2}}{2}(-\sin\varphi_1 - \cos\alpha\cos\varphi_1) & \frac{\sqrt{2}}{2}(-\sin\varphi_2 + \cos\alpha\cos\varphi_2) & \dots \\ \frac{\sqrt{2}}{2}(-\sin\varphi_1 + \cos\alpha\cos\varphi_1) & \frac{\sqrt{2}}{2}(\sin\varphi_2 + \cos\alpha\cos\varphi_2) & \dots \\ \sin\alpha\cos\varphi_1 & \sin\alpha\cos\varphi_2 & \dots \\ \dots & \frac{\sqrt{2}}{2}(\sin\varphi_3 + \cos\alpha\cos\varphi_3) & \frac{\sqrt{2}}{2}(\sin\varphi_4 - \cos\alpha\cos\varphi_4) \\ \dots & \frac{\sqrt{2}}{2}(\sin\varphi_3 - \cos\alpha\cos\varphi_3) & \frac{\sqrt{2}}{2}(-\sin\varphi_4 - \cos\alpha\cos\varphi_4) \\ \dots & \sin\alpha\cos\varphi_3 & \sin\alpha\cos\varphi_4 \end{bmatrix} \quad (4\text{-}47)$$

4.4.6 Discussion

Based on the results of the trade study, a 4 CMG pyramid array has been designed for use inside the V2Suit module. The goal behind the mechanical design was to arrive at a functional CMG unit that would take up a minimum amount of volume. This design ultimately has a 6 inch square footprint and a height of 3.5 inches yielding a total volume of 126 in^3. This result is larger than is ideally desirable for a body worn module. It would likely be cumbersome, especially for use on smaller body segments such as the forearm. As technology continues to improve, there is potential for further minimizing the size of the CMGs. Smaller gimbal and spin motors would reduce the overall module size. Additionally, the cable management system takes up a large amount of space, especially considering the increased size of the gimbal sweep due to the gimbal spool. Eliminating the need for excess cable with a very small slip ring (something not currently available commercially) would reduce the module size.

4.5 Human-System Integration

4.5.1 Qualitative Evaluations

The interface with the human wearer is important for the operational implementation of the V2Suit. Existing countermeasure suits (e.g., Russian "Penguin Suit" or GLCS) do not have a rigid component along the major axis of the bones within the various limb segments. However, for the V2Suit to be effective as a countermeasure system, it requires this infrastructure. The ability of the gyroscope to both resist changes in angular momentum and as a result affect the body segment during movements requires that the module be rigidly attached to the

limb. This is the key to providing the coordinated "viscous response" with a specific magnitude and direction.

To develop an operational system the V2Suit must be easily put on, comfortable to wear, and small and low-profile as to not interfere with normal movements -- all while providing the desired functionality. In addition, the modules must not interfere with normal, daily activities when worn and non-operational. This requires a small form factor that can be integrated with normally worn garments – either as an add-on to existing equipment or designed to be an integral part of the garment.

The V2Suit module sizing, placement and interface to the human body was investigated through computer aided design (CAD) modeling (Figure 4-47), form-factor analysis using a life-size mannequin (Figure 4-48) and through limited evaluations through members of the V2Suit team. The modules were sized according to the anticipated final form factor through technology selection, component miniaturization, and packaging. They were placed near each body segments center-of-mass (e.g., [68]) in an effort to maximize the resulting "viscous resistance" perceptual magnitudes. The CAD modeling (Figure 4-47) provided an initial opportunity to visualize the sizing estimates relative to the anthropometrics, as well as the position and orientation with respect to the individual limbs. Subsequent analysis using a life-size mannequin (Figure 4-48) enabled the visualization of various V2Suit module form factors, the position and orientation of them including the power and processing module, as well as the required cabling to connect the modules to one another. In addition, the V2Suit module interface with the mannequin/garment, as well as the attachment points for the cabling was investigated.

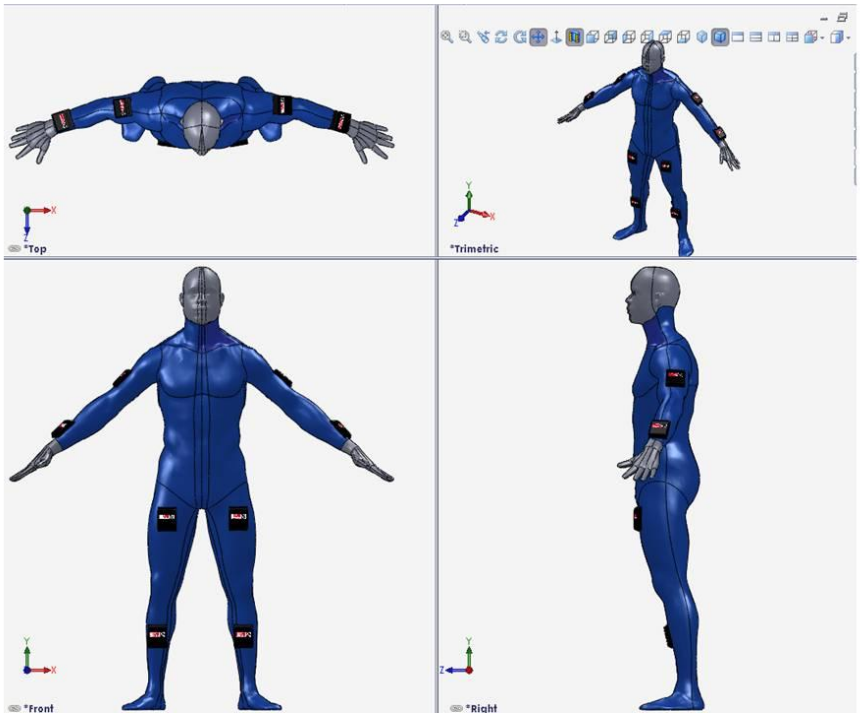

Figure 4-47: CAD modeling of V2Suit module sizing and placement

Figure 4-48: V2Suit module form factor sizing and placement analysis using life-size mannequin

4.5.2 Quantitative Evaluations[1]

An experiment was designed and performed which included a functionality test of placing mock-up V2Suit modules onto the arms. Since astronauts primarily use their arms to move around the spacecraft, interact with equipment, and move objects, designing a suit that maintains the functionality of the arms is of critical importance. It is extremely difficult to capture the microgravity environment on Earth without using a parabolic arc aircraft or some other kind of special environment, so a test that captured some of the general aspects of arm movement and dexterity using common items was required. The module mock-ups had minimal weight to them, as the testing was focused on volumetric constrains and not inertia effects.

Van Tujil et al. reviewed fifteen different standardized tests used to test the functional ability of hand and arm movements, but most of these tests are primarily focused on cases of humans with deteriorated arm and hand use from injury or illness [77]. These types of tests, which are generally used to examine patients who have suffered a stroke or other debilitating disease, would be much too easy for a person with normal hand and arm function and do not accurately

[1] The V2Suit team would like to acknowledge Rebecca Vasquez, Mark Boyer, Dan Montes, and Dilip Thekkoodan for contributing to this section through their work in MIT Course 16.423, Spring 2013.

represent the challenges of space. Similarly, a multitude of tests deriving from Fitts's Law provide a suitable quantification of arm movement versus accuracy, but are only useful for testing single movements in very controlled environments [78-81]. Plamondon and Alimi provide a good overview of the applications of Fitts's Law over the 40 years since Fitts' original publication but do not list any tasks specific to the microgravity environment or to broader functional tests.

Elements from both the functional tests of the physical therapy domain and the Fitts's Law tests of the experimental psychology domain were combined into a new test. The Boyer Upper-body Functionality in Flight (BUFF) Test was developed to mimic some of the broad elements of movement and function in space. The test forced the subject to move in both gross and precise hand and arm movements in three dimensions. The most critical time for an astronaut in space is during an emergency. During an emergency, an astronaut may have to address a cognitively challenging problem while moving through a very constrained and potentially hazardous environment. If astronauts were hindered while addressing emergencies by wearing the V2Suit, it would be a dangerous and un-flightworthy device. Therefore, the test compared the performance of a subject with and without the suit in time-critical tasks to determine if their performance was degraded.

The BUFF Test used 10 rectangular blocks and 5 circular blocks. Each block was a different height and has a different number, English letter and Greek letter written on it one of 5 colors (black, blue, red, yellow, green). The test arena was an enclosed space between a bookshelf and a table. The table was located approximately 5 feet from the bookshelf. The walls on either side that created the corridor were approximately 4 feet wide, enough to allow passage by narrow enough to provide constraint. This was done to simulate the constraints of the space station. The setup can be seen in Figure 4-49.

Figure 4-49: BUFF Test Experimental Setup. The bookshelf was divided into 12 regions, with each of the three shelves containing four quadrants

In a within-subjects experiment, each participant was seated on a wheeled chair in the enclosed space. The subject had to follow one of two exercise scenarios written down step by

step. In each step, the subject had to move the blocks around to achieve some objective. The objectives varied in difficulty from "Place any two blocks into space A1" to "Organize the blocks alphabetically by Greek letters." The variation in cognitive difficulty between the steps was designed to focus the user's attention on the task and away from the test condition. Preliminary studies were done to ensure tasks were do-able by a wide range of participants and would take between two and five minutes to complete on average. Further testing and scenario development could be used to create a set of equally difficult, equal length scenarios to present the participants with a greater variety of tests. In order to mitigate some of the learning effects that occurred with repeated movement activities, the order of events and conditions were counter-balanced using a Latin Squares method, but different new scenarios could further control for learning biases.

The within-subjects functionality testing of gyro mock-ups (boxes) resulted in two dependent quantitative measurements, as well as a subject survey. The test composed of three sleeve configurations (no boxes, small boxes, large boxes) and two different exercises. The test matrix is show in Table 4-3. The performance of the participants was measured task completion time in seconds as well as number of errors committed while performing the test. An ANOVA was performed on both these dependent variables for each of the two exercises (easy, hard). The ANOVA showed that, regardless of exercise, the different box treatments did not have a significant influence on the task completion time (P=0.46, 0.73) but did have a significant influence on number of errors (P=0.003, 0.043). It also showed there was a significant variance among subjects in task completion time for both exercises. These results correspond well with the expected outcomes.

As a low-power method to further characterize the ANOVA results for task completion time, each mean difference between the three box treatments was computed (accepting an increased risk of Type I error). A one-sided dependent samples t-test was performed on each result to determine if the statistical significance of any one difference was greater than another. The p-values calculated for all comparisons fell in the range 0.44-0.51, and consequently it cannot be concluded that there was any statistical impact of the mock-ups on task completion time. The graphical results are shown in Figure 4-50. There was a small positive trend for exercise 1 but it lacks statistical significance.

Table 4-3: Test matrix used for the BUFF test (top) and composition of test sample (bottom)

	Exercise 1	Exercise 2
No boxes	Trial 1	Trial 4
Small boxes	Trial 2	Trial 5
Big boxes	Trial 3	Trial 6

	Test Sample Information
Participant Count	9
Average Age	22.8 +/- 3.4
Composition	Students: 4 Male, 5 Female

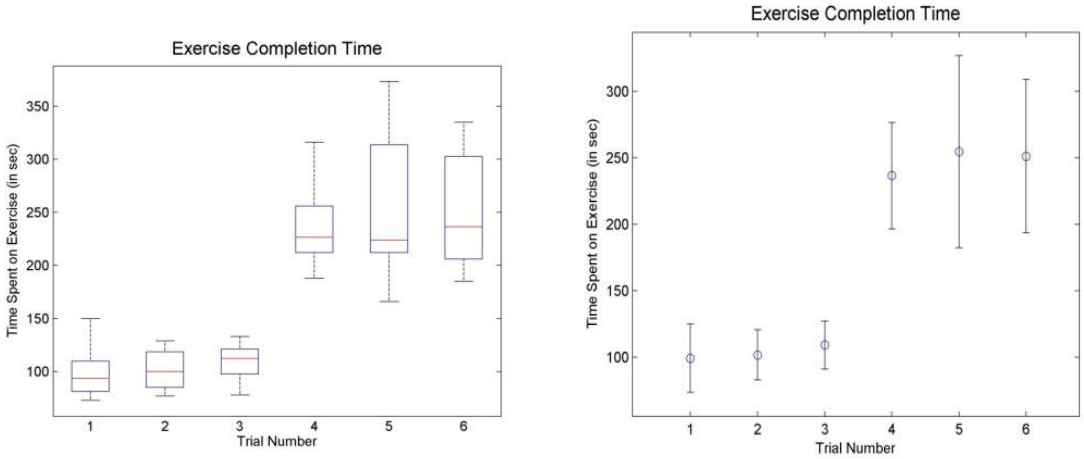

Figure 4-50: (Left) Box plot of the data, and (Right) mean and error spread of the data

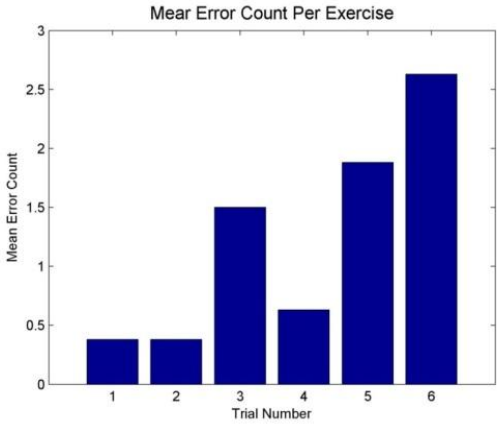

Figure 4-51: Error Count by Trial Number

An analysis of the errors committed for each exercise also showed no statistical significance, although there was a much stronger correlation between appendage size and errors as seen in Figure 4-51 and supported by the ANOVA results.

To determine if there was a correlation between speed and accuracy, as might be stated by Fitts's Law, the times for tasks one and three were plotted against the number of errors. Theoretically, there should be an overall negative correlation since a lower time would result in a higher number of errors as shown in Figure 4-52.

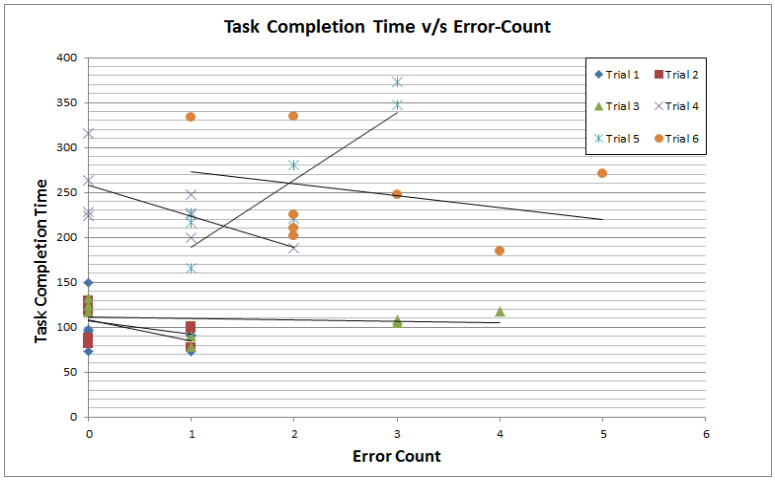

Figure 4-52: A plot of task completion time versus the number of errors committed plotted for all six trial cases for all participants. The expected negative trend is seen in five trial cases

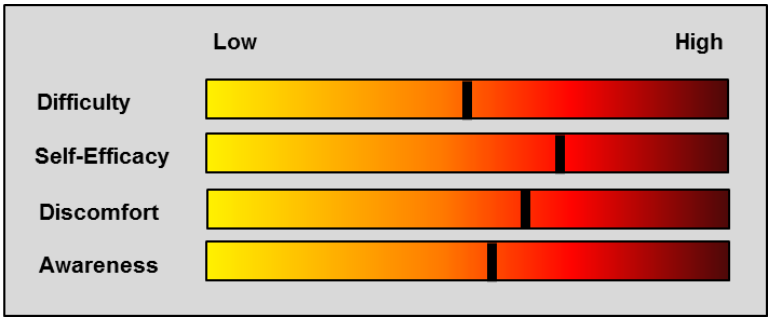

Figure 4-53: Survey results on four metrics (a) task difficulty, (b) self-efficacy, (c) discomfort and (d) appendage awareness

In addition to the performance data, a survey was administered to the participants following the test to measure their perception of how much the mock-ups affected their performance. The data were analyzed across four different factors from the questions on the survey (see Figure 4-53). The most important factor highlighted by respondents was the category of awareness. Respondents noted that they were very aware of the boxes and generally modified their movements because of them.

Although the small sample size precluded a strongly significant result, there were several important results that came from the test data, experimenter observations, and subject feedback. First, there was notable variability in how subjects performed the tasks. Some subjects were very motivated and completed the tasks very quickly while others were much more methodical and took longer to complete the task. This highlighted the importance of collecting data from a representative sample. The sample was not a very accurate representation of the population of interest. The average age of the sample was 22.8 years, and most were students; this differed from the astronaut pool which is an average of 34 years old, many of whom have over 1000 hours of pilot-in-command time in jet-powered aircraft. Upon further development of the V2Suit, testing will need to expand to include a more appropriate subject pool that is more representative.

Second, the way that participants acted during the periods in between the experimental trials was suggestive. Although there were several incidences of participants bumping into walls or objects with the boxes, the most egregious errors actually occurred in the time between the trials when the experiment was being reset. While subjects were conscious that their performance was being graded, they were generally more cautious in their movement. When they were not being graded, this caution subsided somewhat and led to more natural errors, the kind that would most likely be seen when astronauts are not cognizant of their motions.

Third, subjective participant feedback, both verbal and written, showed trends. Several participants remarked that they were more conscious of their movements and many noted that they adjusted their movements while wearing the boxes. This was very insightful because restricted or altered movement is a potential source of injury, a concern since this suit may be worn for most hours of the day and for many months or years.

A deficiency with an exercise like this is the learning component involved. Participants often took more time on the first and second trials as they familiarized themselves with the instructions on each task. While the effect of this may average out by counter-balancing the presentation of the trials, this learning component might skew the results. A way to counter this would be to have a training period using a few equivalent tasks ahead of starting the timed experiments. This was decided against since a) most people have been moving blocks around since infancy, and b) it was desired to get as many volunteers as possible by reducing the time commitment required for these trials.

The functionality test was shown to be a viable first step towards developing a rapid and easy test to determine design and sizing constraints. The newly-created BUFF Test incorporates elements of both Fitts's Law tasks and accepted functionality tests into a cognitively-challenging, three-dimensional motor control task. Initial testing shows that wearing appendages with varying volume does not affect task completion time but may have some impact on the number of errors committed by users. The task provided valuable quantitative as well qualitative data on the impact of wearing boxes while completing a time-critical task.

4.6 Brassboard Prototype Development

4.6.1 LabVIEW[2]

LabVIEW was chosen for the command and control software for the V2Suit module brassboard prototype. The IMU initialization, "down" tracking functionality, and CMG steering laws were implemented in a single framework. The LabVIEW development mirrored the MATLAB/Simulink development implemented previously for the trade study and CMG modeling and simulation.

Implementing the steering laws required establishing communication with the motion controllers (MC) that run the gimbal motors. To give the LabVIEW program correct and complete management of the gimbal motors, the steering laws were ported from Simulink to LabVIEW with the same structure. This ensured that the gimbal motors would rotate properly. Similarly to the Simulink integrated model, the down vector in the MCF and the angular velocities of the IMU were passed to the steering laws section code. The steering laws' final output in LabVIEW was the gimbal motor rates, which were then sent to the motion controller.

Within LabVIEW, a sub-Virtual-Instrument (VI) was created to manage the serial communication with the gimbal motors. The steering law calculations were also placed into sub-VIs to allow for space reduction and logical flow. Instead of using queues to pass data between VIs, global variables were used. A single file was created that stored all global variables used (Figure 4-54). The V2Suit's main VI (Figure 4-55) was only used to initialize variables, start sub-VIs, control IMU initialization, update global variables based on the user-controlled local variables, read values from global variables and display them on the UI, and control the gimbal reset types. There were no direct calculations or any major data flow to maintain simplicity and to have the main VI serve solely as a manager for the other processes. The back panel of the LabVIEW code is summarized in Figure 4-56.

[2] The V2Suit team would like to acknowledge Ostin Zarse for his contributions to the LabVIEW development.

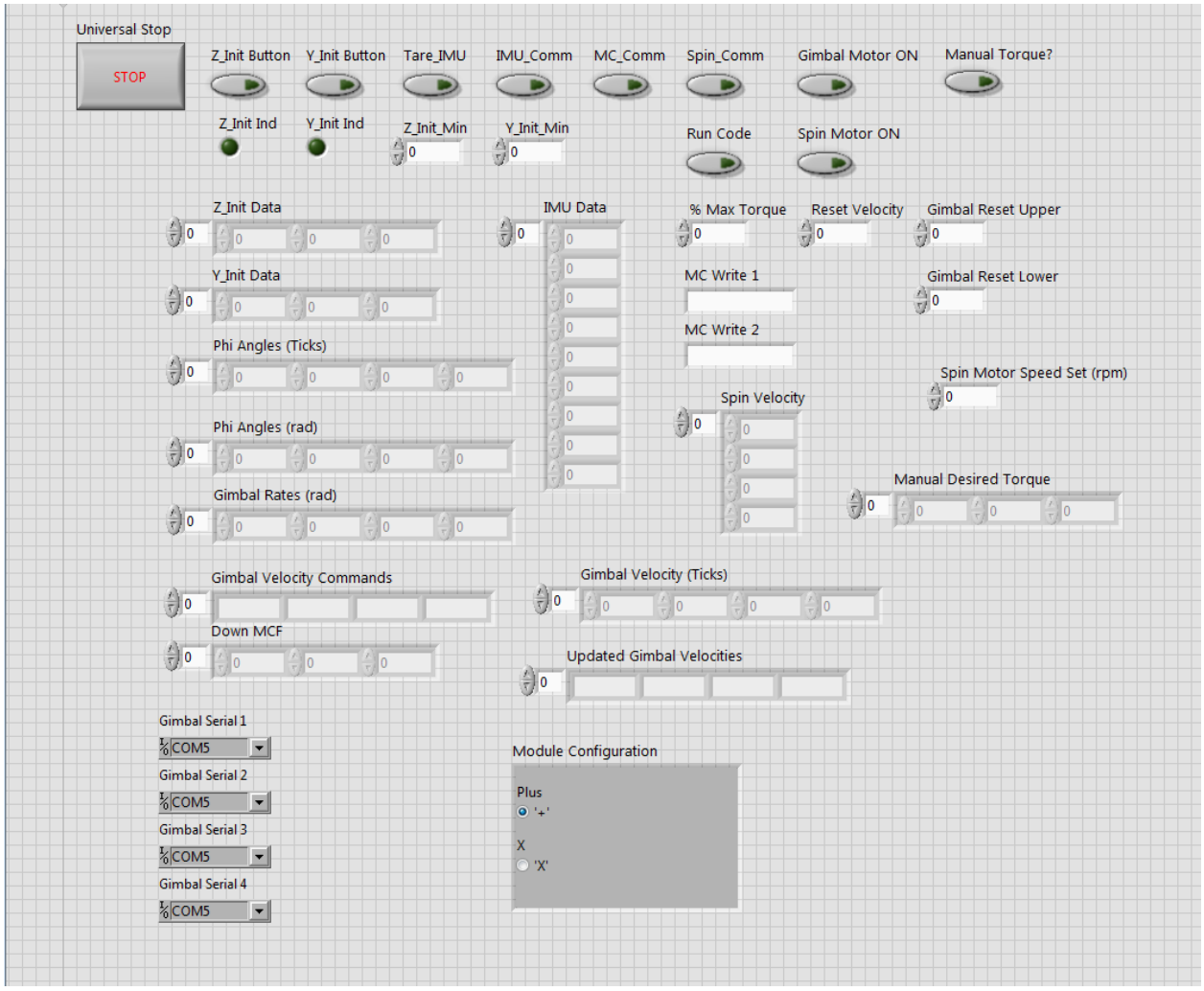

Figure 4-54: Summary of the global variables in the V2Suit LabVIEW implementation.

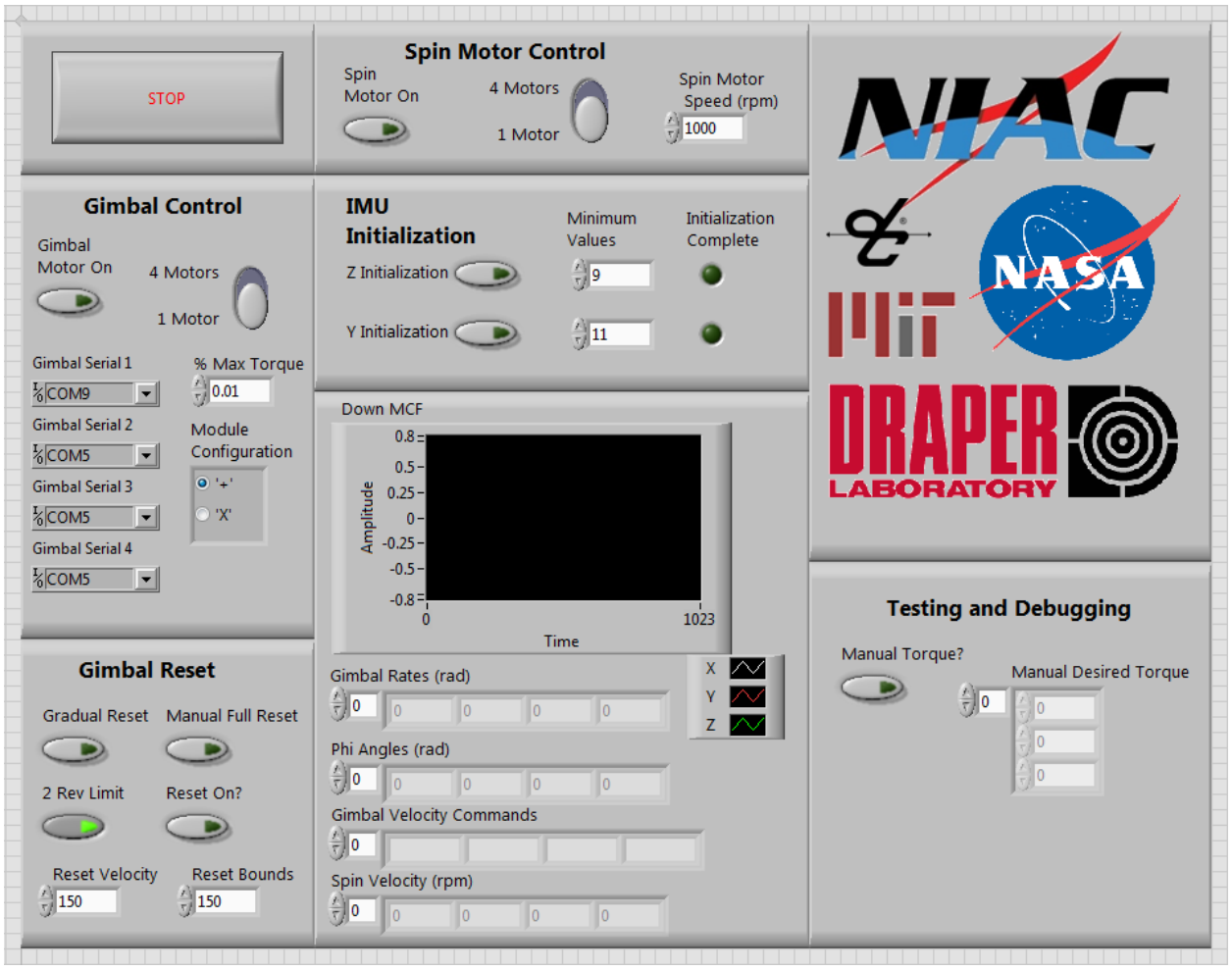

Figure 4-55: V2Suit Main VI Front Panel

Control of either of the four spin motors was added as a user input, as well as control of their velocity. An indicator was placed to display the estimated velocity of the spin motors. Part of the spin motor control VI includes estimating the spin motor velocity by reading pulses from the hall effect sensor in the motors. This measurement measures the period of the pulses and then applies the appropriate conversion factors.

COM port selection for each of the gimbal motors is available to the user. This is necessary, especially if different computers or hardware is being used. Given that the gimbal motors can be rearranged to be either in a "plus" or "cross" configuration, user control was created for an easy switch. Manual control of the desired torque vector was also made for future analysis and testing. Rather than obtain the torque vector from the down-tracking code, the steering law calculations could be fed a user specified vector.

Due to the two revolution restriction for each gimbal motor, safety margins and preventions were added to avoid any hardware damage. A reset chain, with user control, was added that first

checked if any of the gimbal motors' position exceeded two revolutions in either direction. If so, the code would stop and bring all four motors back to the zero position. If not, then user control was given for a full manual reset. If the manual reset button was pressed, all motors would return to the zero position and hold there until the button was released. If the button was not pressed, if any of the motors' velocity was less than a user defined bound, the motor would return to zero at a user defined rate.

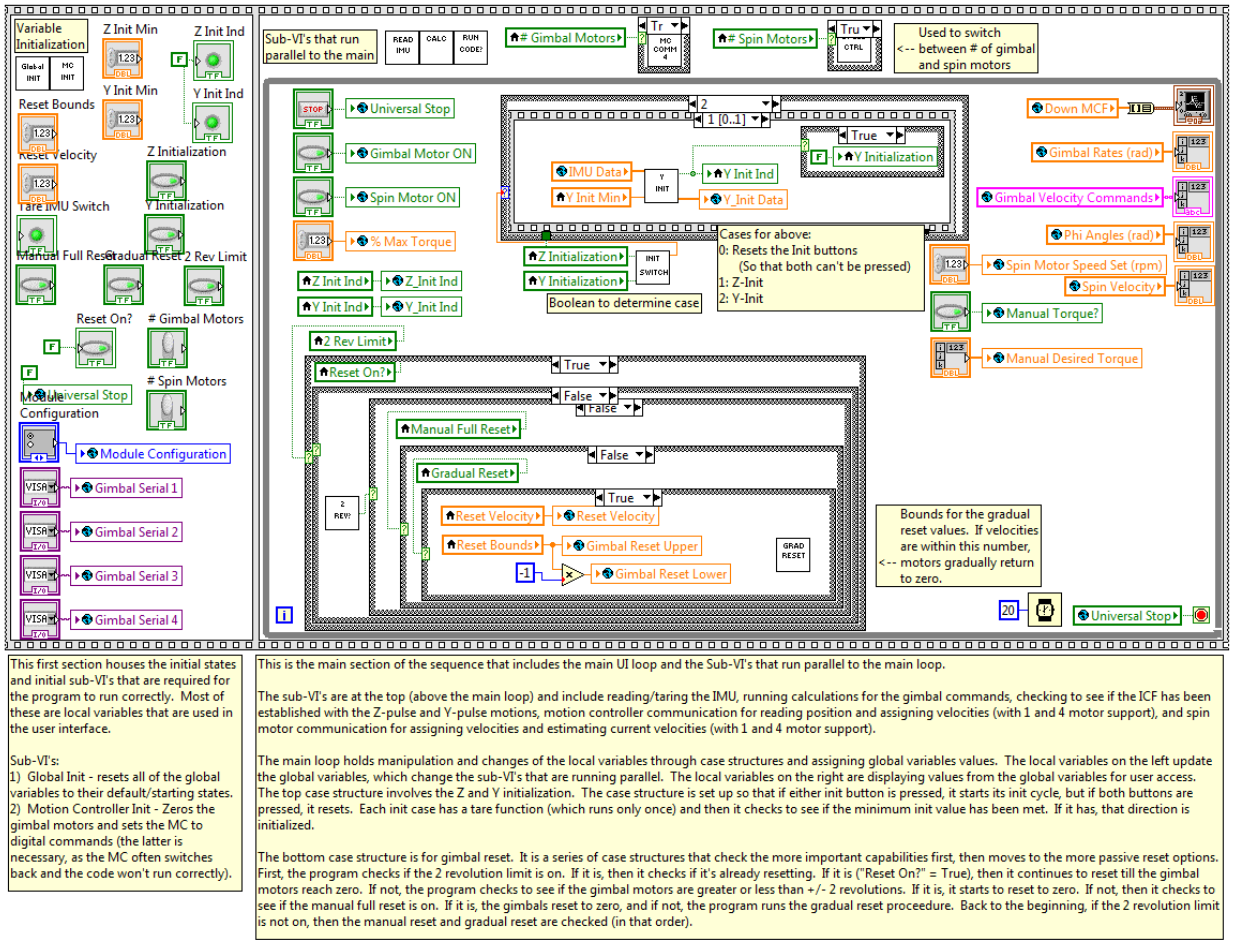

Figure 4-56: Back panel of the LabVIEW code.

4.6.2 Brassboard Unit Images

The V2Suit brassboard unit model was fabricated using commercial off-the-shelf components and custom fabrication, and integrated with the LabVIEW environment for command and control. Power was supplied from an outlet source at 12 VDC. Figure 4-57 shows the laboratory setup with the command and control PC, National Instruments chassis for LabVIEW control, and the brassboard unit within a protective enclosure. The protective enclosure was fabricated to ensure personnel safety during testing.

Figure 4-57: Brassboard unit setup in the laboratory

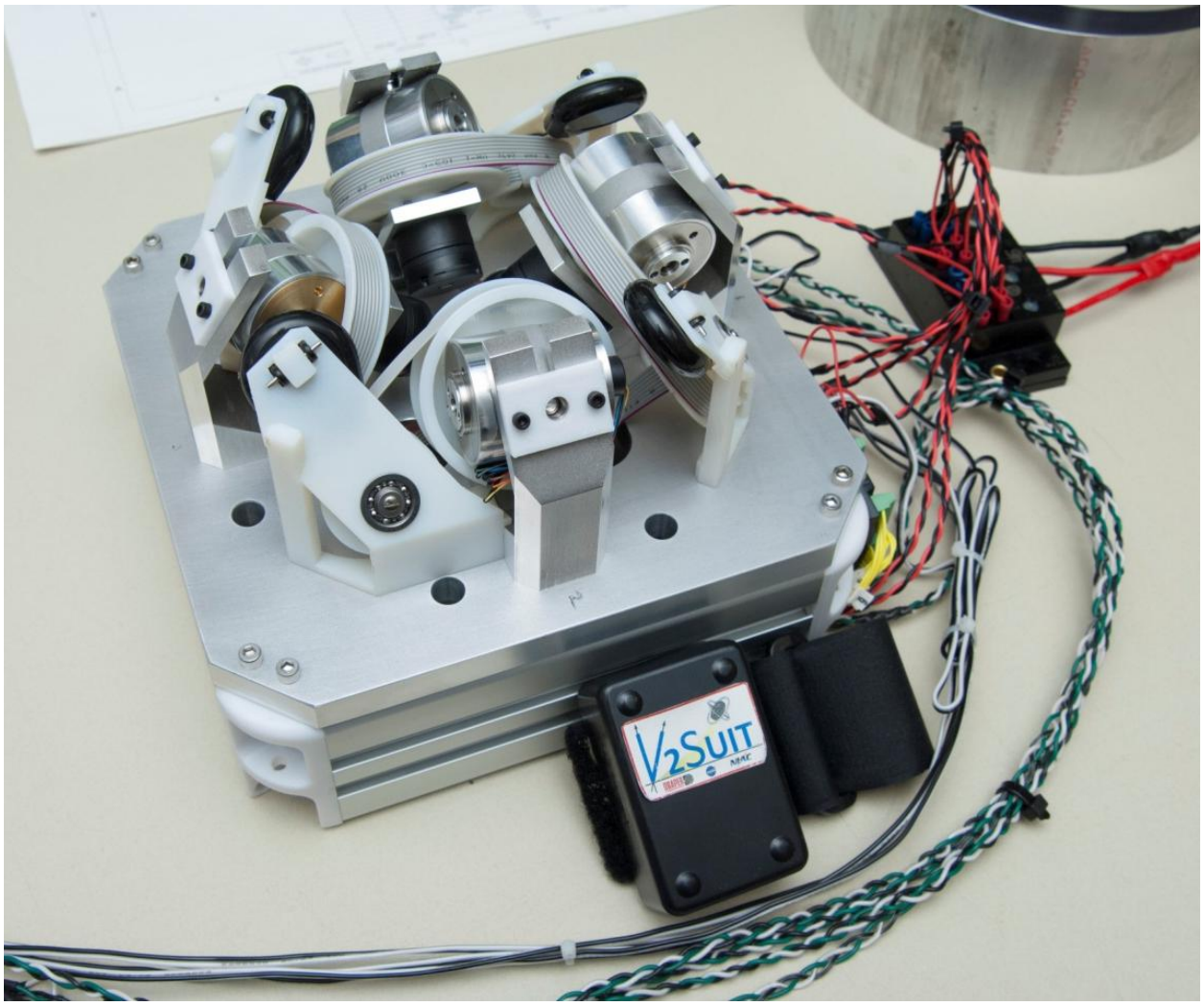

Figure 4-58: Brassboard unit without protective enclosure.

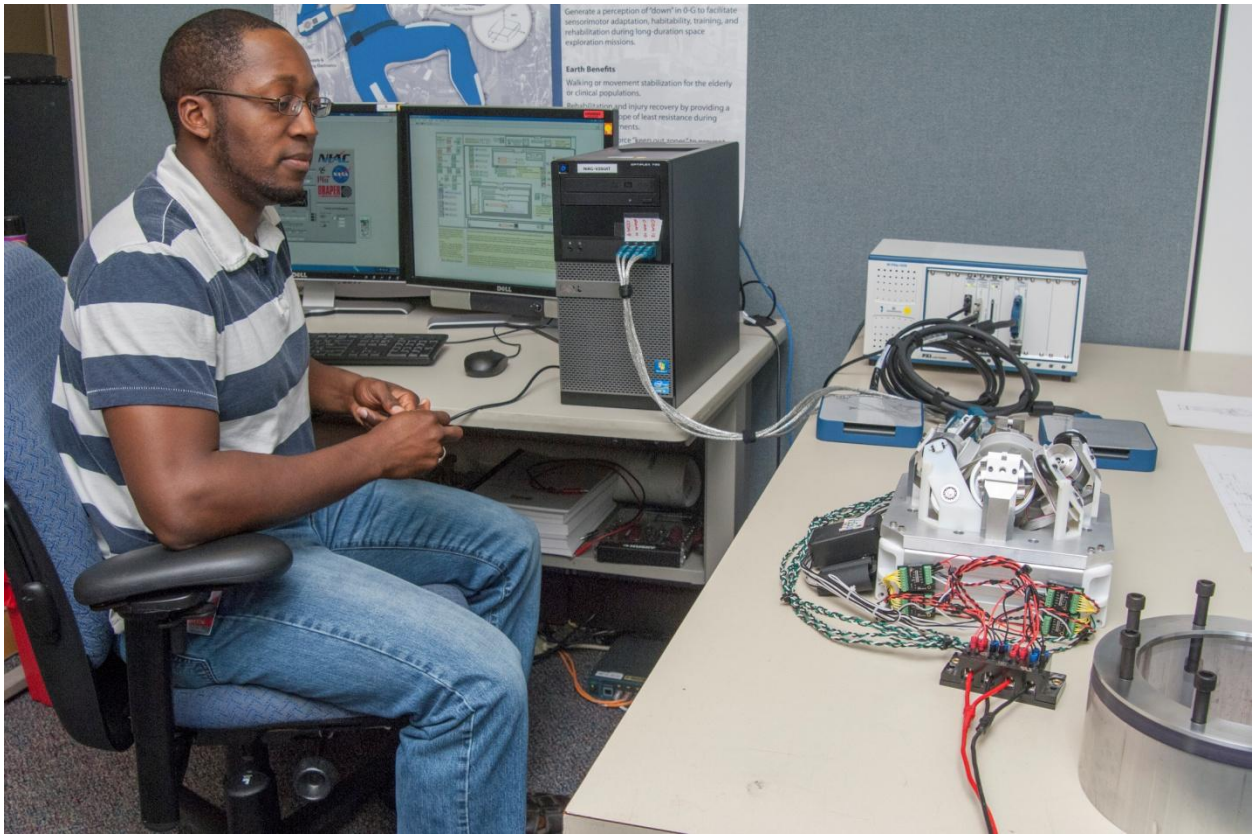

Figure 4-59: Integrated testing setup in the laboratory

4.6.3 Integrated Testing

Several preliminary testing scenarios were developed to evaluate the integrated performance of the V2Suit brassboard prototype. The "down" tracking performance was tested extensively, as summarized in prior sections. Gimbal motion as a result of initialized IMU motion was qualitatively evaluated, and initial estimates of power consumption of the unit were quantified.

Several directions of "down" were initialized, and the IMU was subsequently moved with it remotely located from the desktop brassboard prototype (see Figure 4-59). The movement of each of the CMG gimbal motors was qualitatively evaluated to assess that their motion was in the appropriate direction and magnitude to determine the desired torque (without detailed instrumentation and data logging on the unit it was not possible to record and analyze exact performance). This testing also demonstrated that the gimbal limit safety code as implemented was working correctly: the gimbals, when they reached their limit, reset to zero.

Secondly, there was an assessment of the power consumption of each of the motors when in operation. This was done by quantifying the current draw of each motor controller from the 12 VDC power supply. Initial estimates found that each motor controller was drawing 1 - 1.2 Watts, for a total power consumption of approximately 8-10 Watts per module. This is higher than desirable for a wearable system with multiple modules. However, given that the current

sizing is greater than desired and that assembly was constrained to using commercial off-the-shelf components in this study, it is reasonable to assume that the power consumption will continue to decrease as the design is further refined.

5.0 Key Enabling Technologies

The identification of the key enabling technologies is driven by the operational requirements for the V2Suit system. The integration of these key technologies into the system design is dependent on the development and demonstration roadmap (Figure 5-1). At a high level, it is envisioned that an operational V2Suit system could be ready by the 2020 timeframe, with increasing fidelity system components being developed during the current NIAC Phase II program, as well as subsequent programs. As these components are matured, they will likely be comprised of development components as well as integration of commercial technologies. Each of them will be dependent on the state-of-the-art at that point as well as the V2Suit technology needs. In this section, we detail each of the Key Enabling Technologies and provide individual development roadmaps against the overall V2Suit vision.

Collectively, these high-level operational requirements map to four key enabling technologies that are required to realize a fully operational V2Suit:

- Miniature control moment gyroscopes
- Motion tracking technology and algorithms
- Human-system integration
- Power source technology

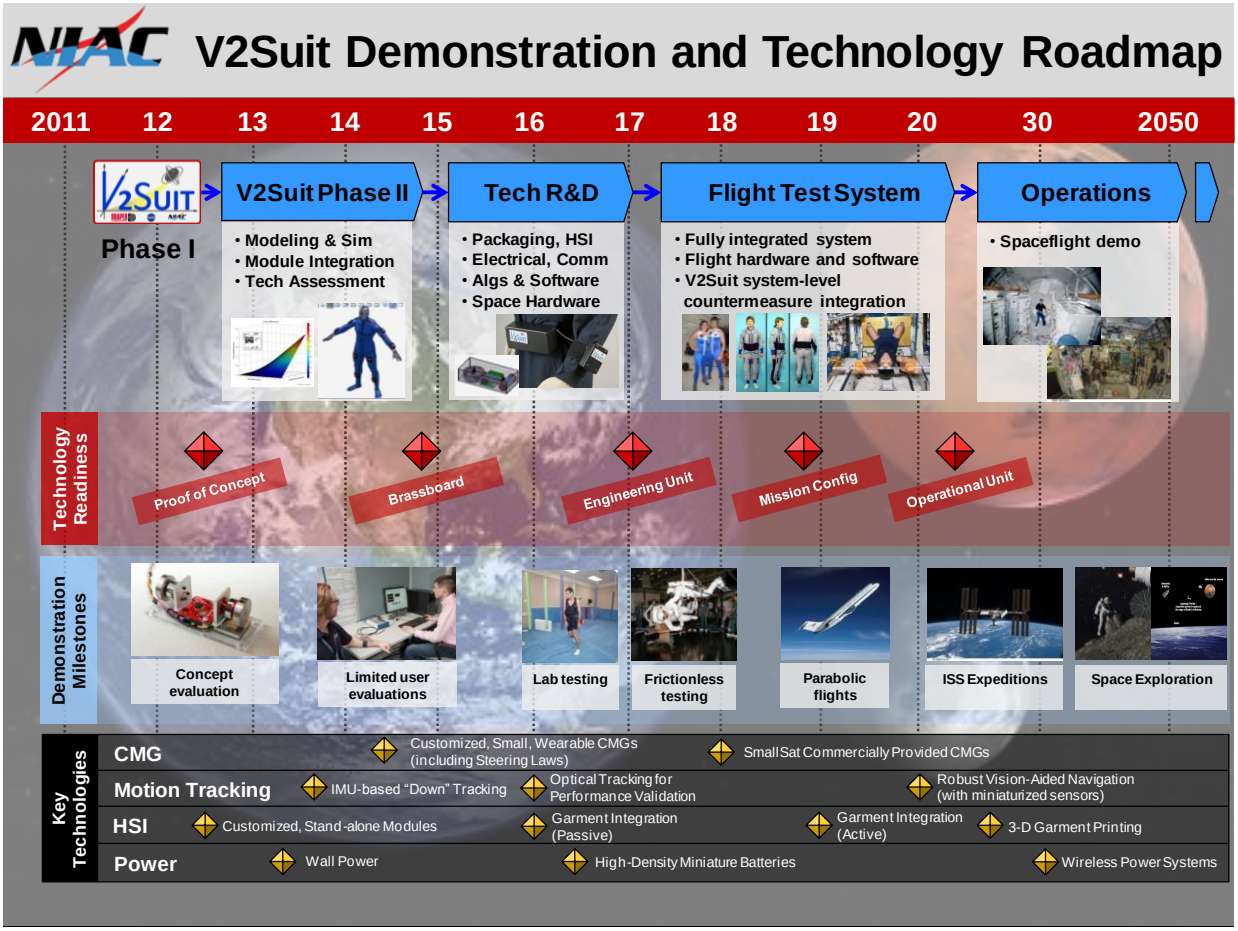

Figure 5-1 – Overall V2Suit Demonstration and Technology Roadmap

5.1 Miniature Control Moment Gyroscopes

Miniature control moment gyroscopes – the hardware and control algorithms (steering laws) – are a key enabling technology for realizing the V2Suit system [Requirements CR-1 and CR-2]. The CMGs are the central technology for providing the viscous resistance to movement, and thus enabling a countermeasure system to the sensorimotor adaptation that occurs during spaceflight.

Technology Need

The V2Suit design utilizes body-worn control moment gyroscopes that are actuated to point the gyroscopic torque vector in the specified direction to resist movement. These CMGs must be miniaturized to fit within the wearable module V2Suit form factor, and the control algorithms must point the torque vector in response to body movements, while simultaneously preventing singularities and momentum saturation. We aim to provide a gyroscopic torque that is at least 0.1 Nm in the specified direction, which is based on prior work that has determined this to be an acceptable magnitude for both being perceptible and affecting limb biomechanics [69].

Background & Design Alternatives

CMGs are comprised of many components to enable their actuation and the resultant pointing of the gyroscopic torque vector (see Figure 5-2). The selection of the specific components and their resultant packaging is dependent on the CMG architecture, which includes both the hardware and the steering laws. The results of the V2Suit NIAC Phase II integrated CMG trade study (architecture and steering laws) determine that a four CMG pyramid configuration enables the greatest torque envelope given the wearable sizing contraints. The architecture and component selection will be based on the performance of the integrated simulation in maintaining the gyroscopic torque vector in response to the commanded direction from the "down" tracking algorithm during representative arm motions.

Challenges

The CMGs-related challenges for the V2Suit are comprised of both the miniaturization of the components/packaging as well as the steering laws (control algorithms) to actuate the CMGs and point the torque vector in the appropriate direction (see Figure 5-2). Each are key challenges that must be addressed through development and technology integration.

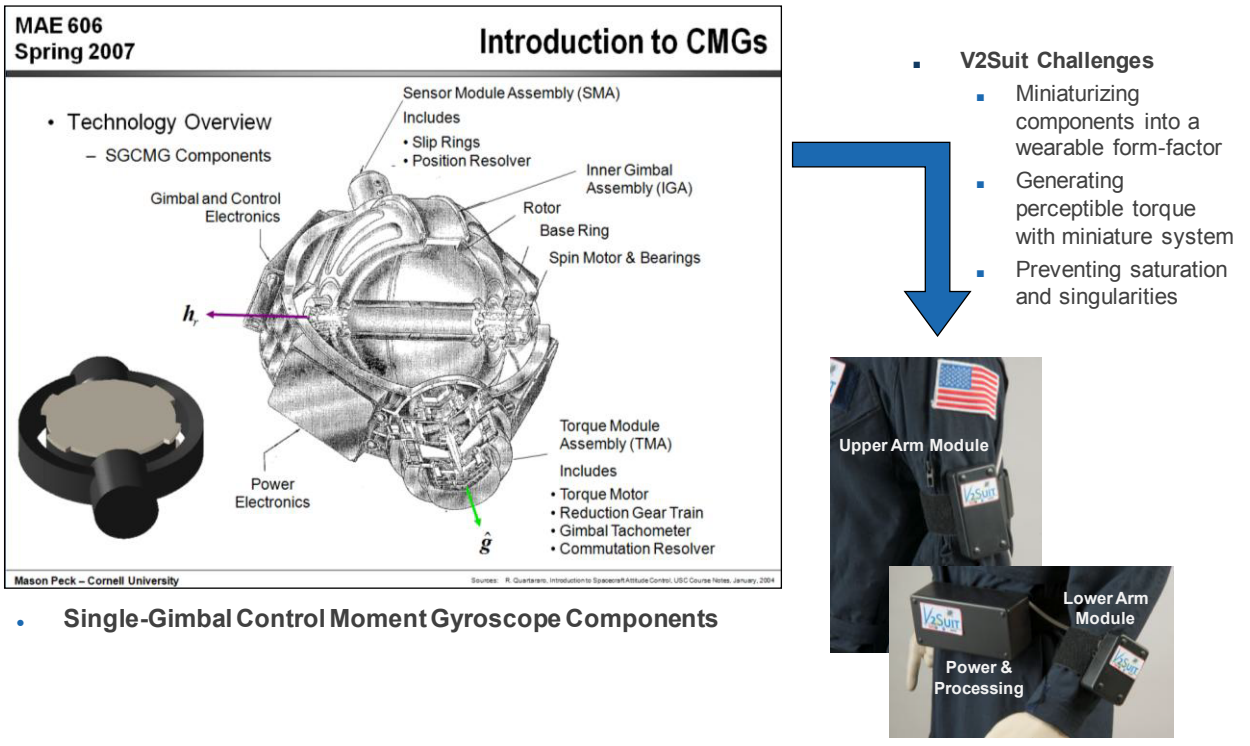

Figure 5-2 – CMG Components and V2Suit System Challenges

The challenge will be to determine the required architecture paired with either commercially available components, or required development activities to package the unit within a low-profile wearable form factor. Existing small CMGs are sized approximately for a CubeSat, and have a volume that is too large for a body-worn form factor (e.g., Honeybee Robotics Tiny

Operationally Responsive CMG (TORC)[3]). Since the V2Suit is proposing to use CMGs in a manner that has not been rigorously considered before, and the required torques are estimated to be less than that required for a satellite system, the V2Suit requirements could push that state-of-the-art in the miniaturization of CMG designs and packaging.

Additionally, the CMG steering laws must accurately, and reliably: 1) point the gyroscopic torque in the specified direction, 2) avoid torque singularities, and 3) avoid momentum saturation. These challenges must be addressed when designing the control algorithms for the specific CMG architecture.

The steering laws will receive a desired direction to point the gyroscopic torque vector from the "down" tracking algorithm. This algorithm will track the orientation and velocity of each wearable module, and then specify torque (direction and magnitude) to resist body movements. Additionally, any module movements that have an angular velocity component will induce additional gimbal rates and (potentially) provide out-of-plane torques – referred to as "base rate effects". These torques could result in resistances that are not aligned with the specified "down" direction, causing potentially distracting motions for a sensorimotor adaptation countermeasure. The steering laws must also take these into account when sending the actuation commands.

Torque singularities occur during CMG operation when the flywheel gimbal motion results in an orientation that produces no net torque in a certain direction. These singularities can be overcome through a combination of steering law design, CMG arrangement/architecture, and/or methods to provide an external torque on the system (e.g., thrusters). For the V2Suit, this is important from a resistance magnitude perspective. If, for example, there are certain points along a movement trajectory where a singularity occurs, there could be a "choppy" feel when the torque zeroes, and then re-appears.

Thirdly, during active attitude control maneuvers, the CMGs may saturate by reaching either gimbal or rotor spin limits. This results in a degradation of available attitude control authority. In spacecraft, the attitude system, including the CMGs, will employ methodologies to prevent the saturation. External torques – such as those from thrusters – may be used to de-saturate the CMGs (i.e., bring the momentum back to the nominal value). This is particularly important in a) scissored pair or pyramid configurations where the gimbal angle is limited, or b) variable speed configurations or reaction wheels that have a limit on spin rate. CMG saturation has a similar effect on the resistance perception for the V2Suit. However, instead of it being a (potentially) momentary zeroing of the torque, there could be an extended reduced torque, or a torque in an inappropriate direction.

Since the V2Suit module design only includes CMGs for generating torque each of these challenges – component miniaturization/packaging and steering laws – must be addressed.

[3] http://www.honeybeerobotics.com/aeromechanical-systems/12-cmg

There currently exists no mechanism to generate an external torque to de-saturate the CMGs or prevent singularities. The complex and continuous body motions during daily activities require robust steering laws to maintain the required torque magnitude in the specified direction, such as being active to provide the resistance to movement as well as sensing quiescent periods to reset the CMG internal states to be ready for subsequent movements. Therefore, the integrated system of tracking the module orientation and motion, along with the CMG control algorithms is necessary to both prevent singularities and saturation to effectively generate the gyroscopic torque to provide the viscous resistance to movement.

Roadmap

The V2Suit CMG Key Enabling Technology roadmap includes both development specific to the V2Suit system as well as the potential integration of commercially available technology. In particular, we aim to initially develop the miniature CMGs and steering laws for prototype and engineering evaluation. Concurrent discussions with commercial CMG providers will allow for assessment of the state-of-the-art, with the opportunity for technology insertion. Over the duration of the V2Suit development roadmap, there is the opportunity for multiple spirals of system development, including the integration of CMG technology and subsequent versions of the steering laws for commanding the array.

5.2 Motion Tracking Technology & Algorithms

The ability to specify and initialize a direction of "down" in a weightless environment, and then track the orientation and motion with respect to that direction is critical to the operation of the V2Suit [Requirement CR-1]. The components that enable this "down" tracking are one of the key enabling technologies for V2Suit implementation and operation.

Technology Need

Commanding of the CMGs to provide a viscous resistance to movement requires knowledge of each of the V2Suit's modules orientation and motion with respect to the specified direction of "down." Operationally, this knowledge should be independent of any external system – enabling the V2Suit to be a stand-alone countermeasure system that is not dependent on the surrounding environment. The performance bounds for knowledge of the state of the module with respect to the specified "down" will be dependent on the perceptible limits from operator evaluations. However, our initial design goal is to maintain knowledge of each module's orientation within 5 degrees of truth, and the ability to sense linear velocities of at least 2 cm/s.

Background & Design Alternatives

Knowledge of the orientation and motion of each of the wearable modules (within the specified performance bounds) with respect to the initialized direction of "down" is critical for the commanding and actuation of the CMGs. There are several technologies, including wearable inertial measurement units (IMUs) (wearable kinematic systems), optical tracking, and vision-

aided navigation systems that can be considered for solving this challenge. In fact, multiple technologies must be employed for characterizing and calibrating performance. For example, a wearable IMU and its "down" tracking performance will need to be characterized against the "gold standard" of motion tracking – an optical system. However, each of these systems cannot be integrated or leveraged without understanding the challenges associated with them.

Table 5-1 – Motion Tracking Technology Options

Technology Option	Description
Inertial Measurement Unit (IMU)	•Integrated accelerometer and gyroscope for measuring linear accelerations and angular velocities.
Optical Tracking	•Multi-camera based system for tracking the position of reflective markers that are placed on the object of interest.
Vision-Aided Navigation	•Camera-based system for determining location and pose of a user with or without *a priori* knowledge of the environment.

IMU

Optical Tracking

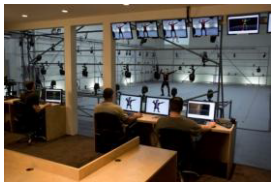

Vision-Aided

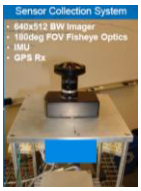

Inertial measurement units (IMUs) provide high-bandwidth linear acceleration and angular rate data, are small, lightweight, often are an integrated system, can operate wired or wirelessly, and are relatively low cost. This enables them to be easily integrated into each of the V2Suit modules. Additionally, kinematic measurements (e.g., limb velocities, body angles) derived from wearable IMUs offer tremendous opportunities to study the biomechanics of human motion outside of laboratory and clinical settings, such as those required when using state of the art optical motion capture systems [51, 70]. Nonlinear Kalman filters, such as the extended Kalman filter (EKF) [71] and the unscented Kalman filter (UKF) [72], represent a class of fusion algorithms that can correct for the drift and integration errors, while providing absolute unit estimation during representative biomechanical movements. Recent work has demonstrated the effectiveness of this technique for tracking orientation of the torso [73] and orientation of the hand [74]. Regardless of the hardware and estimation filter, the performance effects due to sensor drift and/or long-term integration errors must be quantified and accounted for in the system design to ensure adequate performance during extended operation of the V2Suit.

Optical tracking systems are widely utilized in the research and animation communities (see Figure 5-3). The most widely available systems required reflective markers to be placed on an object or person to be tracked via an array of (infrared) cameras to determine the three-

dimensional position of each marker at each sample interval. These systems will generate very precise position measurements of the marker with a well calibrated system; typically no drift errors, relatively high sample rates, and minimal burden on the wearer. Conversely, they are expensive systems that often require a large volume with multiple cameras and markers to get marker position estimates during natural movements. Because of their constraints on the environment, and specialized equipment to be attached to the wearer, they typically are not used in real-time systems. However, their relatively ease of setup and use along with precise measurements make them an ideal candidate to calibrate the measurements and calculations coming from both the V2Suit internal IMU and the outputs of the "down" tracking algorithm.

Figure 5-3 – Example optical motion tracking setup and infrastructure. (www.creativeplanetnetwork.com)

Vision-aided navigation systems are becoming increasingly researched and adopted. These are optical-based systems that analyze scene images to correlate them with a known database to determine location and pose [75]. In integrated systems, the output of the vision-based algorithms may be integrated with an IMU and/or GPS to enhance navigation accuracy [76]. Since the output of these systems can be integrated with IMU results, they can easily be used to correct for sensor drift and improve navigation accuracy. Their implementation can also either track against an a priori generated model of the environment (vision aided inertial navigation), or create an environment model in real-time that can then be tracked against (simultaneous localization and mapping). Regardless, these systems are computationally expensive and the required optics and performance of the cameras can be a challenge to integrate with small, wearable modules such as those proposed for the V2Suit.

Challenges

The principal challenge that a robust motion tracking technology and algorithm will address is the V2Suit "down" tracking element (Figure 5-4). "Down" tracking is required to estimate the orientation and velocity of each wearable V2Suit module with respect to the specified direction of "down." The output of the algorithm provides an input to the CMG algorithms to point the gyroscopic torque vector. The "down" tracking algorithm has been designed such that it receives filtered states (linear acceleration, angular velocity) from the local motion tracking data. It tracks multiple states of the V2Suit module in multiple coordinate systems, for both CMG control and

post-operation analysis (as an engineering tool).

To enable V2Suit operations without erroneous CMG commanding, the "down" tracking algorithm must operate in real-time, receive sensor data with little- or no errors, maintain knowledge of each of the individual module states, as well as their collective states of the modules and core body movements. These challenges can be addressed through hardware selection/implementation or through algorithm development.

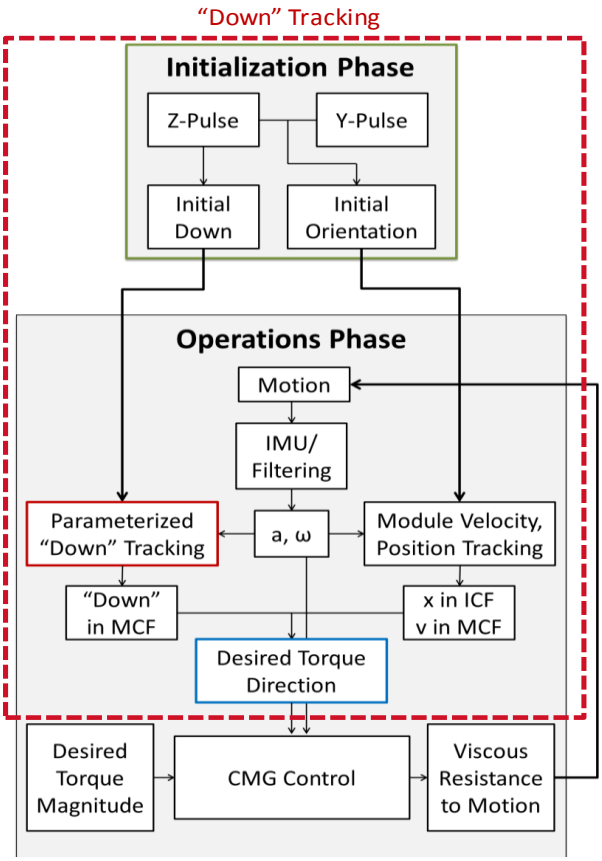

Figure 5-4 – V2Suit "down" tracking element in context of the high-level architecture.

The real-time aspect is important for commanding the CMGs in sufficient time so that there are no perceptible lags between movements and actuation. IMUs provide high-rate data with minimal delay. However, they are susceptible to performance drift and integration errors. Most commercially available systems incorporate filtering algorithms with their sensors – providing an integrated solution. However, they are still susceptible to state estimation errors after extended duration operation. In order to continually provide the appropriate commanding of the CMGs during V2Suit operation, accurate knowledge of the module orientation and motion must be estimated. Validation of these systems will be critical with "ground truth" estimates to determine the magnitudes of the errors and how they propagate over time. These performance specifications will determine the operational time between re-initializing "down."

Lastly, the V2Suit integrated modules must be able to differentiate between whole body movements, and individual limb movements. In the case of when the body core is relatively stationary, the modules must be actuated to provide the resistance to movement in the specified direction. However, when there is whole body translation the central processing will only provide CMG actuation commands to motions that deviate from the whole body movements.

The "down" tracking algorithm is a central technology to the V2Suit system. Therefore the development of the integrated algorithm and motion sensing technology is a key enabling technology. Wearable IMUs are a leading candidate for integration into the system. However, their performance needs to be characterized in the context of the "down" tracking algorithm as well as against "ground" truth to determine the performance envelope for perceptual estimates and determining the time between "down" re-initializations.

Roadmap

Key Enabling Technologies for the motion tracking technology and algorithms are primarily driven by the need for the "down" tracking algorithm performance. The baseline design includes the integration of an IMU into the V2Suit wearable modules, and validation of its performance through optical tracking systems. The performance of wearable kinematic systems, including both the IMU and filtering techniques, provides sufficient navigation accuracy of the modules for laboratory development and test of the "down" tracking algorithms. Future technologies could include vision-aided navigation as well as additional technologies, such as Draper Laboratory's Precise Positioning System (PPS)[4,5], for body motion tracking and improved navigation accuracy.

Figure 5-5 – Top: Contoured plate (lace-in and double-strap versions) (courtesy of David Clark Company Inc.), Bottom: Concept of V2Suit module placement.

5.3 Human-System Integration

The interface with the human wearer is important for the operational implementation of the V2Suit. For the V2Suit to be effective as a countermeasure system it must efficiently transmit the CMG torque to the wearer, all while minimizing the burden for putting on/taking off [Requirement CR-3], and performing activities with the modules attached for an extended duration of time [Requirement CR-2].

Technology Need

The V2Suit must be able to efficiently transmit the CMG-generated torque to the wearer during movements, as well as be comfortable to wear and easy to put on/take off. There is a need for conformal, comfortable V2Suit modules that can integrate with a shirtsleeve environment, or existing intravehicular activity (IVA) suit/garments, and minimize relative motion between the

[4] http://www.draper.com/tactical_gnc.html
[5] http://defense-update.com/products/p/pps_nav.htm

module and the body. A system that is easy to don/doff, comfortable and does not negatively affect performance is more likely to be adopted and used by the crew.

Background & Design Alternatives

There are several design approaches to creating the V2Suit modules so that they conform to the shape of the limb to which it is attached, are comfortable, easy to attach/remove, do not interfere with activities, and effectively transmit the torque to affect limb loading (Figure 5-5). At a high level, there are two categories: stand-alone modules, and those modules that are integrated with wearable garments.

Stand-alone wearable modules contain the CMGs, IMU, and control electronics. They are a self-contained individual enclosure that has a contoured plate and an adjustable strap to secure it to the limb. The limb may be bare or have a standard garment between the skin and the module. To minimize relative motion between the module and the limb, it is likely that the contoured plate would be customized to the wearer. However, based on evaluations it may be determined that standard sizes of contours (e.g., S, M, L, XL) could be developed and leveraged. The power and data communication cables will be run along the body, secured by additional straps (when necessary), and connected to the central power and processing module. The ability to customize to the individual wearer has many benefits. However, this is also a challenge, along with cable management and module placement and fitting.

Integration of the modules, module attachments, and all required power and data cabling with existing, wearable garments offers many advantages. In this configuration the modules (or at least their attachment base plates) (see Figure 5-5) would remain on the wearer as long as the garment is on. The interface with the human could either be passive (maintain rigid attachment via garment compression or tensioning straps) or active (external activation of tensioning). It is envisioned that this approach would ease donning/doffing and facilitate a quick transition from quiescent /standby mode to operations. Two example attachment mechanisms for the modules include a baseplate that can be laced-into garments, or one with a double-strap attachment (see Figure 5-5, top). In this configuration, the V2Suit module would have the mating plate attached to it so that the two would mate and provide a rigid attachment to the wearer.

Several garments have been developed and used operationally that provide means to prevent physiologic adaptation to spaceflight, or facilitate the transition back to a gravitational environment following living and working in weightlessness. These garments, such as the Skylab Orthostatic Intolerance Garment (OIG) (Figure 5-6), Russian Penguin Suit (Figure 5-7), or the MIT Gravity Loading Countermeasure Suit offer garment platforms for integrating the technology for a wearable V2Suit module that limits relative motion, to efficiently transfer the CMG-generated torque to the wearer. In the case of use of a Skylab OIG-type system, it could be worn lose throughout the day, but when you want to activate the modules you could also activate the garment to tighten it up in the necessary locations. This would be achieved via a

simple capstan-type system with an inflation bulb, so it would not require power or a compressed air source. It would be designed to apply the minimum pressure to hold the module tight and minimize relative motion.

In the Figure 5-5 example configuration, each of the V2Suit modules would include a contoured baseplate that has a quick-connect/disconnect with the main module. The baseplate and associated inter-module cabling would be integrated with the garment. There would be two available tensioning mechanisms – 1) a passive system such as elastic and/or Velcro straps for initial tensioning to maintain the conformal attachment, and 2) a pseudo-active system such as an inflation bulb to increase the rigidity of the attachment just prior to activation. Depending on the final size of the modules, they could be continuously worn or would reside in a docking module and attached to the suit via the baseplate connect mechanism prior to operations. The final determination of the attachment approach will be determined, in part, by the size of the modules and preliminary user evaluations.

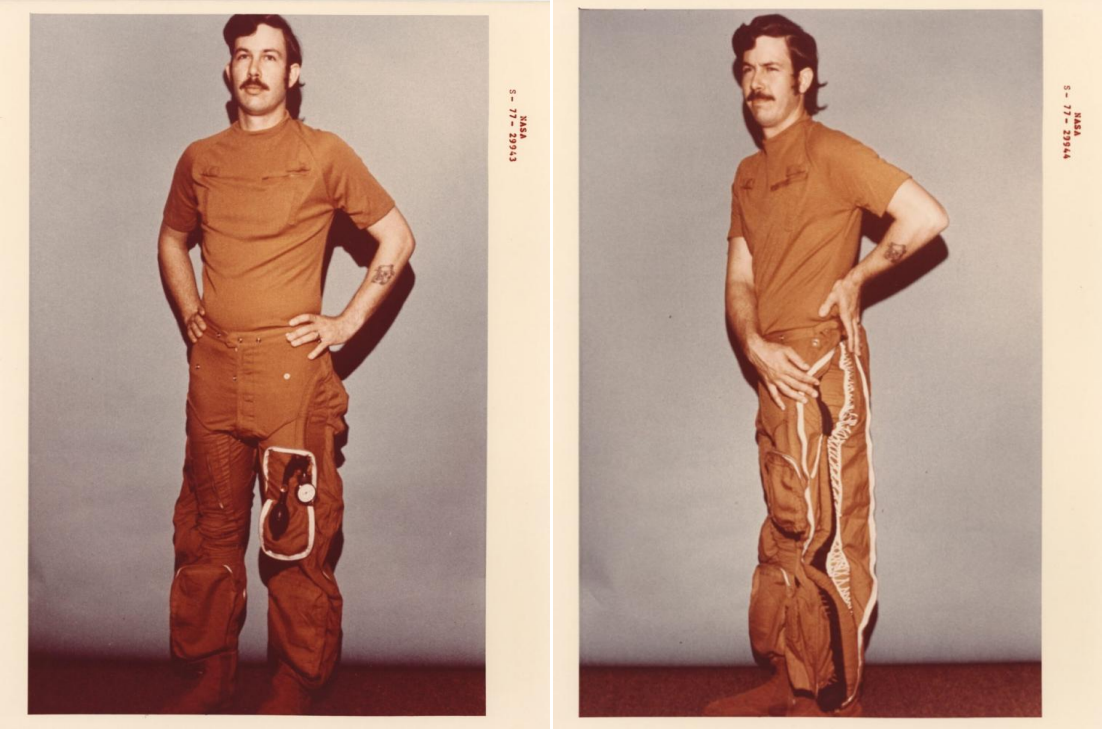

Figure 5-6 – Skylab Orthostatic Intolerance Garment

Figure 5-7 – ISS Expedition 36 crewmembers wearing the Penguin Suit

A future technology that could create fully-customized garments and ensure the V2Suit modules efficiently transmit the torque to the wearer is printable garments. 3D printing of garments is a conceptual technology that is beginning to come online in some areas (Figure 5-8). This technology has the ability to customize the garment and attachment locations to an individual person. The ability to blend comfortable, athletic-type clothing with more rigid segments at or near the site of the V2Suit module attachment offers many advantages for reducing the complexity of the module human-system integration. In addition, the physiologic changes occur over time in space (e.g., fluid shift, weight loss, muscle size and volume reductions) could be accommodated with replacement printing of the garments, as well as replacement due to normal wear and tear. The increasing use of 3D printing technology on Earth, coupled with the plans to send a 3D printer to the ISS[6], make the inclusion of this technology in the roadmap a plausible concept to minimize some of the risks associated with the module human-system integration.

Figure 5-8 – Printable garment conceptual design **(http://jhharris.prosite.com/104313/973830/work/design-for-2050-clothing-printer)**

[6] http://www.madeinspace.us/made-in-space-and-nasa-to-send-first-3d-printer-into-space

Challenges

The key technology challenges to develop an operational system include: easy put on and take off, be comfortable to wear over extended durations, and have small and low-profile as to not interfere with normal movements -- all while providing the desired functionality. In addition, the modules must not interfere with normal, daily activities when worn and non-operational. This requires a small form factor that can be integrated with normally worn garments – either as an add-on to existing equipment or designed to be an integral part of the garment.

Two of the V2Suit operational requirements map to the human-system integration key enabling technology: 1) the worn V2Suit must be comfortable and unobtrusive during at least 8 hours of wear (Requirement CR-2), and 2) take less than 5 minutes to put on or take off (Requirement CR-3). Meeting these requirements, and being an effective countermeasure system requires these technology solutions, and are dependent on the final V2Suit module design and form factor.

Since this system is envisioned to facilitate spaceflight adaptation and maintain human health and performance during long-duration missions, human-in-the-loop evaluations will be critical or the determination of the acceptable form factors, magnitude of acceptable relative motion between the module and the body, and the comfort and garment integration for extended wear and operations. Throughout the development process, prototyping of garment integration concepts with representative module sidings and inertia properties will be critical for the final implementation.

Roadmap

The V2Suit initial laboratory development units will be stand-alone modules. The long-term operational system will be an integrated garment – incorporating the lessons learned from module design and packaging as well as user evaluations. Longer-term technologies that could enhance the human-system interaction, such as active garments and 3D printed garments, will continually be surveyed and the technology benchmarked against the V2Suit system needs. The goal is to have a garment that has all the baseplates in place, all wired together with the wires integral to the garment (e.g., reducing snag hazards), and all one has to do to use the system is snap in the modules, makes sense operationally. With these modules part of garment, they're right where they need to be every time -- just connect and operate.

5.4 Power Source Technology

To realize the V2Suit as an operational countermeasure system, it must be able to operate without attachment to an external power source [Requirement CR-4]. Therefore, a wearable power source that can power the computing, sensing and actuation electronics, including the CMGs, is a key enabling technology.

Technology Need

In the weightless environment of spaceflight, the V2Suit must be able to operate for an extended duration of time in order to be an effective countermeasure. It must also facilitate operation while free-floating, without the encumbrances of a wire power connection. Therefore, small, re-chargeable, high-density power sources with a long useful lifetime are needed. The power source must be able to power and actuate the V2Suit components for at least one continuous hour of operation between charges [Requirement CR-4].

Background & Design Alternatives

Small, re-chargeable, high-energy density power sources (e.g., batteries) are required that can either reside within each of the V2Suit modules, or a single centralized source in the central power and processing module. The power source must be able to power the electronics and actuate the components within the modules for at least one continuous hour between re-charges. Existing technology offers a number of options from conventional outlet power, commercial batteries, to wireless power sources.

Conventional outlet power sources are the most trivial of the enabling technologies, but they provide the required energy for laboratory development and test. By connecting the equipment to a 120V 60Hz alternating current power supply in the laboratory, we have a conditioned power source with virtually unlimited operational duration – a requirement for early stage research and development. It does have limited extensibility to future V2Suit operational scenarios, such as a limited operational volume, cable management, and constraints for living and working in a weightless environment.

Batteries are the most common portable energy device. They consist of one or more electrochemical cells that convert stored chemical energy into electrical energy. Recent advances in battery storage technology have increased the energy density (energy per unit mass/volume) (see Figure 5-9), which as in turn increased the portability and operational duration of many electronic devices. The most promising battery technologies for the V2Suit include Nickel Metal Hydride (Ni-MH), Lithium Ion/Lithium Polymer, and a future technology of Metal-Air (Figure 5-10).

- NiMH. NiMH batteries are a rechargeable power source. Compared to lead-acid battery, NiMH battery has longer lifespan and better high-rate charge and discharge characteristics. And, compared to lithium batteries, NiMH battery is a more mature technology with more advantageous cost competitiveness[7].
- Lithium. Lithium polymer (LiPo) batteries evolved from lithium-ion batteries, and have a lower cost of manufacture, adaptability to a wide variety of packaging shapes, reliability, and ruggedness, with the disadvantage of holding less charge. It's noted

[7] http://www.energytrend.com/research/Lithium_Roadmap.html

that they are applications where small form factors and energy density outweigh cost considerations.[8]

- Metal-Air. Metal-air batteries have a very high theoretical energy density. Lithium-air and zinc-air batteries are recognized as the most likely candidates for next-generation secondary batteries for electric vehicle applications.[9]

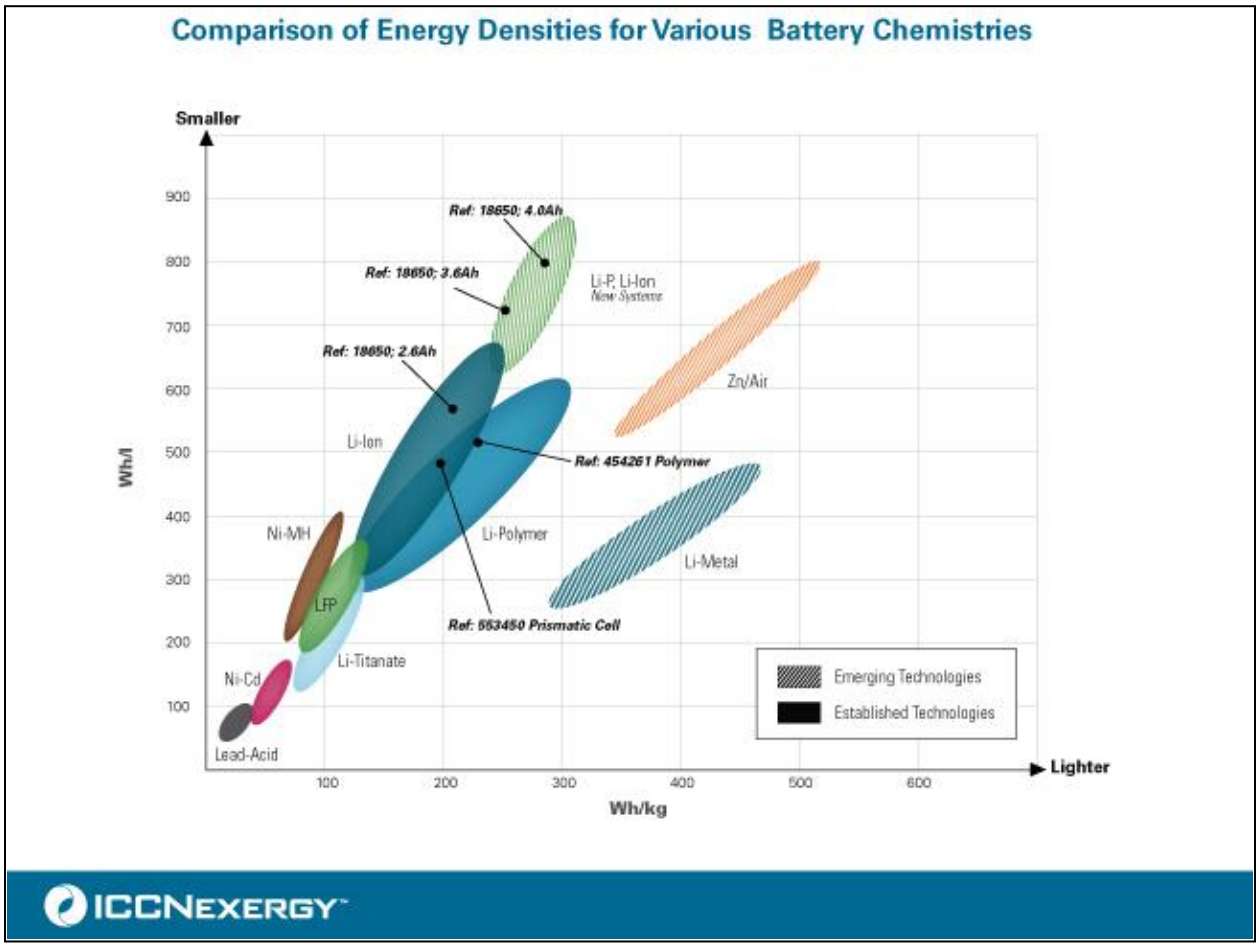

Figure 5-9 – Battery Energy Densities [credit ICCNexergy]

[8] http://en.wikipedia.org/wiki/Lithium_polymer_battery
[9] http://www.prnewswire.com/news-releases/lithium-air-batteries-technology-trends-and-commercialization-prospects-215240681.html

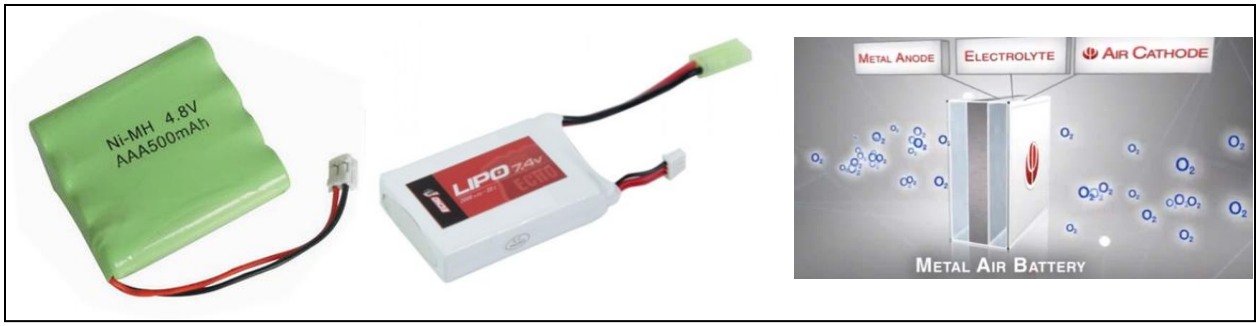

Figure 5-10 – Battery Technology Form Factors and Concepts

Wireless power sources are beginning to become commercially available, albeit over very short distances. There are several categories of wireless power systems that could be considered, some more practical than others for the V2Suit system – electrodynamic induction, electrostatic induction, and electromagnetic radiation. Wireless power systems provide the distinct advantage of being able to power the modules without any cabling or high energy-density batteries, thus potentially reducing the mass and volume of the modules. However, they still require an external power source, maintaining localization within the power transmission/reception volume, as well as environmental confounds due to the spacecraft structure. Wireless power sources are being considered in the V2Suit technology roadmap, particularly for module re-charging in a base station. Their technology for real-time power production is considered to be not mature enough for immediate consideration.

Challenges

The scope of the challenges associated with integrating a self-contained power source to operate the V2Suit system for at least one hour between re-charges cannot be fully realized until our design has matured and electrical and computing components have been selected. Independent of the V2Suit power requirement, there are additional challenges associated with the battery technology that can be discussed – packaging, re-chargeability, and operational lifetime.

The V2Suit system concept includes the wearable modules on the limbs and the central power and processing module. This architecture provides the affordance of having power be locally within each limb module, be within the central power and processing module, or both. A design trade will need to be made once the module designs mature to determine the exact form factor and available volume for battery containment.

The design requirement for operational duration has been specified as one hour, allowing for re-charging of the batteries between sessions. Newer battery technology fully supports re-chargeability. However, the one open question that needs to be addressed is the time required to re-charge. It is likely that the time required will be on the order of a few hours. However, this performance specification needs to be addressed before component selection.

Lastly, batteries may have a limited number of charge/discharge cycles in their useful lifetime.

This is particularly important for specifying the number of batteries to include on a long-duration mission. Cycle testing of the selected battery in an operational system will be necessary to determine the lifetime of the technology.

Roadmap

Power sources are a requirement for any electromechanical system. The existing state of development of the V2Suit enables the use of widely available, conditioned outlet power sources while surveying battery technology for integration into a subsequent development system. Our baseline is to continue development using laboratory power sources, and survey battery technology in parallel as the V2Suit design matures, thus enabling us to make a fully informed decision on the sizing and selection of re-chargeable battery units.

5.5 Key Enabling Technology TRL Summary

Each of the four key enabling technologies for the V2Suit are currently at different estimated technology readiness levels (TRLs) (Figure 5-11). Their estimates are based on composite knowledge of the current status of development or off-the-shelf components for integration to realize V2Suit operations in a long-duration space mission specified by the key operational requirements (refer to Table 2-1).

Control moment gyroscopes (CMGs) are a very mature technology for aerospace applications. However, their miniaturization for body-worn systems is immature, and even further immature is the development of the steering laws to resist movements parallel to a specified direction. Miniature CMG components are readily available (e.g., MICROMO motor systems). However their miniaturized packaging for torque generation has not been developed. Similarly, this NIAC V2Suit Phase II study has advanced the development of the steering laws of a number of CMG architectures to respond to the torque vector recommendation from the "down" tracking algorithm, while avoiding singularities and saturation conditions.

Several candidate technologies for the module state estimation and "down" tracking algorithms are readily available for integration into a V2Suit flight system. IMUs, for example, which are the baseline navigation system for tracking the orientation and motion of each V2Suit module with respect to the initialized direction of down have been used extensively in aerospace systems. The element of this key technology, which has been developed and tested as part of the NIAC Phase II study, is the "down" initialization and tracking algorithm. This algorithm has demonstrated its performance using synthetic as well as actual IMU data and has been identified for integration into the V2Suit system.

Key Technology for V2Suit Applications	Estimated TRL*
Miniature CMGs (for body-worn applications)	**5**
CMG Hardware	*6*
Steering Laws	*4*
Module Tracking Technology & Algorithms	**6**
Module State ("Down") Tracking Algorithms	*6*
Inertial Measurement Units (IMUs)	*9*
Optical Tracking Systems	*9*
Vision-Aided Navigation	*4*
Human-System Integration	**5**
Low-profile, Conformal Form Factor	*5*
Integration with Existing Wearable Garments	*5*
Customized, Printable Garments	*3*
Power Source Technology	**9**
Miniature, High-Density Energy Storage	*9*
Wireless Power Technology	*2*

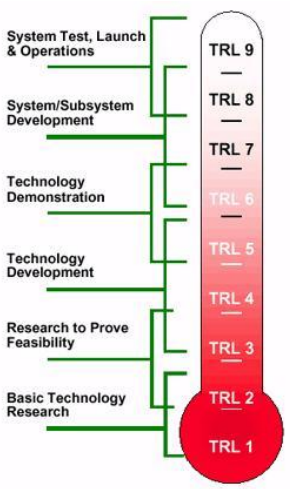

*Current estimate based on existing technology survey for a ground-based operational V2Suit.

Figure 5-11 – V2Suit Key Enabling Technology Estimated TRL Summary

There are several design approaches and technologies available to enable the integration of the V2Suit modules with the astronaut. The key to the development of these technologies will be the sizing of the modules (based on CMG design and electronics), and also informed by user evaluations to ensure comfort and ease of use – two keys for technology insertion and adoption. Several concepts exist for integrating the modules with wearable garments. However, these concepts are relatively immature in terms of design specifics for the modules and V2Suit operations. Additional technologies, such as printable garments, are less mature for aerospace garments.

Lastly, power source technology – particularly battery technology – has a high TRL because of its ubiquitous integration with electronics. The challenge, as mentioned before, will be the specification of the required power to support V2Suit operations and then selecting a battery with the energy density and form factor to meet the body-worn, autonomous operations requirement. Future technology may include wireless power sources. However, at the present time, this technology is considered too immature to consider in the V2Suit baseline development roadmap.

6.0 Earth Benefits and Alternate Uses

The current research, analysis, and concept design of the V2Suit has focused on a wearable system to prevent the physiological adaptation and de-conditioning that is associated with long-duration spaceflight. There are other spaceflight applications of the V2Suit technology (see Figure 6-1). Wearable CMGs could be integrated with a spacewalking astronaut and commanded to provide a "stable" work platform, or counter reaction torques during movement, while operating on or near a low-gravity body such as an asteroid. This type of countermeasure suit also has earth benefits, particularly in gait or movement stabilization for the elderly, or physical therapy/rehabilitation (see Figure 6-1). For example, the V2Suit CMGs could be programmed to provide a kinematic envelope of least resistance during walking – "keeping within stability zones." Therefore providing tactile feedback to the appropriate biomechanical coordination – either to assist in gait correction or facilitate recovery following spaceflight or traumatic injuries. A potential advancement to drop foot gait (a neuromuscular disorder, often occurring after a stroke, where the anterior muscles of the lower leg are weaker) could be made with a wearable device with embedded sensors and programmable network of actuators, such as with the V2Suit modules. With the appropriately sized CMG, it is possible that the gyroscopic torque could prevent falls – a significant contributor to hip fractures in the elderly. In addition, with knowledge of the environment and the planned task, the CMGs could be commanded to enforce "keep out zones" – spatial regions that if encroached with a body limb could cause harm to either the person or the equipment.

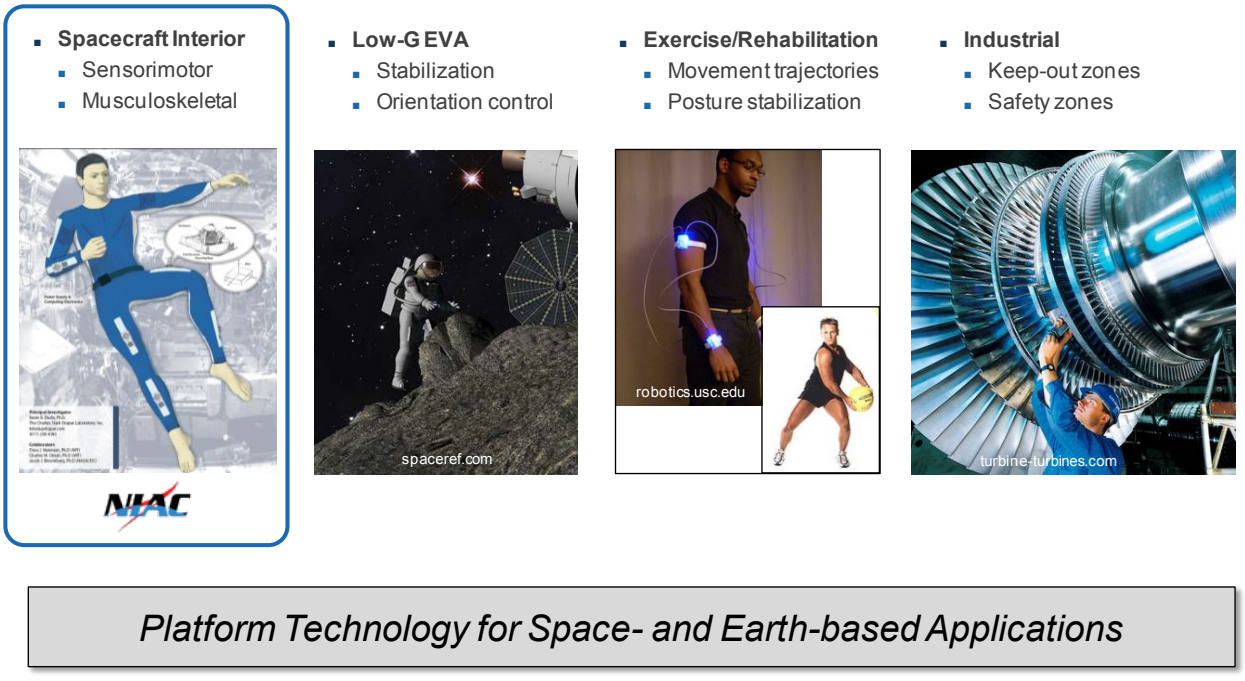

Figure 6-1 – V2Suit Alternate Uses

The V2Suit software and hardware architecture was designed to be module to enable multiple developers or researchers to interface with the system (Figure 6-2). The hardware components include the module kinematics/motion sensing through the on-board IMU and the actuation/commanding of the resistance through the CMGs. With these interfaces, the developers can create their own algorithms for analyzing the module kinematics and CMG steering laws for commanding a resistance to movement. For the initial V2Suit development, we focused on countering the sensorimotor effects of long-duration spaceflight, but there are other applications as well (Figure 6-2).

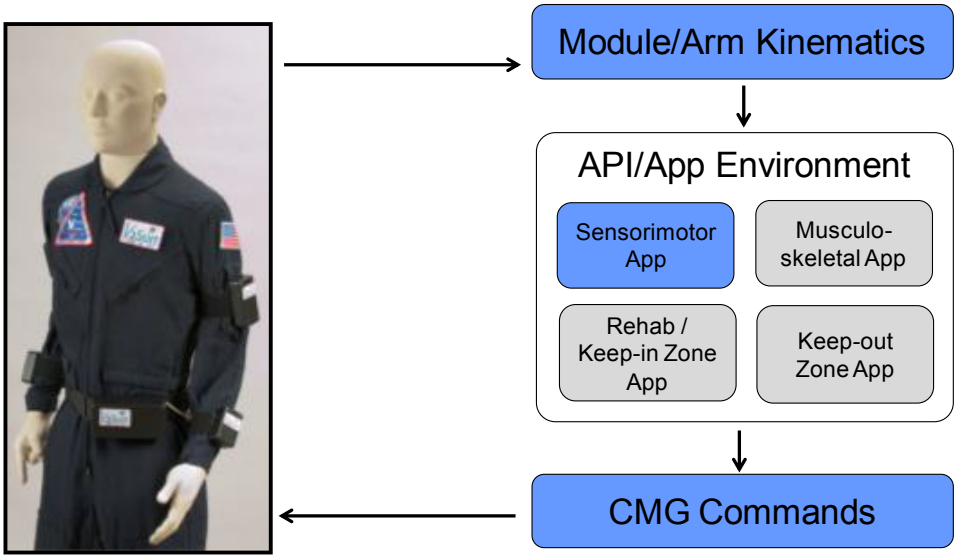

Figure 6-2: V2Suit Developer Integration Architecture

7.0 References

[1] Oman, Charles M., *Chapter 19: Human Visual Orientation in Weightlessness*, in *Levels of Perception*, L.R. Harris and M. Jenkin, Editors. 2003, Springer-Verlag: New York. p. 375-395.

[2] Augustine, Norman R., et al., *Review of U.S. Human Spaceflight Plans Committee: Seeking a Human Spaceflight Program Worthy of a Great Nation*. 2009.

[3] Buckey, Jay C., Jr., *Space Physiology*. 2006, New York: Oxford University Press.

[4] NSBRI. *Research Areas: National Space Biomedical Research Institute*. 2011 [cited 2011 April 19]; Available from: http://www.nsbri.org/Research/index.html.

[5] Paloski, William H., et al., *Recovery of Postural Equilibrium Control Following Space Flight (DSO 605)*, in *Extended duration orbiter medical project final report 1989-1995. NASA SP-1999-534*, C.F. Sawin, G.R. Taylor, and W.L. Smith, Editors. 1999. p. 5.4-1 - 5.4-16.

[6] Bloomberg, Jacob J. and Ajitkumar P. Mulavara, *Changes in Walking Strategies after Spaceflight.* IEEE Engineering in Medicine and Biology Magazine, 2003(March/April): p. 58-62.

[7] Bloomberg, J.J., et al. *Locomotion after long-duration spaceflight: Adaptive modulation of a full-body head and gaze stabilization system*. in *Bioastronautics Investigators' Workshop*. 2001. Galveston, Texas.

[8] NASA-HRP. *Risk of Impaired Control of Spacecraft, Associated Systems and Immediate Vehicle Egress Due to Vestibular/Sensorimotor Alterations Associated with Space Flight*. 2012a [cited 2012 April 27]; Available from: http://humanresearchroadmap.nasa.gov/risks/.

[9] Coolahan, James E., Andrew B. Feldman, and Sean P. Murphy. *Integrated Physiological Simulation of an Astronaut Exercise Protocol*. in *55th International Astronautical Congress*. 2004. Vancouver, Canada.

[10] Duda, Kevin R., Thomas Jarchow, and Laurence R. Young, *Squat Exercise Biomechanics During Short-Radius Centrifugation.* Aviation, Space, and Environental Medicine, 2012. **83**(2): p. 102-110.

[11] Drake, Bret G., ed. *Human Exploration of Mars Design Reference Architecture 5.0 (NASA/SP-2009-566)*. Vol. NASA/SP-2009-566. 2009. 100.

[12] Charles, John B. *Human Health and Performance Aspects of the Mars Design Reference Mission*. in *33rd COSPAR Scientific Assembly*. 2000. Warsaw, Poland.

[13] NASA-HRP. *Risk of Microgravity-Induced Visual Impairment/Intracranial Pressure*. 2012b [cited 2012 May 18]; Available from: http://humanresearchroadmap.nasa.gov/risks/?i=105.

[14] LeBlanc, A., et al., *Muscle volume, MRI relaxation times (T2), and body composition after spaceflight.* Journal of Applied Physiology, 2000. **89**(6): p. 2158-64.

[15] Gopalakrishnan, R., et al., *Muscle volume, strength, endurance, and exercise loads during 6-month missions in space.* Aviat Space Environ Med, 2010. **81**(2): p. 91-102.

[16] Convertino, Victor A., *Exercise as a countermeasure for physiological adaptation to prolonged spaceflight.* Medicine and Science in Sports and Exercise, 1996. **28**(8): p. 999-1014.

[17] LeBlanc, A., et al., *Bone mineral and lean tissue loss after long duration space flight.* J Musculoskelet Neuronal Interact, 2000. **1**(2): p. 157-60.

[18] Oganov, V. and V. S. Schneider, *Skeletal system*, in *Space Biology and Medicine*, A. Nicogossian and O.G. Gazenko, Editors. 1996, American Institute of Aeronautics and Astronautics: Reston, VA. p. 247-266.

[19] Bikle, D. D., T. Sakata, and B. P. Halloran, *The impact of skeletal unloading on bone formation.* Gravit Space Biol Bull, 2003. **16**(2): p. 45-54.

[20] Astrand, Per-Olof, et al., eds. *Textbook of Work Physiology: Physiological Bases of Exercise, 4th Edition*. 2003, Human Kinetics: Champaign, IL.

[21] Gazenko, O. G., A.M. Gernin, and A.D. Egorov, *Major Medical Results of the Salyut-6 Soyuz 18 5day Space Flight.* 1981.

[22] Johnson, R.S., L.F. Dietlein, and C.A. Berry, *Biomedical Results of Apollo*. 1975, Washington, D.C.: NASA.

[23] Nicogossian, A.W., C. Leach-Huntoon, and S.L. Pool, *Space Physiology and Medicine*. 1989, Philadelphia: Lea & Febiger.

[24] Paloski, William H., et al., *Risk of Sensory-Motor Performance Failures Affecting Vehicle Control During Space Missions: A Review of the Evidence.* Journal of Gravitational Physiology, 2008. **15**(2): p. 1-29.

[25] Bock, O., S. Abeele, and U. Eversheim, *Human adaptation to rotated vision: interplay of a continuous and a discrete process.* Exp Brain Res, 2003. **152**(4): p. 528-32.

[26] Oman, C. M. *Etiologic role of head movements and visual cues in space motion sickness on Spacelabs 1 and D-1*. in *7th IAA Man in Space Symposium: Physiologic Adaptation of Man in Space*. 1986. Houston, TX.

[27] Gazenko, O. G., *Medical studies on the cosmic spacecrafts "Vostok" and Voskhod"*. 1964.

[28] Cohen, Helen S., *Update on the status of rehabilitative countermeasures to ameliorate the effects of long-duration exposure to microgravity on vestibular and sensorimotor function.* Journal of Vestibular Research: Equilibrium & Orientation, 2004. **13**(4-6): p. 405-409.

[29] Hoffer, Michael E., et al., *Sensorimotor reconditioning during and after spaceflight.* NeuroRehabilitation. **29**(2): p. 185-195.

[30] Wood, S. J., J. A. Loehr, and M. E. Guilliams, *Sensorimotor reconditioning during and after spaceflight.* NeuroRehabilitation, 2011. **29**(2): p. 185-195.

[31] Harm, D. L. and D. E. Parker, *Preflight adaptation training for spatial orientation and space motion sickness.* Journal Of Clinical Pharmacology, 1994. **34**(6): p. 618-627.

[32] Aoki, H., C. M. Oman, and A. Natapoff, *Virtual-reality-based 3D navigation training for emergency egress from spacecraft.* AVIATION SPACE AND ENVIRONMENTAL MEDICINE, 2007. **78**(8): p. 774-783.

[33] Harm, D. L., et al., *Sensorimotor coordination aftereffects of exposure to a virtual environment.* Visual Computer, 2008. **24**(11): p. 995-999.

[34] Shelhamer, Mark and Kara Beaton, *Pre-flight sensorimotor adaptation protocols for suborbital flight.* Journal of Vestibular Research: Equilibrium & Orientation, 2012. **22**(2/3): p. 139-144.

[35] Bock, O., S. Schneider, and J. Bloomberg, *Conditions for interference versus facilitation during sequential sensorimotor adaptation.* Experimental Brain Research, 2001. **138**(3): p. 359-365.

[36] Waldie, James M. and Dava J. Newman, *A gravity loading countermeasure skinsuit.* Acta Astronautica, 2011. **68**(7-8): p. 722-730.

[37] Kozlovskaya, I., I. Pestov, and A. Egorov, *The system of preventive measures in long space flights.* Human Physiology, 2010. **36**(7): p. 773-779.

[38] Coolahan, J.E., A.B. Feldman, and S.P. Murphey, *Integrated Physiological Simulation of an Astronaut Exercise Protocol*, in *55th International Astronautical Congress*. 2004: Vancouver, Canada.

[39] Buckey, Jay C., *Space physiology / Jay C. Buckey, Jr*. 2006: Oxford ; New York : Oxford University Press, 2006.

[40] Iwase, S., *Effectiveness of centrifuge-induced artificial gravity with ergometric exercise as a countermeasure during simulated microgravity exposure in humans.* ACTA ASTRONAUTICA, 2005. **57**(2-8): p. 75-80.

[41] Zwart, S. R., et al., *Lower body negative pressure treadmill exercise as a countermeasure for bed rest-induced bone loss in female identical twins.* BONE, 2007. **40**(2): p. 529-537.

[42] LeBlanc, A., et al., *Bisphosphonates as a supplement to exercise to protect bone during long-duration spaceflight.* Osteoporosis International, 2013. **24**(7): p. 2105-2114.

[43] Smith, S. M., et al., *Benefits for bone from resistance exercise and nutrition in long-duration spaceflight: Evidence from biochemistry and densitometry.* JOURNAL OF BONE AND MINERAL RESEARCH, 2012. **27**(9): p. 1896-1906.

[44] NASA. *Advanced Resistive Exercise Device (ARED)*. International Space Station 2014 January 9, 2014 [cited 2014 April 23]; Available from: http://www.nasa.gov/mission_pages/station/research/experiments/1001.html.

[45] Scheuring, R. A., et al., *Musculoskeletal Injuries and Minor Trauma in Space: Incidence and Injury Mechanisms in US Astronauts.* AVIATION SPACE AND ENVIRONMENTAL MEDICINE, 2009. **80**(2): p. 117-124.

[46] Marshall-Bowman, K., M. R. Barratt, and C. R. Gibson, *Ophthalmic changes and increased intracranial pressure associated with long duration spaceflight: An emerging understanding.* ACTA ASTRONAUTICA, 2013. **87**: p. 77-87.

[47] Luinge, H. J. and P. H. Veltink, *Measuring orientation of human body segments using miniature gyroscopes and accelerometers.* Medical & Biological Engineering & Computing, 2005. **43**(2): p. 273-282.

[48] El-Gohary, Mahmoud and James McNames, *Shoulder and Elbow Joint Angle Tracking With Inertial Sensors.* IEEE Transactions on Biomedical Engineering, 2012. **59**(9): p.

2635.

[49] Young, D., et al. *Estimation of Lower Limb Joint Angles During Walking Using Extended Kalman Filtering*. in *6th World Congress on Biomechanics*. 2010. Singapore.

[50] Lapinski, M., et al. *A distributed wearable, wireless sensor system for evaluating professional baseball pitchers and batters*. in *2009 International Symposium on Wearable Computers (ISWC)*. 2009. Place of Publication: Piscataway, NJ, USA; Linz, Austria. Country of Publication: USA.: IEEE.

[51] Brodie, Matthew, Alan Walmsley, and Wyatt Page, *Fusion motion capture: a prototype system using inertial measurement units and GPS for the biomechanical analysis of ski racing.* Sports Technology, 2008. **1**(1): p. 17-28.

[52] Lai, Daniel T. H., et al., *On the difference in swing arm kinematics between low handicap golfers and non-golfers using wireless inertial sensors.* Procedia Engineering. **13**: p. 219-225.

[53] Hung, Tran Nhat and Suh Young Soo, *Inertial Sensor-Based Two Feet Motion Tracking for Gait Analysis.* Sensors (14248220), 2013. **13**(5): p. 5614-5629.

[54] Li, Rongxing, et al., *A Multisensor Integration Approach toward Astronaut Navigation for Landed Lunar Missions.* Journal of Field Robotics, 2013. **31**(2): p. 245-262.

[55] Young, Diana and D. J. Newman, *Augmenting Exploration: Aerospace, Earth, and Self*, in *Wearable monitoring systems*, A. Bonfiglio and D.E. De Rossi, Editors. 2011, Springer: New York.

[56] Peck, Mason, *Lecture Notes on Control-Moment Gyroscopes*. 2007: Cornell University.

[57] Giffen, A., P.L. Palmer, and R.M. Roberts, *Exact CMG Steering Laws which Reset Gimbal Angles*. 2012, University of Surrey: Guildford, Surrey.

[58] Wie, B., *Singularity escape/avoidance steering logic for control moment gyro systems.* JOURNAL OF GUIDANCE CONTROL AND DYNAMICS, 2005. **28**(5): p. 948-956.

[59] Wie, B., D. Bailey, and C. Heiberg, *Singularity robust steering logic for redundant single-gimbal control moment gyros.* Journal of Guidance, Control, and Dynamics, 2001. **24**(5): p. 865-872.

[60] Flanders, M., et al., *Using arm configuration to learn the effects of gyroscopes and other devices.* JOURNAL OF NEUROPHYSIOLOGY, 2003. **89**(1): p. 450-459.

[61] Jones, L. L., R. A. Zeledon, and M. A. Peck, *Generalized framework for linearly constrained control moment gyro steering.* Journal of Guidance, Control, and Dynamics, 2012. **35**(4): p. 1094-1103.

[62] Wie, Bong, *Space vehicle dynamics and control / Bong Wie*. AIAA education series. 2008: Reston, VA : American Institute of Aeronautics and Astronautics, c2008. 2nd ed.

[63] Bedrossian, N. S., et al., *Redundant single gimbal control moment gyroscope singularity analysis.* Journal of Guidance, Control, and Dynamics, 1990(a). **13**(6): p. 1096-1101.

[64] Bedrossian, N. S., et al., *Steering law design for redundant single-gimbal control moment gyroscopes.* Journal of Guidance, Control, and Dynamics, 1990(b). **13**(6): p. 1083-1089.

[65] Asghar, S., P.L. Palmer, and M. Roberts, *Exact steering law for pyramid-type four control moment gyro systems*, in *AIAA/AAS Astrodynamics Specialist Conference and*

Exhibit. 2006: Keystone, Colorado.

[66] Kurukowa, H., *A Geometric Study of Control Moment Gyroscopes*. 1998, University of Tokyo: Tokyo, Japan.

[67] Yoon, Hyungjoo and Panagiotis Tsiotras, *Singularity analysis of variable-speed control moment gyros.* Journal of Guidance, Control, and Dynamics, 2004. **27**(3): p. 374-386.

[68] Yeadon, M. R., *The simulation of aerial movement--II. A mathematical inertia model of the human body.* Journal of Biomechanics, 1990. **23**(1): p. 67-74.

[69] Flanders, M., et al., *Using arm configuration to learn the effects of gyroscopes and other devices.* J Neurophysiol, 2003. **89**(1): p. 450-9.

[70] Lapinski, Michael, et al. *A Distributed Wearable, Wireless Sensor System for Evaluating Professional Baseball Pitchers and Batters*. in *International Symposium on Wearable Computers*. 2009: IEEE.

[71] Brown, R. G. and P. Y. C. Hwang, *Introduction to Random Signals and Applied Kalman Filtering*. 1997, New York: John Wiley & Sons.

[72] Julier, Simon J. and Jeffrey K. Uhlmann. *A New Extension of the Kalman Filter to Nonlinear Systems*. in *Int. Symp. Aerospace/Defense Sensing, Simul. and Controls*. 1997. Orlando, FL.

[73] Luinge, H. J. and P. H. Veltink, *Measuring orientation of human body segments using miniature gyroscopes and accelerometers.* Med Biol Eng Comput, 2005. **43**(2): p. 273-82.

[74] Sabatini, A. M., *Quaternion-based extended Kalman filter for determining orientation by inertial and magnetic sensing.* IEEE Trans Biomed Eng, 2006. **53**(7): p. 1346-56.

[75] DeBitetto, P., *Using 3D Virtual Models and Ground-based Imagery for Aiding Navigation in Large-Scale Urban Terrain*. 2010: Joint Navigation Conference.

[76] Wu, Allen D., Eric N. Johnson, and Alison A. Proctor. *Vision-Aided Inertial Navigation for Flight Control*. in *AIAA Guidance, Navigation, and Control Conference*. 2005. San Francisco, CA.

[77] van Tujil, J.H., Y.J.M Janssen-Potten, and H.A.M Seelen. "Evaluation of upper extremity motor functions tests in tetraplegics". *Nature* (2002). Vol 40, Num 2, pgs 51-64.

[78] Fitts, P. "The Information Capacity of the Human Motor System in Controlling the Amplitude of Movement." *Journal of Experimental Psychology*, (1954). Vol 47, pgs 381-391.

[79] MacKenzie, C.L., R. G. Marteniuk, C. Dugas, D. Liske, B. Eickmeier. "Three-dimensional movement trajectories in Fitts' task: Implications for control." *The Quarterly Journal of Experimental Psychology Section A*. (1987) Vol. 39, Iss 4.

[80] Hartsell, C.P. "An Information-Theoretic Model of the Human Operator." *Eighteenth Annual Conference on Manual Control*. (1982). Dayton, OH.

[81] Plamondon, R. and A. M. Alimi. "Speed/accuracy trade-offs in target-directed movements." *Behavioral and Brain Sciences*. (1997) Vol 20, pgs 279-349.

8.0 Appendices

8.1 Publications

Duda, K.R., R. Vasquez, A.J. Middleton, D.J. Newman, and S.E. Jacobs (2013) "Variable Vector Countermeasure Suit (V2Suit) for Space Exploration" [Abstract & Poster] NASA Human Research Program Investigators' Workshop. Galveston, TX. 12-14 February.

Duda, K.R. and D.J. Newman (2013) "Variable Vector Countermeasure Suit (V2Suit) for Space Exploration" IEEE Aerospace Conference. Big Sky, MT. 2-9 March.

Duda, K.R., R. Vasquez, A.J. Middleton, D.J. Newman, and S.E. Jacobs (2013) "Variable Vector Countermeasure Suit (V2Suit) for Space Exploration" [Poster] 2013 NIAC Spring Symposium. Chicago, IL. 12-14 March.

Duda, K.R., R. A. Vasquez, and D. J. Newman (2013) "Wearable Control Moment Gyroscopes as a Spaceflight Adaptation Countermeasure" [Presentation] Invited Panel Session: *Sensorimotor Evaluation and Countermeasures for Space Exploration Missions*, 84th AsMA Annual Scientific Meeting, Chicago, IL, 12-16 May.

Duda, K.R., R. A. Vasquez, and D. J. Newman (2013) "Wearable Control Moment Gyroscopes as a Spaceflight Adaptation Countermeasure" [Abstract] Aviation, Space, and Environmental Medicine. Vol. 84, No. 4. p. 411. ISSN 0095-6562. (Abstract #454)

Duda, K.R., R. A. Vasquez, A. J. Middleton, D. J. Newman, and S. E. Jacobs (2014) "Variable Vector Countermeasure Suit (V2Suit) for Space Exploration" [Abstract & Poster] NASA Human Research Program Investigators' Workshop. Galveston, TX. 12-13 February.

Vasquez, R. A., A. J. Middleton, K. R. Duda, and D. J. Newman (2014) "The V2Suit 'Down' Tracking Algorithm." IEEE Aerospace Conference. Big Sky, MT. 1-8 March.

Duda, K. R., R. A. Vasquez, A. J. Middleton, D. J. Newman, and S. E. Jacobs (2014) "Variable Vector Countermeasure Suit (V2Suit) for Space Habitation and Exploration" *Invited Presentation to NSBRI Symposium* "Designing for the Future: Remote Rehabilitation and Integration of New Technologies in Spaceflight." Houston, TX. 6-7 May.

Vasquez, R. A. (2014) "The Variable Vector Countermeasure Suit for Space Habitation and Exploration." S.M. in Mechanical Engineering, Massachusetts Institute of Technology, Cambridge, MA, June 2014.

8.2 Select News & Media Coverage

Draper Laboratory News Release

Draper Spacesuit Could Keep NASA Astronauts Stable, Healthier in Space

Draper Laboratory's Kevin Duda has begun work on a new spacesuit for NASA, and will deliver an Earth-based prototype to demonstrate on a human arm next year.

CAMBRIDGE, MA – Draper Laboratory began work this month on a new spacesuit that could keep NASA astronauts healthy during long-duration space exploration missions and stabilize them while they work in microgravity.

NASA commissioned the work through its NASA Innovative Advanced Concepts (NIAC) program, which funds efforts based on their potential to enhance future space missions.

The suit aims to stabilize astronauts and allow them to operate far more efficiently during space missions by adding resistance similar to the force of gravity on Earth. During so would help astronauts acclimate to space and avoid body movement coordination-related mistakes in microgravity or other gravitational environments that can make their work more cumbersome.

The suit will use an intertial measurement unit and flywheel gyroscopes to raise or lower resistance during body movements, or stabilize and assist astronauts while working inside or outside a spacecraft, as well as on a planet or asteroid.

"This spacesuit concept will provide a platform for integrating sensors and actuators with daily activities to maintain and improve astronaut health and performance," said Kevin Duda, a senior member of the technical staff in Draper's Human Centered Engineering Group, and the principal investigator for the spacesuit project.

In addition to stabilizing astronauts in space, the suit could also be used to help reacclimate them to the feel of gravity upon return to Earth or other planetary destination. Outside of space, the suit could be adapted for uses including medical rehabilitation to assist in rehabilitation and physical therapy for individuals affected by stroke, spinal cord and brain injuries, as well as the elderly population, as they relearn the proper way to execute common movements by introducing strong resistence when they do not take the proper path.

Over the course of the next year, Draper will develop an early stage Earth-based prototype to demonstrate the capability on a human arm. With continued funding, this capability could be ready for use as a feature in astronaut spacesuits in five to 10 years.

Draper is partnering on the project with Jacob Bloomberg, a senior research scientist at NASA's Johnson Space Center, Professor Dava Newman, director of the technology and policy program at the Massachusetts Institute of Technology's Department Aeronautics and Astronautics, and Charles Oman, a senior researcher in the MIT Aero Astro department.

Draper, MIT Device Could Help Stop Spread of Cancerous Tumors

CAMBRIDGE, MA – Draper Laboratory and MIT have invented a device that may enable drug developers to create medicines that stop cancer in its tracks by allowing them to see how diseased cells migrate.

A longer term goal for the device is to enable hospital labs to create more individualized treatment plans for cancer patients

http://www.draper.com/newsItems.html 8/23/2011

The Washington Post

URBAN JUNGLE

The changing natural world at our doorsteps.

Troubled urban streams

When hurricanes or tropical storms pass through the Washington area, flash flooding can become a problem, not just for houses and businesses in the flood plain, but also for the organisms that live in the waterways being flushed with storm water.

The flow can cause serious disturbances in streambeds, "uprooting aquatic plants, rolling rocks and killing many bottom-dwelling organisms," says N. LeRoy Poff, an ecology professor at Colorado State University.

Heavy rains can also flush pollutants and soil sediments into streams. Although too much sediment in a stream can cause problems, too little can also be detrimental.

"Many streams inside the Beltway have been urbanized for a long time, and there is no longer available sediment from the watershed due to all the impervious surfaces," says Poff. A loss of sediment cripples an urban stream's ability to deposit new banks and bottoms, so the stream becomes incised, cutting an increasingly deeper groove for itself.

Another problem: Roofs, streets and parking lots prevent rainwater from soaking into the ground, sending it as a "flash" through urban waterways. Sensitive species have trouble finding refuge during such an event.

Only species that are pollution-tolerant, have a fast life cycle and are able to handle extremes in flow can survive in such an environment, says Poff.

Asian clams, an exotic invasive species found in local streams, "do very well in extreme flashy environments," says Daren Carlisle, an aquatic ecologist with the U.S. Geological Survey.

Carlisle describes urban-stream fishes, such as the common carp, as generalists: "They can reproduce anywhere and eat anything."

Watts Branch, a deeply incised urban stream, drains almost 3.3 square miles of Northeast Washington and Capitol Heights.

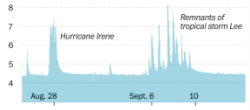

SOURCES: Joel Guyer, USGS Virginia Water Science Center; USGS National Water Information System
PATTERSON CLARK/THE WASHINGTON POST clarkp@washpost.com washingtonpost.com/urbanjungle

HOW & WHY

Brian Palmer

When it comes to fashion, astronauts are way out there

Some people like runway fashion. Not me. I'm much more interested in function than form. From that perspective, no one has a more interesting closet than an astronaut. While they look very much like painter's smocks — their sloppy draping would probably make Michael Kors faint — spacesuits are fascinating, high-tech threads.

Astronaut clothes really boil down to indoor wear and outdoor wear. Let's start with the outdoor ensemble. To state the obvious, space is an inhospitable environment. There's no air. Astronauts are constantly bombarded by ultraviolet-C rays, the high-energy solar radiation that ozone blocks from the Earth. The weather is terrible. A spacewalker's suit can confront freezing temperatures on the front and burning-hot conditions on the back, because the difference between sun and shade is around 275 degrees in space.

Then there's the pressure difference. Space is nearly a vacuum. If an astronaut stepped into the void with lungs full of oxygen in ordinary clothes, the air would expand enough to rupture the lungs. The pressure is also so low that the boiling point of blood drops below human body temperature, a condition that can kill in an instant. Space is also full of micro-meteoroids, tiny projectiles that threaten to pierce an astronaut's armor.

Spacesuits protect astronauts against all these challenges. They have multiple layers to provide insulation and prevent a puncture of the inner coating, which is filled with pure oxygen at a livable pressure. (The pressure difference between the suit and the external environment is daunting, though. Without the improvement in modern spacesuit joints, bending your knee in a spacesuit would be like trying to bend an inflated football.)

A layer of water circulates throughout the suit, interacting with a layer of ice near the outer surface, to moderate the temperature. A ventilation system removes excess body heat when the sun threatens to warm the astronaut too much. For the most part, the temperature remains fairly comfortable, although some space travelers have noted that their extremities — which aren't covered by the water circulation system — can get chilly.

Modern suits have built-in life support systems, so the astronaut can function outside a spacecraft without being tethered to a much larger machine. (Earlier astronauts had to remain attached to their shuttles by large tubes.) The suits are so self-contained that some refer to them as the universe's smallest space vehicles.

Until recently, an astronaut's indoor outfit hasn't had nearly the same sophistication. The international space station, which is still operating despite the end of the shuttle program, has regulated temperature and pressure, plus breathable air. It also protects astronauts from nasty space projectiles.

But this environment has its own challenges. Living in a small orbiting object requires astronauts to adjust to microgravity. It's not just a matter of overcoming the initial clumsiness of movement as they float around the ISS. Since there's very little to resist an astronaut's motion, muscles become deconditioned over months of space life. Bone density also drops, and faces puff up as fluid that is normally pulled toward the feet floats into the head.

To deal with all this, engineers at Draper Labs, an MIT spinoff, are working on a spacesuit that creates the sensation of gravity.

To understand how it works, consider this experiment: If you sit still in a swivel chair holding an upright, spinning bicycle wheel by its axle, then tilt the wheel to the left or right, the chair begins to turn. (Watch the BBC's "office chair fun" on YouTube to see the experiment in action.)

"A flywheel or spinning mass doesn't like to change its orientation," says Kevin Duda. He's leading the Draper team that's developing the spacesuit. "When you tilt the spinning wheel, it exerts a force against your body."

The engineers at Draper think they can use this effect to create a suit that resists an astronaut's attempts to move, in the same way gravity resists us on Earth.

Imagine that an astronaut working in the space station reaches for an instrument on a nearby shelf. As soon as he begins to lift his arm, a computer system inside the suit would order flywheels located along the suit's forearm to begin spinning in a direction that would exert a force against the arm's motion. The faster the flywheel spins, the more the suit would push back against the astronaut.

If it works, the suit would offer a number of benefits. It could ease the transition to life on the space station, and the return to living on Earth. The suit could reduce some of the muscle deconditioning that happens in space.

Beyond the space station, the suit could be used to prepare astronauts for the long, low-gravity trip to Mars and for maneuvering on the Martian surface, whose gravity is only about 40 percent as strong as Earth's.

There may even be uses on Earth. Since the flywheels can make movement more difficult in any environment, Duda thinks the technology could be useful for rehabilitation.

"Some patients have trouble with repetitive movements, such as walking," he says. "The flywheels could train the body to walk by making it difficult for the patient's legs to stray from a proper gait."

Duda hopes Draper Labs will have the spacesuits ready in five years. That should be several years before NASA's first manned mission to Mars, which probably won't come before 2025.

health-science@washpost.com

Space News

www.spacenews.com SPACE NEWS 9
September 12, 2011

Hispasat Picks Ariane 5 To Launch Amazonas 3

Europe's Arianespace consortium will launch Spanish satellite fleet operator Hispasat's Amazonas 3 tri-band telecommunications satellite aboard a European Ariane 5 rocket in late 2012 or early 2013 under a contract Arianespace and Hispasat announced Sept. 7.

Amazonas 3, under construction by Space Systems/Loral of Palo Alto, Calif., will replace the Amazonas 1 satellite now stationed at Hispasat's 61 degrees west orbital slot, where it provides telecommunications in the Americas and between Latin America and Europe. Amazonas 1 was launched in 2004 with an expected 15-year operational life, but a defect in its fuel system has cut its life expectancy by several years.

Given the growing importance of the Americas, especially Central and South America, to Hispasat — the region provided 44 percent of its total 2010 revenue of $214.6 million — the company was forced to order Amazonas 3 sooner than originally expected.

Madrid-based Hispasat also operates the Amazonas 2 satellite at the 61 degrees west slot. Amazonas 2 was launched in October 2009 and is expected to operate for at least 15 years. Amazonas 1 and Amazonas 2 were both built by Astrium Satellites of Europe.

Amazonas 3, based on Loral's 1300 satellite platform, is expected to weigh 6,000 kilograms at launch. It will be equipped with 33 Ku-band transponders, 19 C-band transponders and nine Ka-band spot beams. Hispasat said Amazonas 3 will be the first satellite over Latin America providing substantial Ka-band capacity for broadband Internet connections.

Hispasat is financing Loral's construction of Amazonas 3 through a loan from JPMorgan Chase that was valued at 165 million euros ($236 million) and guaranteed by the U.S. Export-Import Bank. Hispasat said it will be repaying the loan over 10 years.

RapidEye Inks Imagery Deal With NGA Worth $4.6 Million

The U.S. National Geospatial-Intelligence Agency (NGA) has contracted with Canadian-German Earth observation satellite operator RapidEye to purchase up to $4.6 million in RapidEye imagery over the next 18 months, RapidEye announced Sept. 6.

The indefinite-delivery, indefinite-quantity contract is the first NGA purchase of RapidEye data. Brandenburg, Germany-based RapidEye, which was recently purchased by Canada's Iunctus Geomatics of Lethbridge, Alberta, operates a fleet of five identical optical observation satellites, which have been in orbit since mid-2008.

The satellites offer relatively low-resolution imagery but, evenly spaced in low Earth orbit, they are able to cover vast swaths of territory — 4 million square kilometers per day — and offer relatively quick revisits to a given locale.

NGA is the principal U.S. government agency responsible for purchasing satellite imagery from the private sector. It has long-term contracts with high-resolution satellite operators GeoEye and DigitalGlobe of the United States, and also has purchased radar imagery from Italian and German radar satellite operators.

Comments: Brian Berger, bberger@spacenews.com

Blue Origin Acknowledges Test Flight Failure

Blue Origin, the private entrepreneurial space group backed by Amazon.com founder Jeff Bezos, acknowledged Sept. 2 that it lost its New Shepard suborbital spacecraft during a test mishap in Texas.

"Three months ago, we successfully flew our second test vehicle in a short hop mission, and then last week we lost the vehicle during a developmental test at Mach 1.2 and an altitude of 45,000 feet," or 13,716 meters, Bezos wrote in a statement posted on the Blue Origin website Sept 2.

Bezos' statement appeared several hours after *The Wall Street Journal* first reported on the Aug. 24 test failure.

According to Bezos, a "flight instability" drove an angle of attack that triggered the Blue Origin range safety team to terminate thrust on the vehicle. The vehicle roared skyward from the Blue Origin spaceport, roughly 40 kilometers north of tiny Van Horn, Texas, before the failure.

The tight-lipped Blue Origin space company has been focused on suborbital spaceflight, first using its Goddard vehicle and then migrating to the New Shepard spacecraft design at its facility in Culberson County, Texas. New Shepard is seen by the company as supporting the commercial suborbital tourist market. The Goddard vehicle flew on a short, successful test flight in November 2006.

In April, NASA awarded Blue Origin $22 million in funding under the space agency's Commercial Crew Development program for development of concepts and technologies to support future human spaceflight operations. That award followed $3.7 million in NASA funding the company received in 2010 to develop an astronaut escape system and space capsule for ground tests.

NASA retired its space shuttle fleet in July and plans to rely on U.S. commercial spacecraft like those being developed by Blue Origin and other private space companies to transport American astronauts to low Earth orbit.

While the test vehicle that failed last week was a suborbital vehicle, Blue Origin is also developing an orbital space capsule designed initially to launch on an expendable Atlas 5 rocket, then transition to a reusable booster being developed by the company.

"In case you're curious and wondering 'where is the crew capsule,' the development vehicle doesn't have a crew capsule — just a close-out fairing instead," Bezos added in a postscript to his website update. "We're working on the sub-orbital crew capsule separately, as well as an orbital crew vehicle to support NASA's Commercial Crew program."

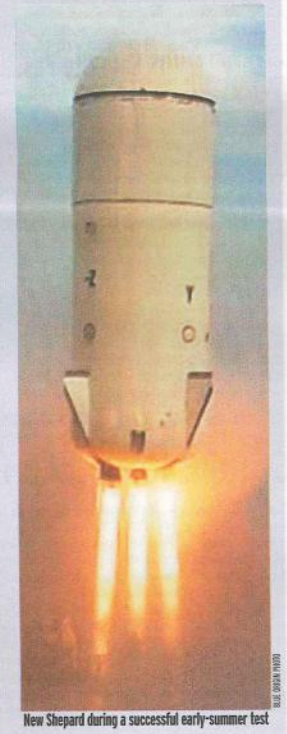

BLUE ORIGIN PHOTO

New Shepard during a successful early-summer test

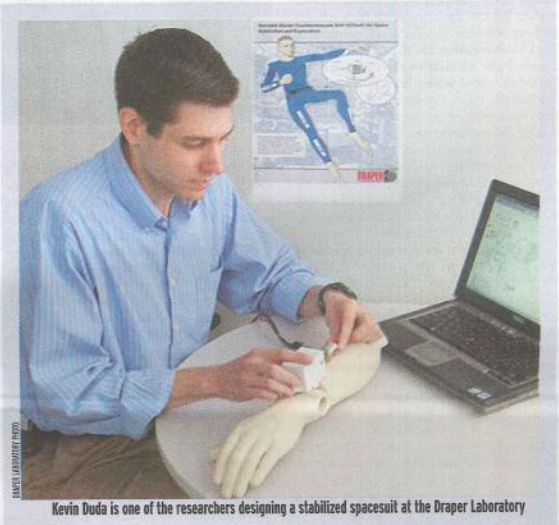

DRAPER LABORATORY

Kevin Duda is one of the researchers designing a stabilized spacesuit at the Draper Laboratory

Spacesuit To Imitate Gravity on Long NASA Missions

Researchers at Draper Laboratory in Cambridge, Mass., are working on a NASA-funded concept for a spacesuit that would help astronauts adjust to weightlessness by resisting movement to imitate gravity.

"We would expect the resistance to simulate movements against a gravitational acceleration when in microgravity," said Kevin Duda, senior member of the technical staff in the Draper Laboratory's Human Centered Engineering Group.

An inertial measurement unit would help the suit gauge an astronaut's movement. That in turn could allow flywheel gyroscopes — spinning devices that resist changes in angular momentum caused by motion — to raise or lower spacesuit resistance for every movement, by increasing speed or changing direction.

First-generation versions of the suit mainly would help astronauts working inside the protected habitat of a space station or spacecraft. But if the concept holds up, it might eventually help stabilize astronauts during spacewalks, as well as on low-gravity planets or asteroids.

"Sensing and adapting to exactly what an astronaut wants to do is difficult," Duda said. "We need to analyze the mechanics and prototype the concept before we can accurately quantify the type of performance we can expect."

Wearing such a suit also might help astronauts ease back into life on Earth, because their muscle coordination would not have to readjust from the resistance-free motions in microgravity.

Another side benefit from the suit could take the form of a space technology spinoff that helps people go through physical rehabilitation. Patients suffering from stroke, spinal cord and brain injuries could make use of the device, as could older people.

"A wearable, full-motion device could be programmed to help you learn, or re-learn, specific movements," Duda explained.

Duda's Draper Lab group has partnered on the project with scientists at NASA's Johnson Space Center in Houston and the Massachusetts Institute of Technology in Cambridge. They plan to first create a prototype for a spacesuit arm by 2012, with funding from the NASA Innovative Advanced Concepts program.

If success attracts continued funds, Duda said, a full-body wearable suit could become a reality within a decade — easily within the time frame for NASA's plans targeting the asteroids, Mars and beyond.

Popular Science – November 2012

November 2012 Issue

Boston Herald

Draper Lab inventions to aid astronauts

Well-suited for space

1

SUITABLE: Draper Laboratory's Kevin Duda, above, with the Variable Vector Countermeasure Suit (V2SUIT) used for space habitation and exploration. The suit is especially important because it could help astronauts adapt to new gravity environments, or offset the effects of prolonged weightlessness. It is being tested at the Johnson Space Center in Texas.